ISSN: 2153-2435
Pharmaceutica Analytica Acta

OPEN ACCESS Freely available online

Research Article

Molecularly Imprinted Polymer Nanostructure for Drug Stability and Binding Affinities in Biotherapeutics

Roongnapa Suedee*, Watchara Pholthien, Krit Prakannoppaku, Nanticha Kaewsud, Khanittha Santipiboon, Pimpisut Getsuvan

Department of Pharmaceutical Chemistry, Prince of Songkla University, Hatyai, Songkhla, Thailand

ABSTRACT

Molecularly Imprinted Polymers (MIPs) are transforming our understanding of protein interactions in the (bio) pharmaceutical arena. These innovative materials are instrumental in developing therapies, optimizing drug delivery, and enhancing diagnostics by enabling effective evaluation of binding affinities. Protein nanocapsules that reassemble at room temperature offer remarkable flexibility. However, fine-tuning their surface remains cutting-edge. These interactions are crucial to unlocking the full potential of Cannabidiol (CBD), particularly in its antioxidant and immunostimulatory roles when interacting with proteins such as human serum albumin. By employing selective membranes, we can precisely identify liquid proteins and uncover epitope variations influenced by excipient density and buffer composition, which significantly impact nanofibril anchoring. Accurate detection of epitopes is essential for lipid and sterol biosynthesis, but variations in the medium can affect protein stability and binding affinity. Additionally, the technique used for drug blending plays a vital role in stability. Utilizing dispersive mechanisms can enhance sustained drug release and further stabilize proteins, thereby improving cellular exposure. Our data demonstrate that CBD levels have no effect on MIP structure or enzyme activity, as confirmed by advanced techniques such as X-ray mapping and Field-Emission Scanning Electron Microscopy (FE-SEM). High-resolution Fouriertransform Infrared (FT-IR) analyses indicate that stabilized Polycaprolactone-Triol (PCL-T) hydrogels promote drug clustering and cell interactions. Moreover, MIPs can mimic natural antibodies by targeting specific markers to deliver epitopes, such as anti-IgE, effectively reducing allergy symptoms. Cutting-edge methods such as Liquid Chromatography coupled with Mass Spectrometry (LC-QTOF-MS) reveal the distinct arrangements of charged residues in proteins, which influence stability and interactions. Additionally, immunoaffinity capture reveals that stable charge states within the PCL-T hydrogel engage with albumin during pH shifts. These dynamic advancements not only enhance the stability and antioxidant properties of CBD but also improve the functionality of larger membrane protein sites created through imprinting. The efficiency of cysteine-rich regions facilitates insightful studies into CBD's role in inhibiting cellular processes. The remarkable potential of cannabinoids extends beyond reducing inflammation to boosting antimicrobial effects. Using innovative techniques such as Scanning Electron Microscopy (SEM) and fluorescence laser microscopy, we discovered intriguing protein-protein interactions in both solvent and non-solvent environments. Our findings on pH- and cholate-anchored Molecularly Imprinted Polymers (MIPs) showcase the dynamic nature of nanocapsules, which significantly influence drug degradation and amino acid absorption. Moreover, variations in nanoparticle and protein mobility highlight the essential role of Adenosine Triphosphate (ATP) in the behavior of antibodies and insulin's binding to Human Serum Albumin (HSA). This research makes a meaningful contribution to biopharmaceutical science, delving deep into biomolecule concentrations, protein folding, and cutting-edge imaging techniques. We're excited to introduce blue-light-responsive photoswitches, which demonstrate how nanocapsule size can impact hydrogel stability and ion interactions at the protein-hydrogel interface. The correlation between weight loss at melting temperatures and aggregation in water-hydrated Immunoglobulin G (IgG) during freeze-drying is noteworthy. Our Nuclear Magnetic Resonance spectroscopy (NMR) studies link biomolecular concentration to protein folding, thereby enhancing the efficiency of antibodies and enzymes. In conclusion, these findings reveal the potential of cannabinoids to improve stability and prevent protein aggregation, paving the way for innovative bioprocess and formulation development. Nuclear Magnetic Resonance (NMR) insights also suggest that lipid bilayers containing thermoresponsive proteins behave as hybrid materials, thereby optimizing drug delivery.

Correspondence to: Roongnapa Suedee, Department of Pharmaceutical Chemistry, Prince of Songkla University, Hatyai, Songkhla 90112, Thailand, E-mail: roongnapa.s@psu.ac.th

Received: 25-May-2026, Manuscript No. PAA-26-31672; Editor assigned: 27-May-2026, PreQC No. PAA-26-31672 (PQ); Reviewed: 10-Jun-2026, QC No. PAA-26-31672; Revised: 17-Jun-2026, Manuscript No. PAA-26-31672 (R); Published: 24-Jun-2026, DOI: 10.35248/2153-2435.26.17.844

Citation: Suedee R, Pholthien W, Prakannoppaku K, Kaewsud N, Santipiboon K, Getsuvan P. (2026). Molecularly Imprinted Polymer Nanostructure for Drug Stability and Binding Affinities in Biotherapeutics. Pharm Anal Acta. 17:844.

Overall, we are enthusiastic about these advancements that can positively impact biopharmaceutical products and enhance treatment safety and effectiveness.

Keywords: Molecular imprinted polymers; Affinity-based proteomic profiles; LC-QTOF-MS; Fluorescence lifetime imaging; Immunoassay hplc; Nanohybrid materials; Multimodal self-management

Abbreviations: MIPs: Molecularly Imprinted Polymers; CBD: Cannabidiol; FE-SEM: Field-Emission Scanning Electron Microscopy; SEM: Scanning Electron Microscopy; LC-QTOF-MS: Liquid Chromatography coupled with Mass Spectrometry; HSA: Human Serum Albumin; IgG: Immunoglobulin G; NMR: Nuclear Magnetic Resonance; IMN: Immunonanocapsules; FLIM: Fluorescence Lifetime Imaging; NIP: Nonimprinted Polymers

INTRODUCTION

Delivering oral biopharmaceuticals, such as engineered peptides and proteins, is promising yet challenging due to enzymatic degradation, low membrane permeability, and unpredictable absorption. MIPs are valuable in drug discovery, offering robustness and resistance to degradation, as demonstrated in studies [1]. The remarkable potential of nanocapsules and MIP for targeting tumor antigens in immunotherapy is revolutionizing the field. Localized binding facilitates advantageous structural changes in the human Fragment crystallizable (Fc) domain of antibodies, significantly enhancing their interaction with the neonatal Fc Receptor (FcRn). This critical interaction extends the half-life of antibodies, transforming the landscape of targeted drug delivery. MIPs, meticulously designed to emulate natural antibodies, enable precise targeting of specific cell-surface markers, thereby greatly enhancing diagnostic accuracy and delivery efficiency for both small molecules and biopharmaceuticals. Responsive MIPs enable controlled drug release, making them useful for insulin, anti-allergen agents, and cannabinoids such as CBD. MIPs mimic natural antibodies, targeting cell markers with precision, such as anti-IgE antibodies that reduce allergy symptoms by modulating IgE activity while maintaining mast cell functions [2]. Allergies involve excess IgE binding to receptors, forming immune complexes cleared *via* bile salts. Developing allergy treatments requires strict contamination controls and strategies-analytical process-based or premixed-to ensure safety. MIPs improve diagnostics and the delivery of small molecules and biopharmaceuticals, including mRNA and plasmid DNA, by effectively simulating antibody-drug interactions, which are crucial for drug development. Recent studies show that combining albumin, catalase, and frameworks creates nanotheranostic membranes with clinical potential, as reported by Chen, et al. [3]. Interactions among chiral amino acids, Complementarity-Determining Region (CDR) fragments, and MIP binding sites on serum albumin enhance charge insulation, which is vital for binding peptides and small molecules.

We are advancing research on MIPs to improve clinical product development and therapeutic effectiveness by addressing process variability in continuous process monitoring and optimizing protein complexes. Our goal is to study protein stability and their responses to stimuli, leading to better treatments. The stability of human Fc domains and antibody fragments is vital for effective receptor binding, thereby affecting drug efficacy and patient outcomes. This stability depends on their structure, on HSA's role in reducing drug diffusion, and on the membrane protein's structure. We focus on developing monoclonal and multivalent proteins using innovative synthesis techniques to push the boundaries of biological medicine. Techniques such as glycosylation, sialylation, and peptide fusion are used to address stability and solubility challenges. HSA and ATP are essential to fully grasp their roles within biological systems. The dynamics of plasma protein binding and free drug levels play a pivotal role in antioxidant activity. Safeguarding enzyme-sensitive regions within the Fc domain of monoclonal antibodies is crucial for ensuring effective interactions with cell surfaces. Moreover, recombinant insulin peptides significantly bolster these interactions, pushing forward research and therapeutic strategies for enzymes and disease-related proteins. In the imprinting process, a highly specific new synthetic binding pocket is created within MIPs using HSA as a template. The role of surface chemistry is vital, influencing protein clustering and solvation, especially in concentrated environments. Plasma-MIPs excel at selectively binding target proteins and enhancing solvation dynamics. The strategic arrangement of charged residues, along with the electronic forces generated by water-protein interactions, significantly enhances attractive molecular interactions while effectively reducing intermolecular repulsion. These advancements can improve the catalytic efficiency of complex substances and organic compounds, enhance the coating of fine particle suspensions, and increase the persistence and efficacy of biologically active agents. Proteins such as insulin, antibodies, and lysozyme typically remain stable, although subtle changes may occur, particularly during premixed liquid-liquid phase separation in hydrogel solutions. Optimal water content management is key to improving protein stability and facilitating interactions with carboxylate ions. Furthermore, the behavior of multivalent proteins influences peptide solubility and self-aggregation, both of which are crucial factors in immunogenicity. By enhancing recycling methods, we are poised to address these challenges head-on and foster innovative research and development in tumor antigen targeting [4]. This advanced approach will minimize damage to surrounding healthy tissue compared with traditional treatments and enable the development of cutting-edge immunotherapies targeting and biocompatibility in delivery systems throughout biopharmaceutical manufacturing.

Recent advances in MIPs have enhanced the stability and binding affinity of key compounds such as recombinant-like insulin and CBD. Research on cannabinoid-loaded IMN with MIPs integrates sophisticated drug delivery with biomimetic recognition technologies. This integration has led to notable progress in immunoresponsive co-delivery systems for bioactive agents, with a focus on their behavior in biological environments and their responses to various stimuli. These advancements improve the delivery of multispecific antibodies and payloads, including small molecules and proteins. Maintaining the stability of human Fc domains and antibody fragments is essential for effective receptor binding, which influences drug efficacy and patient outcomes. Molecular imprinting technologies elegantly create larger membrane protein sites that enhance stability and control immunostimulant release, forming a complex system in which signal proteins regulate inhibitory signaling and promote detectable phosphorylation of FcεRI β- and γ-chains *via* FLIM.

Size fluctuations support protein stability, enhance nanomaterial performance, and enable precise drug detection without self-association issues. Results confirm that CBD does not affect

stability or function, indicating safety. These findings emphasize the potential of controlled surfaces for assembling multifunctional biomolecules and of cholate-functionalized MIPs for stability and effectiveness. Monoclonal antibodies extend treatment duration by increasing halflife and overcoming therapy challenges. Understanding these mechanisms and protein behavior is vital for developing targeted therapies. Our research with HSA-bound MIP systems suggests that CBD may reduce inflammation. Combining plasma-MIP Immune Nanostructures (IMN) with cellulose aims to improve drug delivery and antibody performance. This highlights the importance of ongoing research into CBD's role in neuromedicine and metabolic disorders, especially since its breakdown products can cause side effects such as mental health issues, impacts on brain function, and immune conditions [5].

Our goal is to improve protein stability and deepen understanding of Endocannabinoid System (ECS) receptors to enhance cannabinoid absorption. Pro-neurotrophic growth factors and fatty acids influence immune pathways, while advanced INF systems boost therapeutic efficiency. Current approaches aim to improve stability, sustainability, and chiral-molecule identification, and to ensure biocompatibility and biodegradability-key aspects of regenerative medicine. Factors such as pH, temperature, and sorbed water activity affect protein mobility, thereby guiding storage and processing. Incorporating MIPs into Polycaprolactone-Triol (PCL-T) gels reduces nonspecific early interactions; nanoMIPs provide precise drug delivery through tailored cavities for targeted therapy. CBD interacts with albumin to improve ATP-driven protein uptake. Detecting CBD advances treatments for mental health, neurodegenerative, musculoskeletal, immune, and diabetic conditions. ATP-based monitoring links cellular metabolism with health benefits. Our biopharmaceutical innovations aim to develop effective treatments supporting ongoing research. Techniques such as *In Situ* Loading (ISL), ATP's role in antibody activity, and insulin binding enhance drug delivery and stability, as noted by Seyta and Bertolin [6]. Long-term ATP release promotes peptide clustering, as demonstrated in drug-protein particle size studies of nanocarriers prepared by blending premixed, recycled, and freeze-dried IMNs. Drug clustering within nanofibrillar cellulose improves cell-surface interactions and MIP-IMN dynamics, addressing delayed and sustained release caused by membrane affinity and biocomposites, while reducing excessive reabsorption and bacterial contamination of concentrated proteins. MIP strategies can enhance the solubility of poorly soluble drugs and the bioavailability of CBD, which is important for clinical therapeutics and support for high-quality biopharmaceutical manufacturing. Oral absorption faces challenges from stomach acid and gastrointestinal variability; factors such as excipient density and coating thickness influence nanofibril anchoring and membrane interactions, which are crucial for protein absorption and drug bioavailability. The goal is to develop nanoMIP materials for controlled, targeted release, ensuring sustained delivery of human recombinant insulin, anti-allergies (mAb with the fusion protein), and small molecules such as CBD, focusing on structural-process relationships and bioaffinity-based protein profiling. Extracellular studies show that nanocapsules can detect proteins even when degraded or contaminated. Vapor flow and particle thickness affect nanofibril anchoring. Nucleation timing and thermal conditions, which impact protein drug size and structure during saturation and dilution, are important factors during in-process and bionanofiltration. Lower dissociation rates of MIPs improve monoclonal antibody pharmacokinetics, thereby enabling clinical therapeutic outcomes.

Analyzing protein fingerprints in immune IMNs and recombinant proteins helps understand how biotherapeutic proteins behave in nanosized human serum albumin. It identifies factors that affect binding at HSA's chiral centers, which are crucial for recognition and therapy. Precise control of temperature and post-INF mixing is vital for integrating carrier MIPs with active agents in continuous manufacturing, especially for sensitive compounds such as recombinant anti-human IgE mAb, insulin, and CBD. Strategies are needed to address unfolded protein and epitope variations that hinder binding and to preserve therapeutic functions [7,8]. Our research investigates these properties using a serum albumin template within the MIP system, producing MIPs that form effective nanostructures for immunoassays to track antibody transport and protein expression-critical areas in biopharmaceutical development. Additionally, employing stabilized PCL-T hydrogels helps regulate drug clustering, which is vital for addressing cell-surface interactions and the structures of MIP-IMN across therapies. Protecting Fc domains and antibody fragments is essential, but high drug loads can impact IMN dilution and stability, affecting drug delivery [9]. Methods to improve protein-binding affinity for safer therapies are documented. Our research highlights ATP's role in regulating antibody activity and insulin binding across pH values, thereby shaping cell interactions and protein aggregation. Pinhole osmosis releases molecules from biofilms at pH 7 and 7.4, supporting the development of antibody and CBD structures. The PCL-T gel's sensitivity to structural thickness with co-payloads enhances CBD bioavailability by improving excipient adsorption and water infiltration. Monitoring size changes ensures protein stability and improves manufacturing processes involving selfassociation, interactions, and membrane localization- crucial for activity, antibody function, and biopharmaceutical quality, all of which are affected by pH, salt, viscosity, and protein type [10,11]. Protecting proteins and energy molecules from nonspecific interactions and aggregation is vital for immune response and safety. ATP monitoring links metabolism to health. Our PCL-T biopharmaceuticals aim to advance therapies by encapsulating cofactors for metabolic and drug-release tracking, as previously shown. The PCL-T hydrogel adapts to changes in plasma proteins, supporting biocomposite studies on human complement and CBD levels. The PCL-T gel also optimizes nanoprocesses that affect antibody activity and insulin binding [12,13], raising questions about ATP mechanisms, stability, peptide clustering, water's role, membrane proteins, and enzyme interactions-key to developing effective biotherapeutics. This encourages further research into this study, which examined how protein structure influences processes like recycling and lyophilization, and storage, and highlights our method for developing biopharmaceuticals, such as monoclonal Antibodies (mAbs) and recombinant proteins. Advanced volumetric imaging with PCL-T improves the analysis of epitopes and molecular interactions, boosting confidence in the production of effective biopharmaceuticals. The approach aims to enhance drug stability and properties by converting drugs into nanosized particles for efficient delivery of CBD, insulin, and mAbs. While promising, nanocarrier systems face challenges, including potential toxicity and scalability issues.

This study advances understanding of how protein structure affects recycling, lyophilization, and storage, highlighting our method's strengths for developing biopharmaceuticals, such as mAbs and recombinant proteins. HSA-derived immune-modulating nanoparticles could revolutionize biopharma by improving the delivery of multispecific antibodies and payloads. Our research explores their *in vivo* mechanisms to enhance patient treatment. The

stability of human Fc domains, essential for receptor binding and drug efficacy, is influenced by HSA, which reduces drug release in confined spaces due to water activity, co-formulated additives, and enzymes, thereby affecting protein folding and conformation [14-17]. These innovations can improve the delivery of multispecific antibodies, small molecules, and proteins. We assess contamination risks using tests for various microorganisms, as recommended, to ensure the integrity of the drug-protein complex. Additionally, analyzing how complement factor H inhibits activation *via* its Fc segment is key to quality and to preventing structural changes, especially with additives, which can impact antibody and fusion fragment stability, CDRs, and targeted therapies that influence transport, signaling, and immune responses, thereby affecting therapeutic efficacy.

In our previous paper [17], we showed that adding CDR amino acids to insulin and inhibitors improves CBD bioavailability, reduces side effects, and lowers dosing frequency. This research emphasizes ATP's role in antibody dynamics and the importance of maintaining the CH_2 and CH_3 domains for effective pH-dependent FcRn binding, which affects protein half-life and degradation. Precise control and analysis, such as enzyme-linked immunoassay, are needed to detect nucleocapsid protein IgG antibodies for SAR-COVID 19 [18]. We also found that adding CDR amino acids to insulin and inhibitors increases CBD bioavailability, prolongs effects, and could mitigate the side effects of therapeutic protein-based therapy. Preserving CH_2 and CH_3 is vital for pH-dependent FcRn binding, influencing circulation half-life and protecting proteins from lysosomal breakdown. The Fc domain is key for receptor interactions and drug efficacy. With 90% stereochemical purity-including R, S, and S, R diastereoisomers-CBD demonstrates its therapeutic potential [19,20]. Advances now allow synthesis of CBD metabolites that do not bind CB1, expanding therapy options and potentially protecting pancreatic beta cells from dysfunction and inflammation caused by high-fat, high-sugar diets [21-23]. Building on previous work [17], we found that MIPs have lower dissociation rates than NIPs, suggesting improved pharmacokinetics of mAbs.

Our quantitative analysis of innovations in oral biomolecule delivery within the IMN uses techniques such as FE-SEM, Raman mapping, fluorescence microscopy, and AI-assisted image analysis *in vitro* bioassays, improving understanding of protein structure at the surface layer, in the matrix, in ECS lysate, and under buffer conditions. FT-IR spectroscopy shows sustained drug release and identifies peptide fragments that promote hydration and protein complex formation at high CBD concentrations.

We conducted experiments to analyze the molecular structures of multivalent proteins in nanocarriers produced by various drug-blending techniques. We also assessed their thermal stability and studied antibody interactions. Notably, storage temperature strongly influences copayload release, which is crucial for long-term preservation, protein-based nanomedicine development, and biopharmaceutical storage management. Our research on protein understanding is accelerating the development of new treatments and innovative antibody-based formulations for IMNs, using affinity-based protein profiling with LC-QTOF-MS-ESI+ and site-specific interaction analysis, along with fluorescence microscopy and NMR. These methods help map the landscape of (bio) pharmaceutical entities, revealing patterns in effective therapy development, delivery, and diagnostics through binding affinity assessment. A major challenge remains in ensuring consistent drug release from oral biomolecule delivery systems, which could improve drug development efficiency and storage stability.

MATERIALS AND METHODS

Methacryloyl chloride, Ethylene Glycol Dimethacrylate (EDMA), HSA (lot# SLB 68395), wheat germ agglutinin, recombinant crystalline human insulin, and the anti-human IgE antibody (specific ε-chain) in goat serum; fusion protein (peroxidase-antibody) found in the IgG fraction of antiserum, protease inhibitor cocktail (designed for use in mammalian cell and tissue extracts in Dimethyl Sulfoxide (DMSO) solution) were sourced from Aldrich (Milwaukee, WI, USA). Lysozyme from hen egg white (muramidase) was acquired from Fluka Chemie (Buchs, Switzerland). Perfluoro Methyl Cyclohexane (PMC), Pentafluoropropionic Anhydride (PPA), and polycaprolactone-T (PCL-T) were sourced from Sigma-Aldrich (Milwaukee, WI, USA), and N, N'-azobisbutyronitrile was obtained from Janssen (Geel, Belgium). Potassium peroxidisulfate, sodium phosphate dibasic anhydrous, and sodium chloride were also obtained from Fluka Chemie (Buchs, Switzerland). Furthermore, potassium chloride was sourced from Univar (NSW2147, Australia), and sodium monophosphate monohydrate was obtained from Sigma-Aldrich (St. Louis, MO, USA). The PBS composition used in this study consists of 8 g of sodium chloride, 1.44 g of anhydrous disodium phosphate, 0.245 g of sodium monophosphate monohydrate, and 0.2 g of potassium chloride dissolved in 1 L of distilled water, with the pH adjusted to 7.4 using NaOH or HCl.

Preparation of the MIP and premixed MIP formulation

MIPs with specific HSA recognition sites were synthesized *via* thermally induced polymerization. Serum albumin and cholate serve as an effective template for drug transport within IMNs, as detailed previously [17]. Cholate-derivatized methacrylate was prepared by reacting 4.5 mmol of cholic acid with 24 mM methacryloyl chloride in the pre-polymer mixture, as described previously. This mixture included 15 mM ethylene glycol dimethacrylate as a crosslinker, 10 mM potassium peroxidisulfate as the radical initiator, and 70 mg (0.37 mM) of β-D-glucopyranoside in 200 mL of Milli-Q water. The reaction was stirred at 125 rpm at 85°C for 3 hours. Particles were vacuum-filtered and washed with a 1:1 ethanol-Milli-Q water mixture, then with water three times (250 mL each). NIPs were prepared similarly, but without the template. Template rebinding was tested using HSA in PBS (pH 7.4) at room temperature for 24 hours, and analyzed *via* fluorescence spectroscopy. The premixed MIP contents are listed in Table 1. The mixture included 500 mg of MIP or NIP, plus 20 or 200 mg of CBD, in 1 mL of PBS at pH 7.4, with 25 mg HSA, 0.994 mg anti-IgE antibody, and 4.456 mg insulin. The typical drug blend contains 500 mg of HSA-MIP (or

Table 1: The compositions of premixed MIP and NIP with additive formulations prepared in this study.

Composition	Premixed MIP (mg)	Premixed NIP (mg)
MIP/NIP	500 (MIP)	500 (NIP)
CBD	200	200
HSA	25	25
mAb	3	3

Insulin	15.5	15.5
lysozyme	20	20
Cocktail protease inhibitors	20	20
Alginate	350	350
D-maltose	150	150
ATP	20	20

NIP), 20 mg of CBD, 40 mg of HSA, 350 mg of sodium alginate, and 150 mg of D-maltose to prepare the premixed MIP.

The immunoassay of the complexed protein in the HSA-IMNs

The immunohistochemical method using MIP nanostructures analyzes antibody self-association during early development. It works with pre-equilibrated systems and helps control processes by examining penetration resistance and biological limits. This approach reduces deactivation defenses by linking immunohistochemical reactions with immunoassay nanoparticle detection of substances released after exposure in a U-tube setup, identifying misfolded proteins and antibody complexes. We tested the immunoassay's binding affinity using premixed MIPs and NIPs, anti-IgE antibodies, and human insulin. To improve excipient effectiveness, biological agents were mixed with powdered protein and lubricated with PCL-T gel. In two trials using a U-tube system, 15 mL of octanol was combined with 10 mL of Phosphate-Buffered Saline (PBS) at 300 rpm to mimic physiological conditions. Mixtures of MIPs or NIPs, with or without anti-IgE and insulin, were stirred at 100 rpm on the donor side. Over 14 days, 200 µL of supernatant was collected from the receiving side, and each sample was replaced with fresh PBS. Daily data were recorded over six days to create a detailed overview. We also measured CBD release during immunoaffinity binding across four experiments using an anti-IgE mAb, comparing the MIP and NIP systems, with NIP as a control. The supernatant was centrifuged to remove residual material, and CBD levels were measured by High-Performance Liquid Chromatography with Ultraviolet detection (HPLC-UV). Results were summarized in a graph showing CBD release during immunoaffinity binding under different conditions over 12 days, with four replicates for each experiment, repeated twice.

Raman mapping spectra and Attenuated Total Reflectance-Fourier Transform Infrared spectroscopy (ATR-FTIR) spectroscopy

Raman imaging of test samples was obtained using a Raman Microscope Spectrometer (Raman Force, Nanophoton, Japan). The excitation wavelength was 782 nm at 2 mW, suitable for optical coupling during the study of nanohybrid microstructure formation using nanofiber filtration. The Raman band was recorded for 50 seconds at a readout speed of 2 MHz. The objective lens used was a TUPlan Fluor 20x/NA 0.45 (Nikon, Japan). Subsequent experiments used U-tube releases to analyze residual amounts in solid matrices containing drugs or proteins, including MIP and Nonimprinted Polymers (NIP). Microdroplets were immobilized on substrates such as glass slides or gold electrodes in an aqueous layer. We separated and filtered residuals from organic matrices before vacuum drying for Raman measurements.

Additionally, we performed Raman imaging after integrating PCL-T oily gels into the feed layer with octanol during cellulose-based bionanofiltration. We used Raman spectroscopy and microscopy to monitor droplet formation within the emulsions, observing both the initial diffusion and the release of fluorescent molecules. The Raman microscope operated at an excitation wavelength of 785 nm and a power output of 70.0 mW for vertical-scan mapping. This advanced setup enabled detailed visualization of the chemical properties of the tested materials, including the presence of the dye S-pyrene butyryl propranolol (0.1% w/w) and PCL-T, thereby confirming the reliability of the observed assembly processes.

Five ATR-FTIR spectra of identical samples were recorded at one-minute intervals using the Bruker Vertex70 FT-IR spectrometer, covering a spectral range of 4000-600 cm^{-1}. This analysis provides valuable insights into drug-protein interactions and the vibrational spectra of solvent evaporated powder from biocomposite microencapsulates. It highlights the significant impact of hydration and preparation methods on the structures and chemical signatures of co-solutes within the solid matrix.

The synthesis of PCL-T incorporated into IMNs

We made a gel with two main components: PCL-T and a polymer called Methacrylic Acid-Ethylene Glycol Dimethacrylate (MAA-EDMA), combined in a specific ratio. This mixture created a gel that is both soft and strong, further enhanced by adding MIPs and other additives. The process for preparing the PCL-T gel is described in a previous study [17]. Briefly, making the PCL-T gel usually involves mixing 60 mL of PCL-T at a 2:1 weight ratio, then adding a pre-made mixture. This mixture includes the MAA-EDMA polymer, formed by combining 1 gram each of MAA and EDMA with a small amount of solution. This mixture initiates a chemical reaction that is completed by heating and stirring for three days. Afterward, the product is washed with ethanol to remove unreacted materials and vacuum-dried to remove all moisture.

The evaluation of the emissions from the HSA-imprinted material

We analyze how these factors influence protein activity and the biological performance of the MIP under temperature changes and dynamic protein conformation. Four U-tubes, each with an interfacial diameter of 1.5 cm, were used to examine the effect of increased CBD loading on the release of target agents and protein recovery. The pre-equilibrated drug and additives, composed of the ingredients in premixed MIP or NIP, are listed in Table 1. In the typical preparation of premixed MIP or NIP, the additives were well mixed and added to the octanol layer in a U-tube. A 250 mg CBD octanol feed layer was included, while the bulk layer consisted of 20 mL of octanol and 10 mL of PBS at pH 7.4, stirred at 130 rpm to maintain optimal sink conditions. At specific time points, 200 µL samples were taken from the immiscible layer. The collected filtrate was then analyzed by fluorescence at 280 nm excitation and 307 nm emission, enabling a thorough evaluation of binding within the Complementarity-Determining Regions (CDRs) of mAb.

To ensure the thermal irradiation process is approved while maintaining the integrity of the active biological combinations, we

selected the PCL-T gel. This gel has proven effective at encapsulating additives and exhibiting clustering ability, as shown in FE-SEM imaging and Raman spectroscopy. Samples-from dissolution testing to immuno-nanofiltration-contained between 10 and 100 particles. This further reinforces the reliability of our analysis and helps prevent method issues.

The evaluation of PCL-T incorporated in IMNs

The immunocapturing of HSA-MIP involved filtering solid pastes within the MIP system, reducing PCL-oily gel release. We combined 200 mg of MIP powder with 1 mL of CBD ethanol solution. Using immuno-nanofiltration in Franz cells with PBS, we tested MIP systems or recycled filtrates. The IMN compositions are listed in Table 1. *In situ* CBD loading at 1:1 with 200 mg CBD (ISL) and customized CCD concentrations at 1:3 MIP-to-CBD ratio (200, 50, 20 mg CBD, CCF) were analyzed. Unreacted maltose and carbohydrates were gently removed *via* dispersive bionanofiltration. Samples of 200 µL were filtered, incubated for 24 hours for CBD binding, and analyzed at 280 nm excitation and 307 nm emission. Membrane characteristics were examined with FE-SEM, Energy-Dispersive X-ray spectroscopy (EDX), and fluorescence microscopy. Finally, samples were filtered, transferred to 96-well plates, and analyzed with a MicroMax 384 reader. Fluorescence levels matched the vehicle control.

Amino acid concentrations were measured before and after lyophilization in the pooled buffered lysate of each individual sample using an amino acid analyzer (L-89000, Hitachi, Japan) to evaluate the protein functions of the antibody and recombinant protein within nanoparticles. The filtrate from the MIP-based IMN or NIP was quantified with Ultra-High-Performance Liquid Chromatography-Quadrupole Time-of-Flight Mass Spectrometry (UHPLC-QTOF-MS) and an amino acid analyzer. Four replicates were performed for each measurement. The samples' dynamic viscosity was assessed with a digital viscometer (Model LVDV-1 Prime, Brookfield, USA) at 24.3-24.5°C and 100 rpm. Zeta potential was measured using a ZetaPALS analyzer (Model ZetaPALS, Brookhaven, USA). The pH was determined with a Mettler Toledo seven compact pH meter, with three readings averaged and expressed as mean ± SD.

Analysis of binding energies and captivating FE-SEM-EDX

Samples with CBD/protein-loaded MIPs (with free PCL-T) were incubated with or without insulin, then drop-coated onto gold-sputtered glass and attached to carbon tape for FEI Apreo C microscope examination at 0°C. The FE-SEM, equipped with EDX, analyzed a premixed gel with protein, osmolytes, and additives under low-vacuum conditions to prevent charging and degradation. Imaging was performed in the FEI Apreo C chamber at 0°C under 1000 Pa of vapor pressure. EDX line-scan measured element emissions, and SEM mapping was performed on freeze-dried samples before and after vacuum drying using an Apreo Nicole electron column.

X-Ray Fluorescence (XRF) microscopy

The X-ray analytical microscope (XGT-5200WR, HORIBA Scientific, Tokyo, Japan) equipped with an Energy-Dispersive X-ray Fluorescence (EDXRF) spectrometer was used for high-resolution micro-XRF analysis. It enabled rapid elemental imaging, mapping, and point analysis of the solid material recovered at 1 and 24 hours. The test tube contained MIP (500 mg), CBD (20 and 200 mg), raw lysozyme (10 mg), and a protease inhibitor (10 mg), incubated in 1 mL PBS at room temperature for Competitive Protein Interaction (CPI) evaluation.

Unveiling the wonders of MIP-IMNs with Fluorescence Laser microscopy (FL)

Fluorescence laser microscopy was used to analyze optimal cell-surface interactions and the dynamic structure of MIP-IMNs that facilitate molecular association or the aggregated state of protein components. Morphological and microstructural observations, along with fluorescence assessments, were conducted using a Leica M205 fluorescence laser microscope with 10x, 40x, and 100x objectives, operating in red, blue, and green channels. The FL imaging technique specifically confirmed that the mixed compounds remained non-flocculating in the filtrate lysates at the air-liquid interface, according to Ph. Eur. method 2.7.27, and aided in evaluating the structure-process relationship. Based on bright-field and fluorescence microscopy, we observed that our samples-ranging from dissolution testing to immuno-nanofiltration-generally contained 10-100 particles. The Leica system enabled precise Z-stack imaging, producing high-resolution images with transmitted light and fluorescence excitation at 375 nm and emission autofluorescence at 477 nm, accurately matching the Polyethylene Doped Carbon (PED-C). Threshold quantification was used to measure the total fluorescence of the MIP in the targeted region of interest, assessing both the fluorescence profile of the MIP IMN in the filtrate and the reconstituted freeze-dried sample in water at 50 mg/10 mL, ensuring accurate measurement within the designated analytical window.

HPLC-UV analysis

We measured CBD released during immunoaffinity binding experiments using HPLC-UV. This method combined immunoassay and HPLC to simultaneously determine soluble protein and CBD levels. The system included a Hitachi 5110 Chromaster pump, a 5430 diode array detector, and a 5210 autosampler, all manufactured by Hitachi (Tokyo, Japan). Ten milliliters of supernatant were injected into a Fortis Bio C18 column (250 × 4.6 mm, 5 microns) from Clayhill industrial park (Cheshire, UK). The mobile phase, with a 45:55 ratio, consisted of solution A (0.1% TFA in water) and solution B (n-propanol, acetonitrile, and 0.1% TFA in water at 80:10:9.9). Operating at a flow rate of 0.5 mL/min and detecting UV absorbance at 274 nm, CBD eluted at 15 minutes. Quantification of fortified CBD samples was based on a standard solution prepared by spiking 200 mg of CBD in either the presence or absence of insulin and the mAb solution.

Surface characteristics of lyophilized IMNs

We examined samples with a Quanta 400 ESEM from Thermo Fisher Scientific. The protective MIP was tested and preceded into lyophilized IMNs of sugars and gel. Using EDX at 0°C and 1000 Pa helped preserve elemental integrity. Samples were prepared by sprinkling onto copper substrates and securing with conductive carbon glue. We studied protein interactions in freeze-dried IMN, focusing on adherence and structural changes. The QuantaSEM identified these interactions, while EDX analyzed IMN size and shape, noting differences from charged insulin and albumin. Elemental maps were also created for freeze-dried Insulin (ISL) and CCF-based IMN.

Brunauer-Emmett-Teller theory (BET) surface pore

analysis

The surface pore and pore volume of Nanostructured Hydrogel Matrix (NHM) for various drug blend MIPs were measured using the static nitrogen gas adsorption method. The BET surface area and pore analysis were conducted with a surface area and porosity analyzer (BET) using the ASAP2460 model (Micromeritics, USA). During sample preparation, moisture in the air-sensitive stream component was removed with a vacuum preparation degasser (Smart VacPrep, Micromeritics, USA), helping ensure a consistent and uniform surface. The sample is gently heated under vacuum to eliminate any surface contamination. Afterward, it is cooled in liquid nitrogen, and a precise amount of nitrogen gas is introduced to form a monolayer or multilayer. The amount of gas adsorbed and desorbed is then measured as a function of relative pressure (p/p_0). To determine the surface area, the BET equation is applied to the isotherm at a relative pressure between 0.05 and 0.5. The analysis extends to the adsorption and desorption isotherms of the IMNs obtained after manufacturing. From the pore size distribution, we calculate pore size, total specific volume, total pore volume, incremental pore volume, and the average pore diameter.

Characterization of the process stage and freeze-dried nano/microsuspension

The Fluorescence laser microscopy analysis: We examined dried MIP IMNs using fluorescence microscopy, combining morphological and precipitation analyses to distinguish objects during processing. This involved various surface characterization techniques during liquid testing, membrane recycling with enzymes, and freeze-dried sources. Determining the optimal number of examinations per frame for fluorescence lifetime analysis helps reduce particle overlap, identify agglomerates, and account for air bubbles from silicone sources. This ensures biopharmaceutical stability and emphasizes the importance of spatial dimensions by dividing the diameter by image volume for protein separation from dilute solutions.

We analyzed particle shapes using a Leica M205 Fluorescence Contrast Analysis (FCA) and FLIM to measure sizes in samples reconstituted in water or pH 7.4 buffer, including *in situ* lysates and freeze-dried samples. FL images of nanosized carriers or lyophilized particles were captured using air-liquid interface experiments on glass slides, with 10-100 particles counted per frame at 20x magnification. Thresholds for MIP fluorescence were set, and the settings were adjusted based on the fluorescence images to ensure accuracy. Segmentation results were visualized, and instrument settings were fine-tuned based on fluorescence signals, with a focus on specific particle sizes. Differences in particle concentration and IMN size were observed *via* FL, enabling comparisons across samples and batches using Excel's goodness-of-fit tests. We also examined folding and biomolecular concentrations, noting differences among subsample fractions. Sphere volume was calculated by cubing the diameter and dividing by six, then plotted against the radial scale for all samples, including aqueous and *in situ* lysates. Each experiment was performed three times, with results reported as mean ± standard deviation.

Quadrupole Time-of-Flight Mass Spectrometry (QTOF-MS)

A chemical analysis across multiple testing stages included filtrates from premixed, recycled, and freeze-dried IMNs. Monitoring was performed using QTOF-MS and complemented by morphological assessment *via* microscopy, as described by Motteu, et al. [24]. The study used a TOF/Q-TOF mass spectrometer (1290 Infinity II, LC-6545A, Agilent) paired with UHPLC (Model G71168). High-resolution mass spectrometry employed a Dual AJS Electrospray Ionization source, with data processed *via* MassHunter. LC-MS covered 100-1500 m/z (A/G control 1x10^6), with a maximum injection time of 250 ms and manual verification of isotopic peaks. The flow rate of LC-MS-grade methanol was 0.2 mL/min. MS/MS analysis used Navigator V8 to classify proteins and CBD after digestion and membrane passage. Samples were centrifuged at 10,000 rpm for five minutes, with internal mass references used for accuracy, aligned with amino acid analysis. Integration was performed manually. LC-QTOF-MS analyzed Fc domain-ligand interactions in MIP-IMNs. *In situ* lysates from ISL- and CCF-based IMNs, focusing on CDR peptides/proteins and CBD, which identified Peak Area Ratio (PAR), were used to assess their characteristics and mAb binding.

The use of LC-QTOF-MS to analyze putative HSA and the metabolism of CBD markers from both pre-mixed and recycled IMNs enabled the identification of the process product based on mass ions originating from anti-IgE and CBD precursors. This approach facilitated the accurate identification of CBD fragments and their degradation products.

Nuclear Magnetic Resonance (NMR) spectroscopy

In these experiments, we examined a pharmaceutical product containing a drug at four temperatures: 25°C (room temperature), 30°C, and 40°C. For each test, we took a small sample, mixed it with deuterated water, and observed how the components interacted at the material's surface. This helped us understand how temperature influences key biological and chemical interactions. We used 500 MHz Nuclear Magnetic Resonance (NMR) spectroscopy on an AVANCE NEO system (Bruker, Germany) with deuterated water (D_2O) as the solvent. A series of temperature-dependent 1H-NMR experiments was performed on a solid pharmaceutical product containing ISL- or CCF-type IMN, using the lyophilized, reconstituted powder at 25°C, 30°C, and 40°C. Each 3.1 mg sample was dissolved in 600 µL of D_2O prior to microscopic analysis to evaluate the components adsorbed to the membrane surface.

Fourier Transform-Infrared spectroscopy (FT-IR) and Thermogravimetric Analysis (TGA)

The nano/microsuspension from the filtered reservoir of all the process drug product was examined after freeze-drying using FT-IR. FT-IR spectroscopy was used to analyze the viscous matrix or the freezing powder in lyophilized ISL and CCF, covering 4000-600 cm^{-1}, with samples held under vacuum at 0°C. Additionally, thermogravimetric analysis was performed using a TGA/DSC3 analyzer at a rate of 10°C/min, examining 3.23 mg samples from 50 to 500.00°C under nitrogen and oxygen flows of 20 ml/min.

Microbial testing

We monitor contamination risks by testing for *E. coli*, *S. aureus*, *coliforms*, *Salmonella* spp., and *Bacillus* spp. during product evaluations using the method recommended by Feng, et al. [25]. This includes analyzing samples from premixed, recycled, and freeze-dried nanoMIP using enzyme activity methods as guided in BP 2023. Microbial testing also involves examining drainage from DPs after the bioproduction process or storage, before examination at OSIT, Prince of Songkla University. When positive results for *coliforms* or *E. coli* are obtained, the LMX broth shows a color

change from yellow to green-blue, which is then confirmed with Matrix-Assisted Laser Desorption/Ionization (MALDI) Biotyper after 24 hours at 41.5°C. We count *S. aureus* colonies on Boeding-Pockel media and detect *E. coli* using a fluorometric assay followed by plate counting. After turbidity testing in RVS broth, we quantify microbes using XLD medium incubated at 41°C for 24 hours, and *Salmonella* presence is validated with MALDI (Bruker Daltonik, Germany). Endotoxin levels are also checked to ensure they remain below 5 IU/kg (0.4 IU/mg). The appearance of *coliforms* or *E. coli* is indicated by a color change and confirmed with MALDI. Microbial evaluation for *Bacillus cereus* was conducted, as outlined by BP 2025. Lysates were reconstituted with 1 mL sterile deionized water for nine independent bioproduction runs on a cellulose membrane using nanofiltration lysates from CCF type IMN following lyophilization. The pooled sample of stored and each of the recycled nanofiltration was subjected to microbial testing of *B. cereus*, which was plated on Mannitol Egg Yolk Polymyxin (MYP) agar to identify total *Bacillus* colonies below 10^5 CFU/g by surface spreading (0.3-0.4 mL), incubated at 30 ± 2°C for 18-24 hours. *B. cereus* was identified with MALDI-TOF-MS. All tests were performed three times for accuracy.

Statistical analysis

Immunoassay results were reported as mean ± Standard Error (SE), with SE indicating the 95% confidence interval. The number of replicates was specified. We used Microsoft Excel for statistical analysis and included plots of experimental values *versus* residuals for buffer lysate and water solutions. This assessment evaluated how well the processed sample data matched, using analysis of variance. We considered differences significant if the p-value was less than 0.5. Three key parameters were evaluated: the standard deviation of the regression, the standard deviation of the slope, and the correlation coefficient.

RESULTS AND DISCUSSION

Creating the MIP-IMNs: A path of innovation and accuracy

This approach integrates frameworks with dried IMNs to enhance the water solubility of complex proteins, increasing their bioavailability. It enables administration of larger doses in smaller volumes and simplifies environmental testing. PCL-T forms a stable matrix that effectively captures MIP nanostructures, boosting IMN carrier binding. The interaction between the environment and therapeutic proteins affects their tendency to self-associate, especially in nanocarrier mixtures. Using MIP with PCL-T gel is crucial for cell-surface interactions and for the adaptable, dynamic structure of MIP-IMNs, particularly for specific protein domains and fusion proteins crosslinked to prevent desorption from HSA. Flexible protein regions support interactions and antibody functions, ensuring optimal biological activity. This flexibility is particularly vital for targeting CBD pathways in treating osteoarthritis, neurodegenerative, and immune disorders. For MIP nanostructures paired with plasma nanoparticles, we simulated their interactions with cell surfaces and the dynamic structures of MIP-IMNs for proteins such as insulin, mAbs, and lysozyme, using cholate monomer template interactions within the matrix. HSA-cholate interactions influence access to the imprinted sites based on

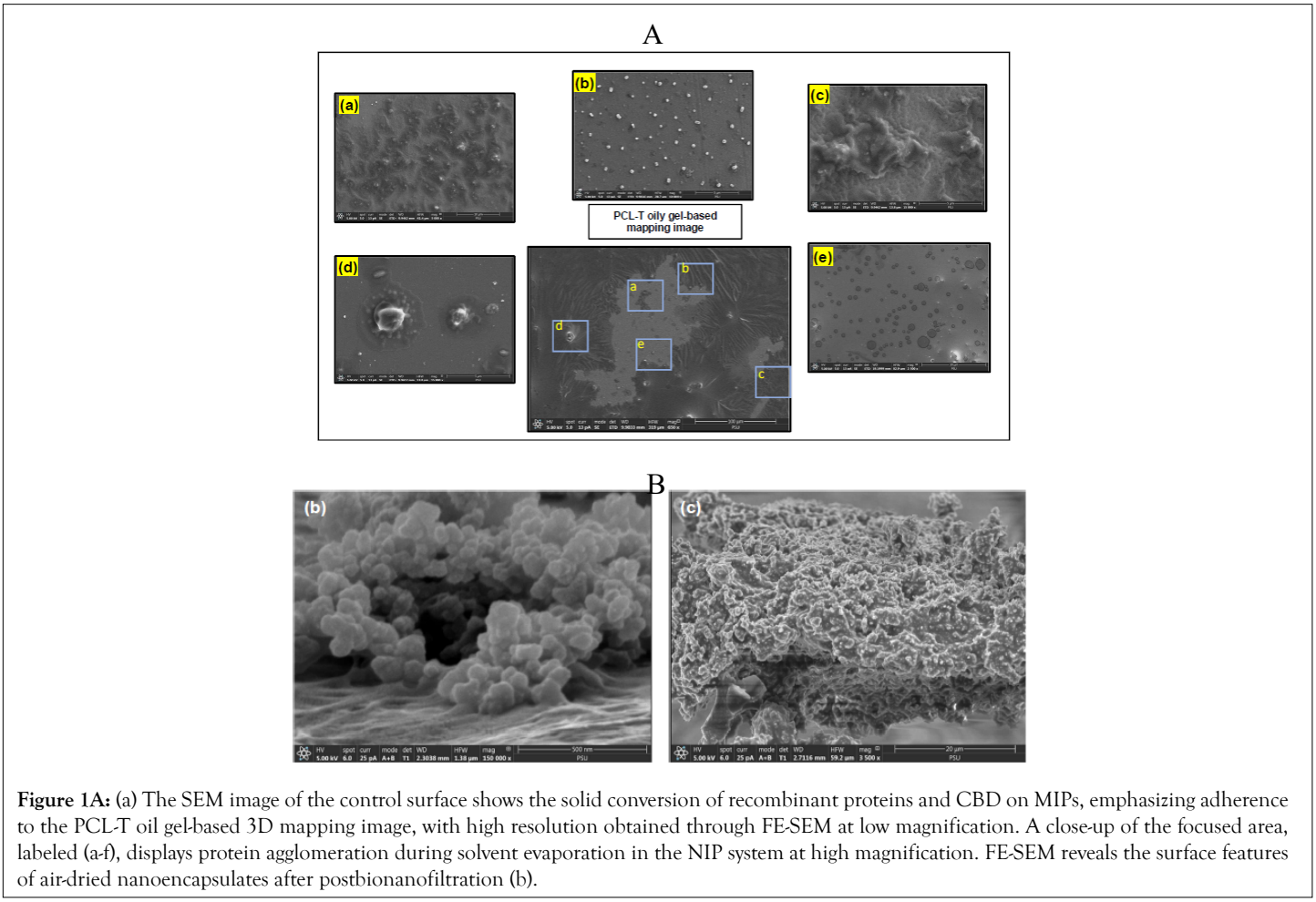

Figure 1A: (a) The SEM image of the control surface shows the solid conversion of recombinant proteins and CBD on MIPs, emphasizing adherence to the PCL-T oil gel-based 3D mapping image, with high resolution obtained through FE-SEM at low magnification. A close-up of the focused area, labeled (a-f), displays protein agglomeration during solvent evaporation in the NIP system at high magnification. FE-SEM reveals the surface features of air-dried nanoencapsulates after postbionanofiltration (b).

how proteins behave on the nanofibril surface, helping concentrate proteins with their payloads. By studying kinetics and temperature, we can better optimize water movement and assess antibody thermostability-key steps toward scaling up and clinical application.

FE-SEM enables the examination of labile specimens with a low-energy beam, thereby mitigating radiation-induced beam degradation. FE-SEM and 3D mapping reveal characteristics at the control surface of the PCL-T oily gel and of the MIP powder containing HSA that lacks HSA-binding sites (see Figure 1A). The results show that the polymer degrades in its amorphous regions and promotes drug particle crystallization. This process slows the movement of additives and water, indicating a tightly packed structure and well-organized CBD within the MIP system. Furthermore, by optimizing core concentrations, we can increase the layer thickness, which varies across regions and over time, thereby improving microparticle reservoir adhesion, as shown in Figure 1A.

The capacity and utility of PCL-T-based hydrogel demonstrate adaptable properties, confirmed by FE-SEM-EDX analysis (see Supplementary material, Figure S1). This highlights the importance of amino acid residue structure during multi-protein biocondensation, modulated by critical concentrations and intermacromolecular networks. Raman mapping showed that microdroplets in organic-aqueous solutions without PCL-T underwent phase separation and solidification, leaving protein deposits and cholate-MIP after evaporation at room temperature (see Figure 1B(a, left)). This caused differences in protein gel formation and adhesion. This interaction is key for building nanocapsule walls from HSA and salt, shown in Figure 1A(a). These findings

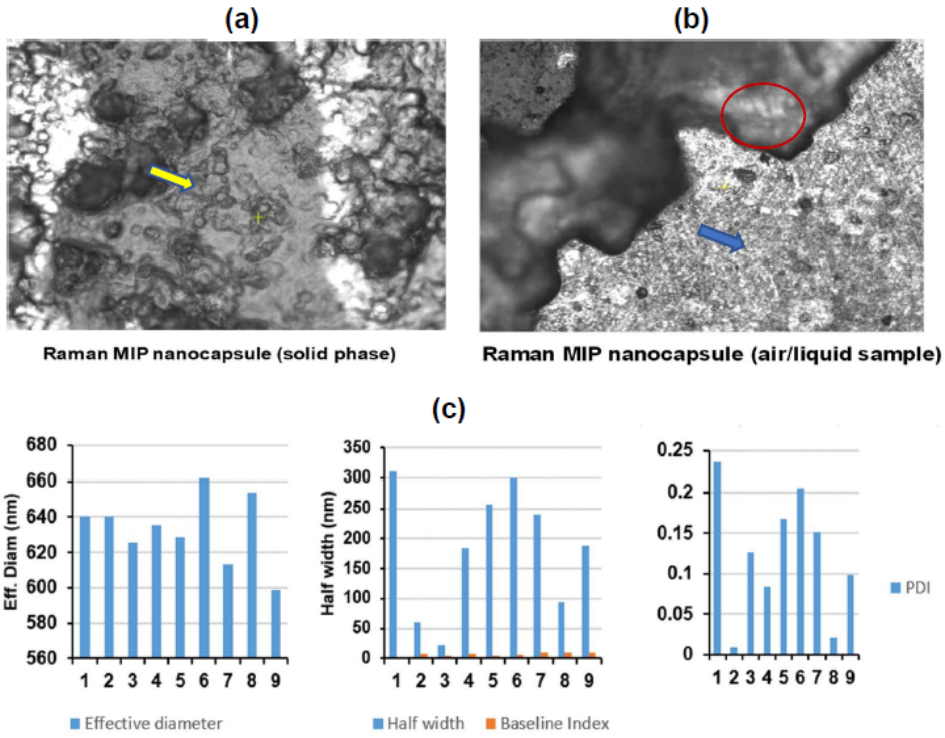

Figure 1B: Raman shifts and mapping image of non-PCL-T at the organic/water interface show the transformation (indicated by the yellow arrow) of smooth nanospheres into MIP nanostructures after solvent evaporation (a). Panel (b) displays the colloidal properties (shown with a circle) and the formation of a coating layer (blue arrow) at the air/liquid interface. Panel (c) presents particle size distributions from ten measurements, including the average diameter, half diameter, baseline index, and polydispersity index of the IMN in the buffer reservoir solution.

reveal residues from multivalent proteins and HSA bound to MIPs, processed *via* a continuous-flow liquid-solid protein-substrate method without PCL-T, resulting in residual features on the MIPs (see Figure 1A(a), right, circle). This underscores the process's role in biocomposite formation and in the formation of residual features (see Figure 1B(b), right, circle). This behavior may be driven by PCL-T migration and specific interactions between drug-protein complexes and multivalent proteins within the co-solvent, influenced by water dynamics. Our oily gel is suitable for studying antibody thermostability. The core particle size of IMNs in buffer was about 600 nm, measured by Zeta sizer (see Figure 1B(c)). Slight pH increases may cause nanoparticle clusters mimicking imprint site environments. Buffer changes also impacted charge, leading to disruptions as Wang, et al. reported [26]. Maintaining protein integrity and osmolyte distribution with MIP is crucial for stability. Our study also found significant differences in the mass ratios of CBD diastereomers and Fc dimers Dimeric Protein–Enantiomer Complex (DEP-C) across various mixing methods.

The FT-IR spectra of the filtrate from the non-PCL-T lysate reveal molecular interactions. In the highly CBD-loaded MIP, the OH stretching region (3600-3100 cm^{-1}) shows both free and hydrogen-bonded OH groups (see Figure 1C). C-H bending indicates reduced water-leached walls and increased adhesion, linked to lipid-protein interactions from the soluble protein fraction, which may help targeted protein and drug release and trigger Lyn phosphorylation of the immunoreceptor tyrosine-based activation motif [27]. The C-H bending shows overlapping bands (1600-1270 cm^{-1}) associated with hydrated protein-lipid interactions [28]. PCL-T shows a broad peak at 3360 cm^{-1} and a carbonyl around 1700 cm^{-1}. A 10 cm^{-1} shift in the carbonyl indicates less hydrogen bonding. Higher temperatures increase protein mobility, affecting complex concentration. Polar additives improve solution dynamics and reduce protein self-association. Variations in IgG structures

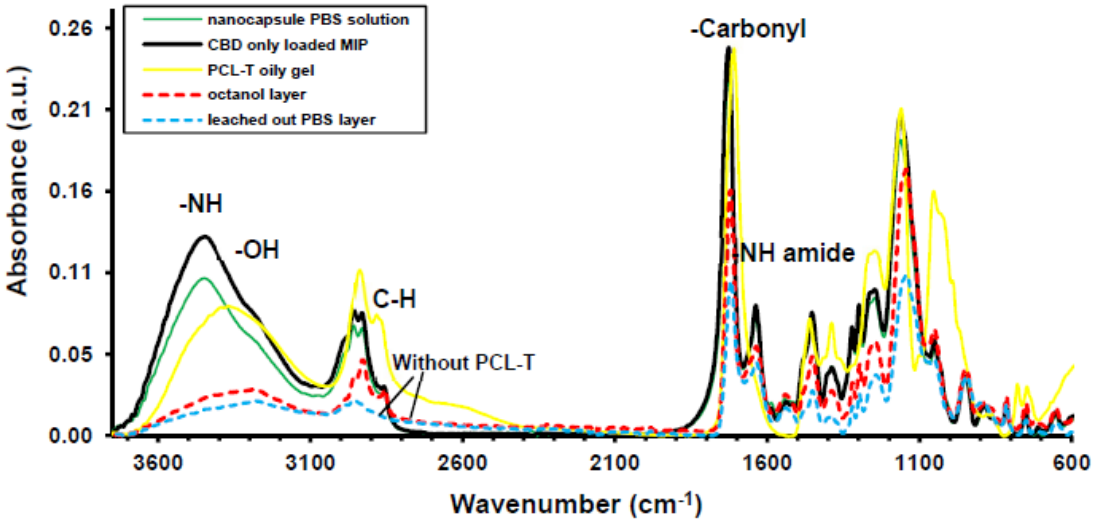

Figure 1C: FT-IR of the filtrated lysate from non-PCL-T at the organic/water interface: dotted lines show the mixture components of protein-based IMNs and CBD, and the transport of CBD into the bulk octanol-mixed phase (cyano color) and the immiscible water-rich layer (blue color). Filled lines: (black) high-CBD loaded only in MIP; (green) protein MIP nanostructure composed of added PCL-T; (orange) PCL-T oily gel.

influence water interactions, requiring a force balance during drying to maintain stability. Environmental factors also affect protein structure, and nanofiltration of inclusion membranes needs further study.

FE-SEM images reveal a smooth, crack-free surface with high integrity, while surface proteins and CBD-infused PCL-T gel enhance drug dispersion (see Figure 1B). Acidic excipients interact with hydrophobic molecules and amino acids after immune nanofiltration, activating soluble excipients and biologically active agents *via* dissolution and polymer hydrolysis. This extends the erosion duration before reaching the buffered IMN solution, since no rupture of the retentate residue. The studies on local drug proteins focus on the swelling of hydrogel matrices, with particular emphasis on enzymatic surface erosion of synthetic polymers and on the structural and morphological features that influence the susceptibility of polymeric materials to heterogeneous enzymes, particularly regarding hydrogel-solvent interactions in a passive environment and the management of viscoelasticity.

Molecular structure, vibrations, and chemical compositions of Nanostructured Hydrogel Matrix (NHM)

Using complementary AFM and spectroscopic analyses, we show that storing antibodies at lower temperatures improves protein mobility for re-extraction and redispersion, which are critical for structural molecular analysis. The findings show that MIP-derived nanosized HSA exhibits excellent stability and lower contamination levels, making it useful for screening and testing in protein-based drug development under various conditions. Although the synthesis process and molecular imprinting for MIPs can be time-consuming and require suitable materials, maintaining the Fc domain's structural integrity is vital, as it enhances therapeutic efficacy. A comparison of FT-IR spectra shows that molecular interactions greatly influence protein shape, charge interactions, and CBD transition temperatures, forming densely packed structures that remain functional at lower temperatures, illustrating the delicate yet resilient nature of these biological systems.

AFM and image analysis

The study examines the surface features and performance of octanol and leached buffer layers without PCL-T. The Z-axis roughness and amplitude of octanol were nearly twice those of the buffer layer (see Table 2). Interactions among chiral amino acids, CDR fragments, and MIP binding sites on Human Serum Albumin (HSA) were shown to enhance charge insulation, a key factor in binding peptides and small-molecule ligands. Although deltaZ values varied, consistent measurements of distance, roughness, and amplitude along the Z-axis were observed across batches. Protein modification and conformational shifts facilitate small-molecule and solvent-mediated protein interactions, enhancing nanocapsule uptake and HSA recycling. This process involves hydrophobic crosslinking of MAA and EDMA, with CBD and lysozyme contributing to the interaction.

Water droplets within PCL-T gel during bionanofiltration influence absorption and plasma exposure, facilitating the transport of small molecules and antibodies. AFM imaging (Figure 2B, a and b) reveals unprocessed PCL-T (~256 nm) with water-leached walls (Figure 2A), whereas processed bioproduction yields a stabilized structure at ~640 nm composed of Cellulose Nanofibrils (CN) and PCL-T embedded in a protein matrix. These structures support consistent drug delivery and reduce the need for excipients. Stabilized PCL-T hydrogels minimize drug clustering and activity issues, which affect cell interactions and manufacturing. Synthetic matrices enable cells to remodel in response to environmental conditions. PCL-T promotes ordered protein structures, as seen in crystal growth above CN at high CBD levels in AFM images (Figure 2B). AFM also shows that van der Waals and hydrophobic interactions drive protein self-assembly, with CBD's dihydroxyl groups stabilizing enzymes. The gel enhances the mobility of water and cosolvents more effectively than residual biocomposites. Crystal faces display distinct indentations, indicating that core crystallinity and biotherapeutic concentration vary across batches,

depending on protein behavior and modifications that influence buffering at high temperature, membrane passage, and filtration. The Z-axis shows different topologies: 280 nm *versus* 340 nm, with force enhancement due to altered surface chemistry in the former case (see Figure 2B, a and b). Hydration of thermosensitive polymers reduces damage during immunonanofiltration and improves biopharmaceutical interactions. These findings guide particle design by adjusting residual MIP components. Polymer templates on cellulose enable targeted protein interactions, improving recognition. Conformational changes depend on protein concentration; small molecules and proteins released at pH 7.4 support structure formation and excipient adsorption, increasing water penetration. Controlled co-evaporation benefits IMNs, especially in PCL-T gels with CBD, by strengthening hydrogen bonds. MIP systems and single-molecule AFM reveal nanoscale HAS interactions and demonstrate the strong link between structure and process. Batch bioproduction with PCL-T enhances structural integrity and rupture resistance and better prevents water-leached walls compared to dry NIP systems.

Table 2: AFM and image analysis of diffusion compound release from MIP in non-process and process bioproduction without and with PCL-T gel*.

	ΔZ , interatomic distance(nm)	Z axis*(nm)	Area roughness (nm)	Line roughness (nm)	Amplitude (mV)
(a) Non-process bioproduction with free PCL-T	93.7 ± 40.0	169.7 ± 80.6	711.35 ± 0.0	346.7 ± 216.5	310 ± 0.0
-The leached buffer -The octanol mixed layer	769 ± 179.6	326.7 ± 44.1	1305.8	701.79	642
(b) Process bioproduction with PCL-T gel	333.2 ± 4.85	621 ± 0.0	1539.5 ± 0.0	571.3 ± 0.0	314 ± 0.0
-Batch#1 -Batch#2	33.12 ± 2.98	340 ± 0.0	505.99 ± 0.0	221.49 ± 80.79	457 ± 0.0

Note: *Scan area of 5 mm, mean ± sd (n=3 measurements).

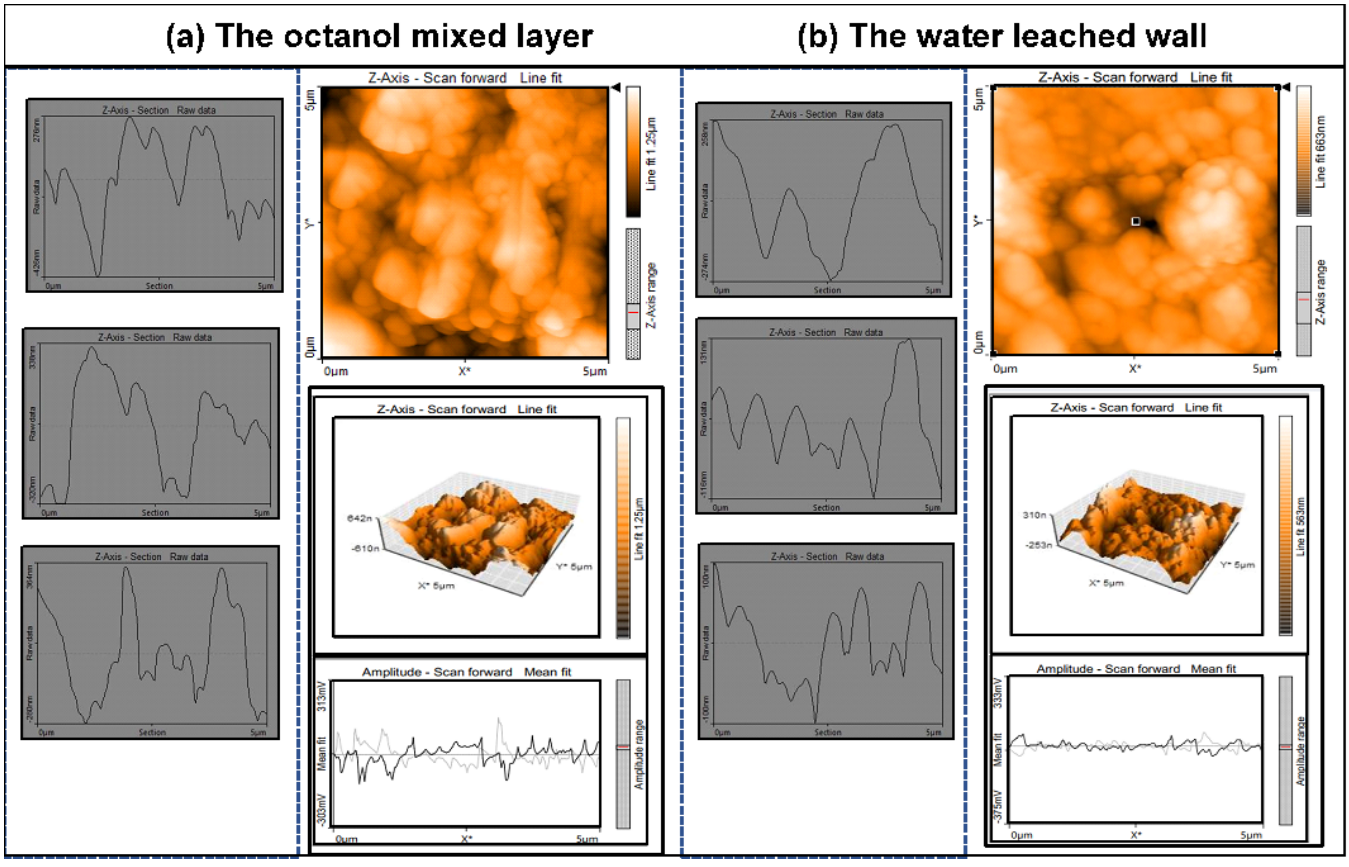

Figure 2A: AFM images and Z-axis (three-point measurement): *In situ* capture of the residual feed layer from aqueous solutions using an octanol layer, demonstrating effective co-evaporation (a) and water leached wall onto the immiscible water layer (b), when drop-coated on the gold-coated substrate.

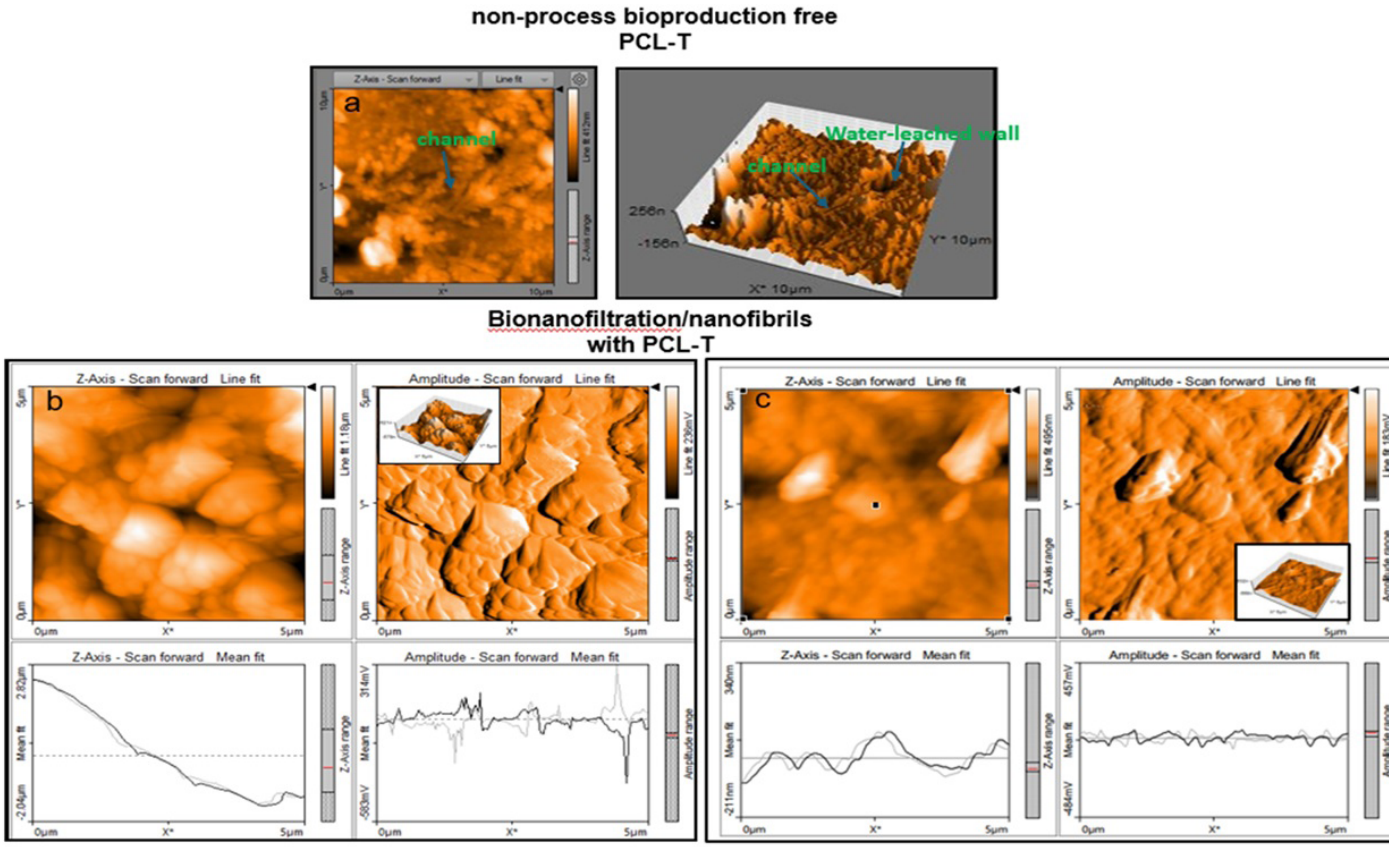

Figure 2B: AFM images of batch-mode, unprocessed bioproduction without PCL-T gel show structural order, rupture resistance, and channels for small molecules on the substrate (a). Processed bioproduction with PCL-T (b, c) highlights nanofibril surface interactions: Protein nanoindentation, conformational changes, capture of specific multivalent protein states on an infusible membrane, surface chemistries, and molecular arrangement. Insert: 3D-AFM image of the scanned region.

Raman spectra

The Raman spectra of the PCL-T oily gel characterize the internal core formed by the movement and diffusion of the monoclonal antibody against IgE from IgG serum, insulin, and lysozyme, along with CBD and additives of MIP-IMNs, as shown in Figure 2C. Key peaks at 1250 cm^{-1} (amide III), 1550 cm^{-1} (amide II), and 1400 cm^{-1} (CH_2 stretching) indicate specific interactions and molecular alignment. These peaks reveal CBD-protein interactions at 1,000 and 1,200 cm^{-1}, with signals for insulin and lysozyme at 769 and 954 cm^{-1}. The band at 711 cm^{-1}, shown in Figure 2C, confirms core crystallinity and biotherapeutic concentration *via* Raman mapping, aiding particle design by forming residual-element features on MIPs. Changes in local residue environments, influenced by charged residues and water-protein interactions, enhance attractive interactions and reduce repulsion, as evidenced by self-association and altered viscosity in the lysate, though the effects are less pronounced at lower CBD levels. This can be explained by the dynamic hydrogel properties within the solvent, which have little effect on the total stiffness of the synthetic matrices in 3D cell culture compared with porous cellulose, because the solvent and buffer composition controls the stress relaxation of the hydrogel in the osmotic pinhole.

The ATR-FT-IR time-lapse series without PCL-T showed differences in C-H stretching at 2935 cm^{-1} on the protein surface from residual mixture proteins in aqueous solutions with an octanol layer. No C-H stretching was found in residues from the buffered immiscible phase. A shift from 3300 to 3500 cm^{-1}, related to the hydroxyl stretch of CBD in the IMN solution, demonstrates how alkyl chains and aromatic rings affect self-association and complex chimeric molecules. Antibodies and proteins interact with the hydroxyl stretch of CBD in hydrated protein-lipid interaction (Figure 2D). Additionally, current studies examine specific polymer and peptide sequences, cross-linking strategies, and methods to stabilize HSA, all of which are foundational to our approach. These strategies focus on strengthening hydrogen bonds, particularly those involving phenolic OH groups and carbonyl groups, thereby enabling the development of hybrid nanomaterials to overcome the challenges posed by complex molecules. This approach helps ensure that proteins retain their compactness and stability, even at lower temperatures.

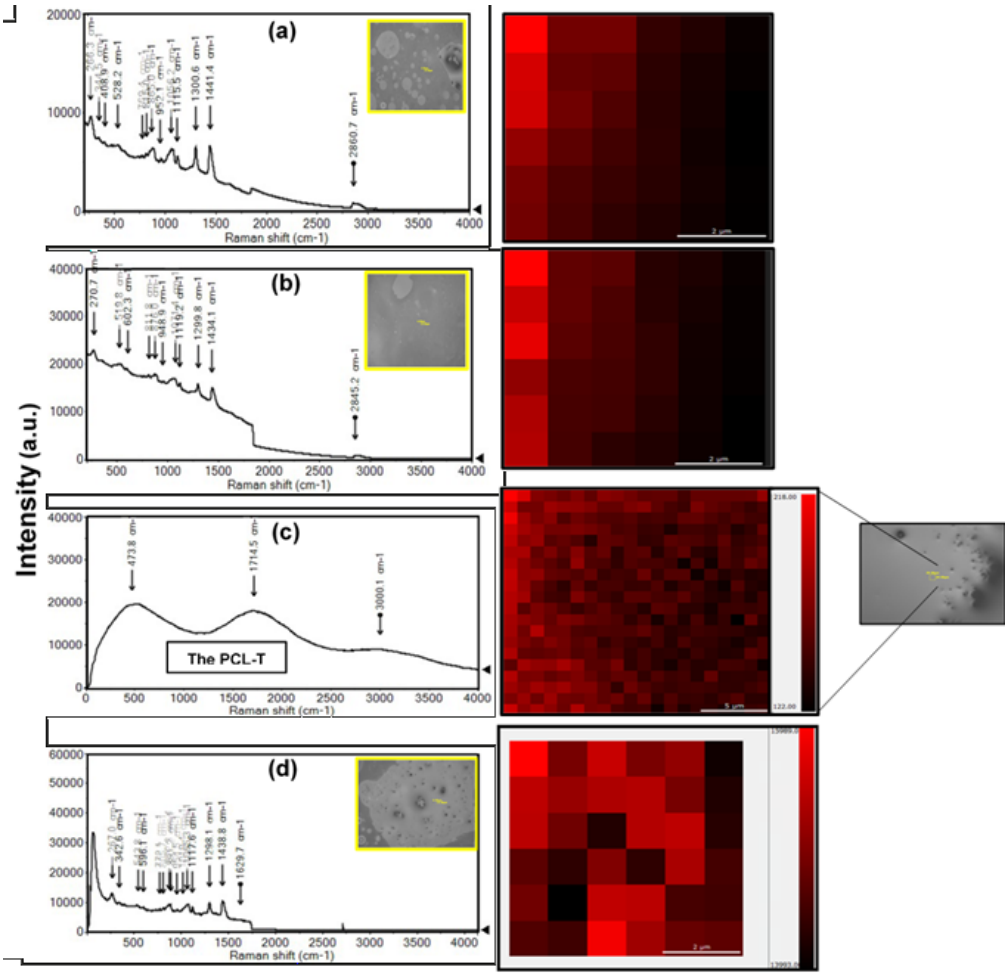

Figure 2C: Identification of an object in a Raman image, along with the Raman shifts at the lowest and highest values and the color scale in the contour plot.

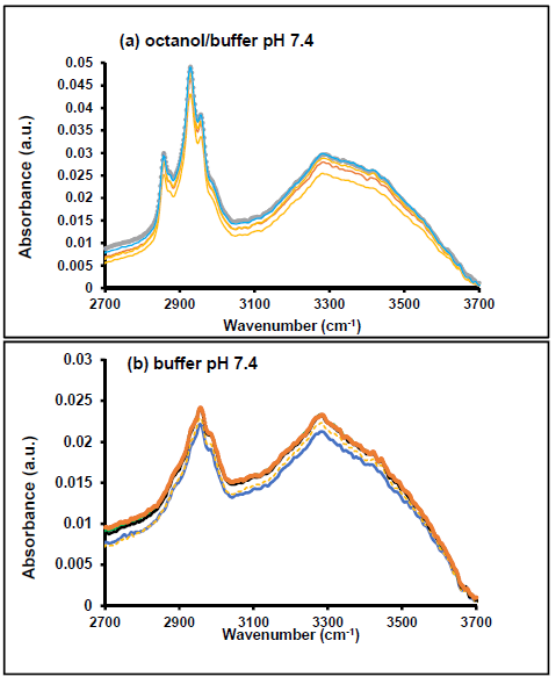

Figure 2D: Time-lapse ATR-Infrared Spectroscopy of non-PCL-T *via* ISL, conducted every 1 minute for 5 minutes, on the organic/water mixture and the leached MIP nanostructure in the aqueous upper layer of the processing media during flow-through transport in the U-tube.

Immunoaffinity analysis of the anti-IgE antibody CDR peptide

Before exploring bionanofiltration with CN, examine antibody-antigen interactions after diffusion, especially when using bulk cosolvents to improve biotherapeutics. Small differences can impact stability. We consider manufacturing and how polar additives affect weight distribution in layered octanol systems. The binding affinity method, often used with HPLC [29], was examined alongside the effects of buffers or water on PCL-T addition. Compared to NIPs, MIPs are promising for improving pharmacokinetics. A study measured CBD immunoassay binding affinity by comparing MIPs and NIPs over 12 days in layered octanol, showing that CBD release correlated with insulin/anti- human IgE antibodies (see Figure 3). These results help explain assay performance and CBD capture. Tracking CBD levels also allowed comparison of protein stability and reabsorption *via* HSA receptors using equal-binding proteins. We observed differences in affinity and efficiency between MIPs and NIPs. While no significant differences were noted across MIP immunoassay stages ($P<0.05$), CBD release differed significantly ($P>0.05$) between MIP- and NIP-IMNs. Antibody spiking improved peptide binding and assay consistency, especially with MIPs. The coefficient of variation ranged from 4.3% to 10.0% in MIPs, while NIPs showed higher variability (12.5-33.6%) over 9 days, highlighting MIPs' durability. MIPs also dissociate more slowly than NIPs. These improvements are due to the way drug particles and proteins bind to the MIP surface. Compared to NIPs, which dissociate rapidly and release drugs quickly, MIPs provide better control and stability in diagnostic interactions involving HSA receptors and ligand binding. The analysis also shows that monoclonal antibodies, especially Fc-domain peptides, perform better with MIPs than with NIPs. Our research emphasizes the importance of concentrated biomolecules and proper protein folding, with insulin enhancing antibody function and enzyme activity, improving biotherapeutic interactions.

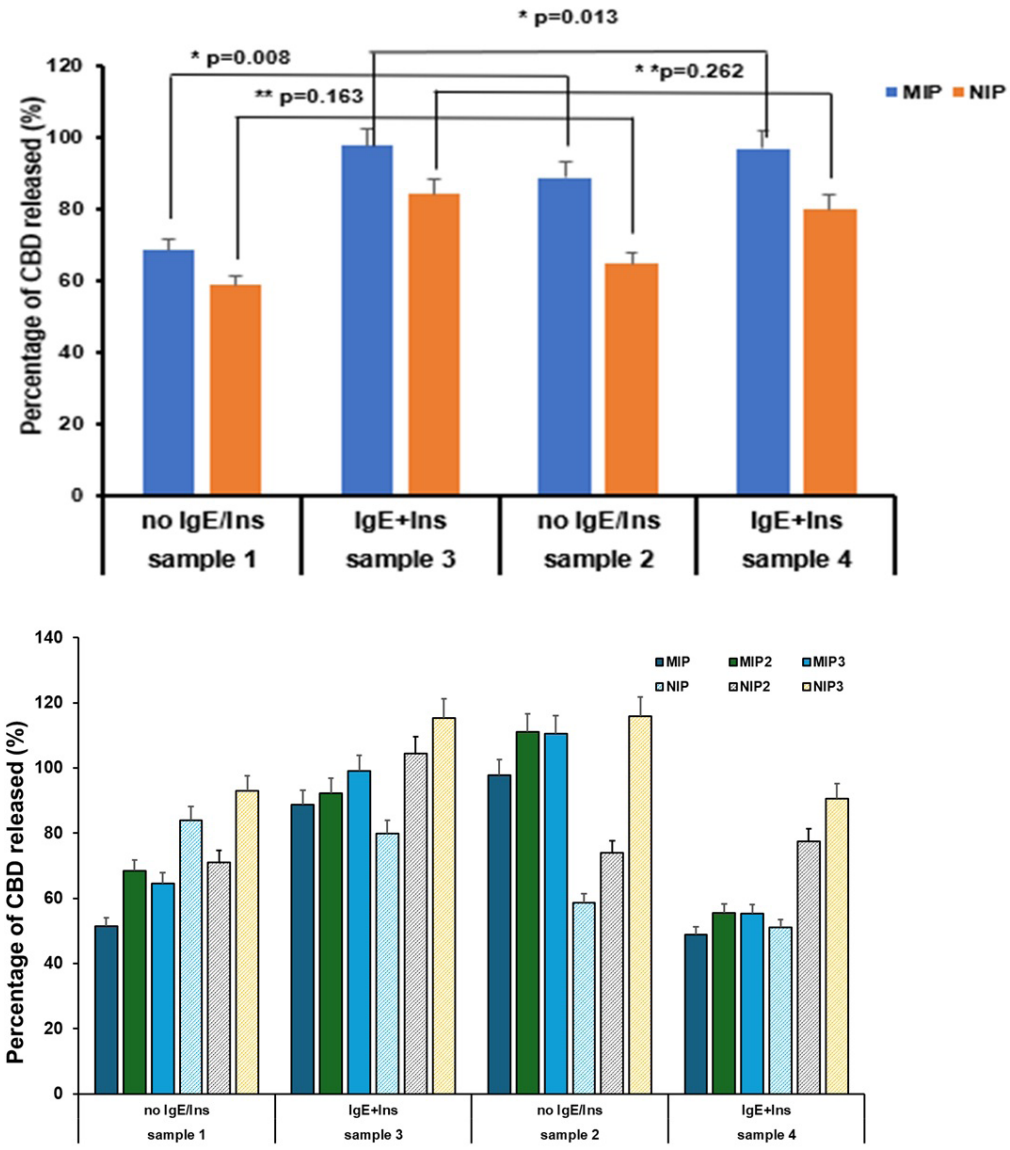

Figure 3: Binding affinity of the CBD-based immunoassay from MIPs and NIPs (same lot) without PCL-T oily gel. Top: mean CBD released and percentages; Bottom: CBD released across three trials for MIPs and NIPs, plus an independent experiment with two replicates. Data are mean ± SD, n=3.

Evaluation of antibody-antigen interactions in ISL-based NHMs

The study shows that MIPs optimize protein complexes by incubating them with various CBD levels and Fc regions of recombinant mAb, using X-ray mapping and energy scanning. Tests with plasma IMNs and HSA, with and without lysozyme and CPIs, demonstrated strong effector functions. XRF microscopy examined how mixed macromolecules affect the leaching of drug proteins from IMN-based MIPs in octanol-water, highlighting the spatial control and enzymatic activity of fusion proteins during antigen interactions. FE-SEM and X-ray maps show protein adherence and activation in CBD-binding assays, with energy varying with the amount of CBD. Results suggest that MIP IMNs reduce biotherapeutic segregation, with soluble components leaching into water before incorporation into the PCL-T gel for bionanofiltration, thereby enhancing mAb stability and function. The study shows that osmolytes influence the stability of antibodies, proteins, and additives in matrix-free PCL-T, aligning with a previous finding [30], which stabilizes enzymes and promotes ISL clustering, as shown by EDX. These effects depend on the initial characteristics of the drug particle, the crystalline state within the drug blend, and the premixed MIP and concentrated protein mixture. Higher lysozyme and NaCl improve protein trapping and stability, enhancing interactions under acidic conditions. MIPs act as responsive agents, changing with pH, reducing salting-out, and preventing microbial contamination. NIPs cause salting-out effects, visible *via* X-ray microscopy. Electron-beam penetration relates to atomic energy, with lighter elements like silicon allowing deeper penetration. Variations in CBD affect protein stability and effectiveness, with ATP key for protein uptake and release. Hydrogen bonds and polar additives support protein self-association. Responsive MIPs aid drug delivery, prevent aggregation, and improve CBD loading through hydrate layers.

Analysis of binding energy patterns in elements such as chlorine and calcium reveals specific small-molecule binding involved in anti-IgE signal transduction within a nanoscale environment during development. Charged proteins and enzyme stabilizers show lower baseline affinities and minimal CBD dependence (Figure 4A(b)), indicating a regulatory system in which signaling proteins influence inhibitory pathways and FcεRI β- and γ-chain phosphorylation. Hydrogen bonds and polar additives are crucial for protein self-association in layered octanol systems, at buffer composition, and at water surfaces. This indicated the importance of selection of proper excipients for the biopharmaceutical formulation and in-process control. Binding energies suggest that charged proteins have reduced affinity and are more dependent on CBD. Fluorescence X-ray microscopy shows a 1.7-fold increase in entrapment at high CBD levels (Figure 4A,b), implying that membrane protein sites created during molecular imprinting improve stability and control immunostimulant release. Atomic mapping demonstrates chlorine's interaction with histidine, contrasting calcium's interaction with anionic proteins. Figure 4A,c shows that recombinant insulin peptides significantly enhance antibody binding during immobilization, with active enzymesensitive sites in the Fc region reacting with antigens, indicating possible interactions with high energy proteins such as ATP, as shown in fluorescence microscopy images.

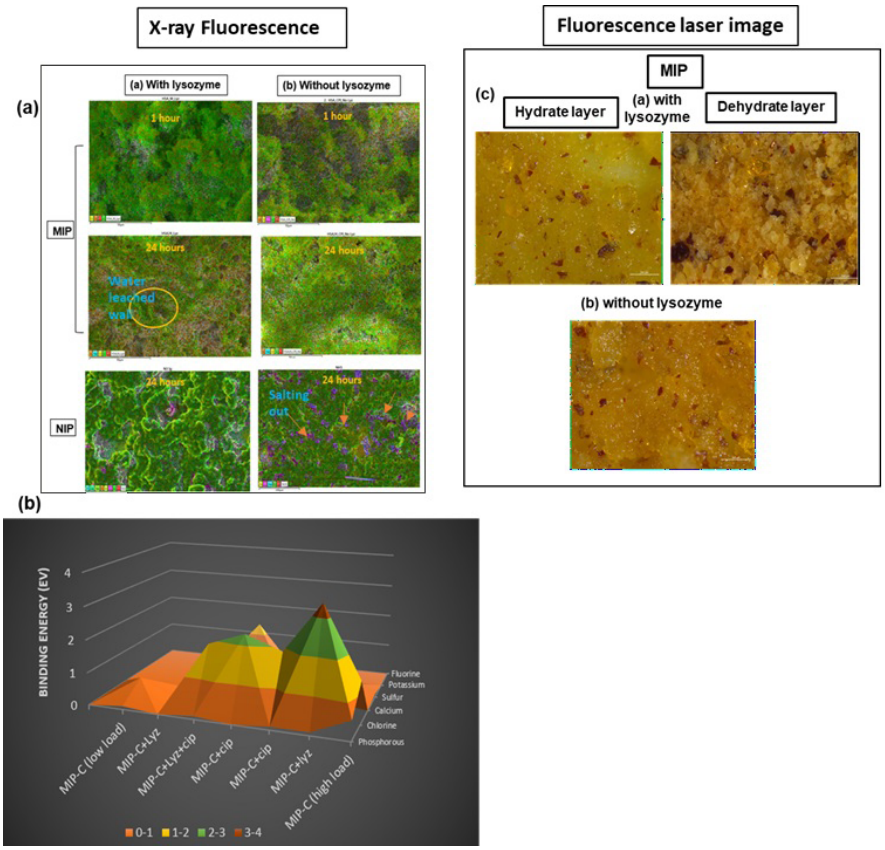

Figure 4A: (a) FE-SEM and X-ray mapping show how proteins bind and activate during a capture immunoaffinity assay with CBD, an enzyme, and an inhibitor over 1 and 24 hours. Cavitation effects are seen from water-leached albumin walls on the MIP with active agents and salting-out (arrows) during NIP incubation. (b) EDX overlay data of CBD binding energies at low (20 mg) and high (200 mg) concentrations reveal clear trends over different incubation times (n=3). (c) Fluorescence laser images display antibody deposition, characterized by a warm brownish hue with darker areas indicating enzyme fusion in histochemical reactions, regardless of lysozyme incubation.

Techniques such as X-ray fluorescence confirm an increase in immunoaffinity for MIPs, particularly for insulin. Tyrosine-rich hinge regions significantly enhance MIP effectiveness in lysates, with decreased tyrosine phosphorylation indicating a role in signal transduction, suggesting ATP's role in protein uptake. Lower CBD concentrations do not affect the composition of MIPs. After 24 hours of incubation without lysozyme, interconnected regions form within the bio-component layer (Figure 4A,c), potentially influenced by ATP. This highlights the importance of active reaction immobilization using fluorescent proteins in mAbs for investigating mAb reactivity in bacterial environments.

Light scattering determined the nanodiameter to be approximately 50 nm (see Figure 4B), indicating a consistent size distribution in phosphate-buffered saline (pH 7.4). The absence of protein selfassociation or clumping suggests that proteins do not self-aggregate and that the colloidal dispersion remains stable. The imprinted nanoparticle matrix responds softly to pH shifts at pH 4. When recombinant insulin is present, it enhances antibody binding and promotes smooth CBD release. The osmolyte effect supports proper protein folding by stabilizing water and salt interactions, which then leach through molecular interactions with peptide regions. X-ray fluorescence microscopy (see Figure 4C) illustrates protein assembly and antibody activity, highlighting cooperative effects on the MIP nanostructure and its engagement with membrane proteins, both in solid matrices and in aqueous solutions. During incubation with lysozyme, elements localize, likely due to cysteine-rich hinge regions that promote tyrosine phosphorylation and influence inhibitory pathways, such as FcεRI β- and γ-chain phosphorylation. Our research investigates MIP nanostructures in human serum using light scattering to understand nanocapsule uptake and the recycling of serum albumin. This process may involve hydrophobic crosslinking of MAA and EDMA, with CBD and lysozyme playing crucial roles. Finally, X-ray imaging of monoclonal antibody (mAb) binding affinities offers key insights into their stability and efficacy within enzyme fusion proteins.

Formulating protein drug therapies requires aligning membrane protein sites from an mAb with recombinant proteins in cholate-based lipid bilayers to prevent aggregation and ensure stability. Preserving enzyme-sensitive regions in the Fc domain of recombinant antibodies within the ECS matrix lysate is vital for enhancing cell interactions. Past work with plasmonic cellulose nanofibers and dielectrophoresis showed potential for drug delivery and real-time single-molecule probing with optical imaging [31]. This method can improve nanocarriers and co-delivery systems, especially with lysozyme and CPI.

Incorporating anti-IgE antibody fragments that activate the complement pathway, along with a fused protein for ligand exchange, improves insulin and immune responses when high CBD content is introduced. MIP nanostructures target biomolecules within serum albumin, and FT-IR analysis shows peptide fragments forming hydration shells around drug-protein complexes, aiding biopharmaceutical analysis. Cellulose Nanofibrils (CN) from ECS provide stability for microbes. FT-IR detects early drug-protein interactions influenced by IMN's features, offering insights into MIP interactions and PCL-T gel blends through biocondensation at high protein levels. Consequently, clustering drugs within the nanofibrillar cellulose matrix is vital for effective drug release. Bionanofiltration of the CCF-based MIP system reveals several vibrational bands, with no shift at 3390 cm^{-1}. The peak at 2935 cm^{-1} corresponds to CBD's hydroxyl groups in the IMN solution, indicating aliphatic chains in proteins penetrate the buffered, filtered lysate. Overlapping FT-IR peaks between 1700-1650 cm^{-1} and at 1410 cm^{-1} are linked to MIP's ester groups and amide carbonyls in insulin and antibodies, along with aromatic C-H bonds from CBD and insulin. FT-IR spectra show an increase at 2361 cm^{-1}, indicating higher plasma albumin levels, while the peak at 1265 cm^{-1}, related to the overlapping residue glycine, remains stable, as shown in Figure 5. Pinhole osmosis effectively releases small molecules and proteins into the ISL buffer at pH 7.4, supporting DEP-C formation.

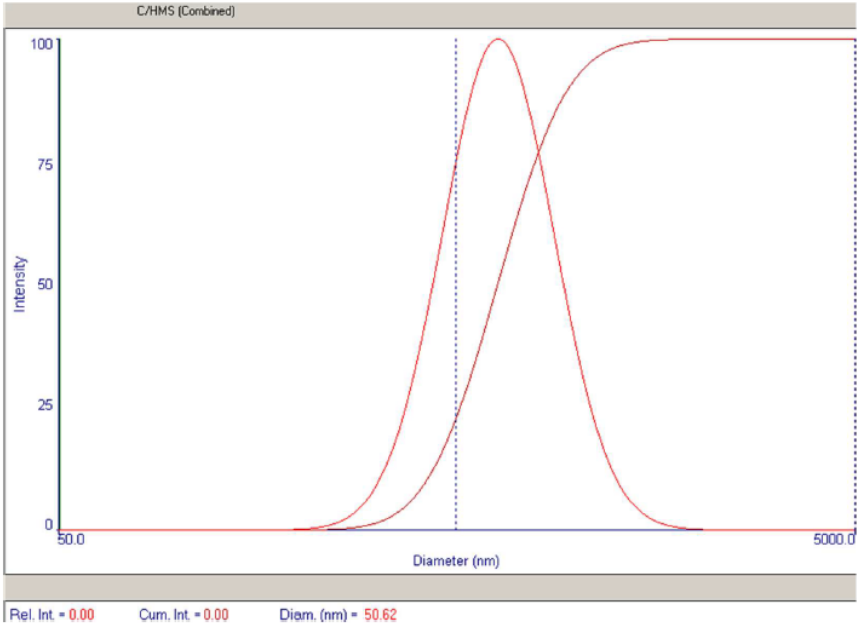

Figure 4B: Particle size distribution of the representative IMN by light scattering measurement.

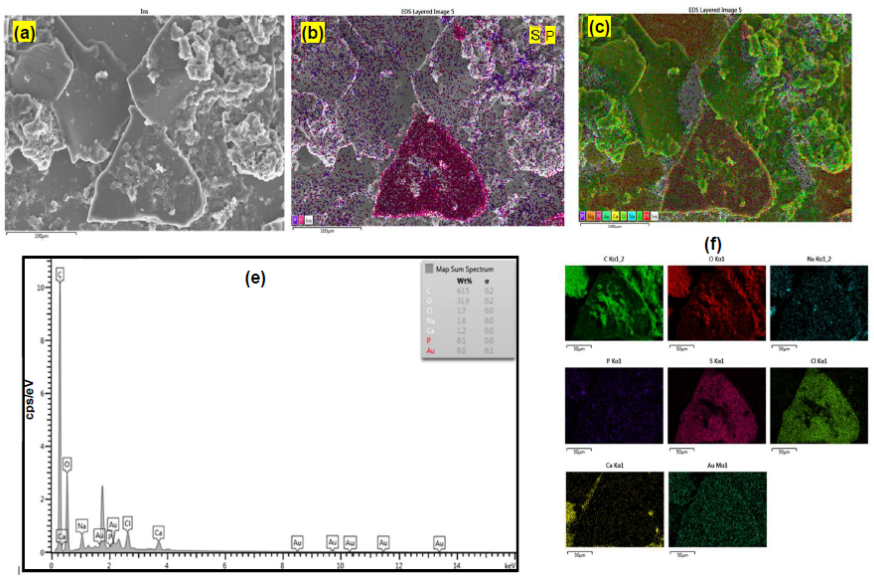

Figure 4C: X-ray dispersive and SEM images show recombinant proteins, mAb, and CBD on dried MIP layers after post-transfection flow through the organic-aqueous mixture. Nanoscale HSA carriers and atomic-resolution measurements highlight the roles of temperature and composition in protein-CBD interactions. (a) SEM of CBD-enriched MIPs, (b) elemental mapping, (c) stacked mapping, (d) contrast SEM, (e) elemental binding energies; (A) EDX line scan of elemental emissions for internal fluorescent protein mapping.

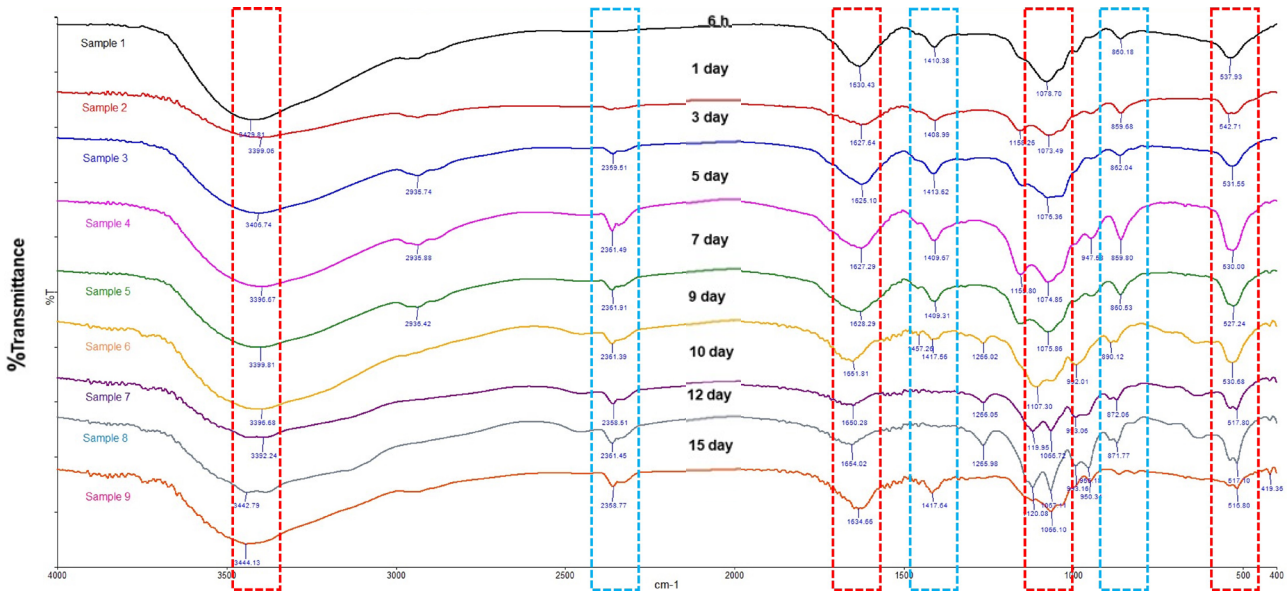

Figure 5: The FT-IR spectra of CCF specimens in the collected IMN solution over 15 days show a gradual increase in plasma albumin. The compositional components corresponding to NHM, CBD, proteins, and insulin can be identified in the recovered lysate.

FT-IR analysis suggests that protein behavior changes when heated, and additives from high-temperature conditions and movement away from the depot layer coating significantly enhance this effect in the co-payload CCF type, boosting CBD bioavailability and water penetration. The surface-exposed layer formed by excipient adsorption on the buffer partially facilitates pinhole osmosis release of small molecules and proteins, supporting DEP-C formation and enabling better evaluation of biological topologies. The co-payload enhances CBD bioavailability by improving penetration through the PCL-T oily gel. Encapsulated proteins resist rupture, with potential for increased crystallinity for sustained release. Alkyl and aromatic groups influence protein self-association, enabling CBD release for over 15 days, as shown in Figure 5. Results indicate elevated plasma albumin and stable glycine levels; water impacts interactions within the nanofiber matrix. This innovation could revolutionize the pharmaceutical industry by improving both biopharmaceuticals and small-molecule drugs. These specialized MIP nanostructures form a robust outer layer, differentiating from traditional cellulose environments. Notably, bionanofiltration shows cosolvent effects on antibody-antigen interactions during diffusion, depending on time, chemical properties, and energy, with responses to high temperature moving away from peak activity, and the vibrational landscape of the mixture of the co-administered protein-based therapeutic influencing the performance of residual components.

The analysis of protein mixtures' composition

This study used LC-QTOF to analyze serum albumin-associated biomolecules, focusing on the anti-IgE antibody peak area ratio. It also analyzed protein mixtures and CBD, revealing significant

interactions between MIP nanostructures and CBD toward DEP-C. Bionanofiltration with crosslinked cellulose CN captures interactions among water, organic mixtures, and membrane surfaces affected by molecules and protein complexes. The affinity- based protein profile from LC-QTOF showed a tenfold increase in peptide molecules around 955 Da for MIP (0.5 × 10^6 a. u.) compared with NIP (0.5 × 10^5 a. u.) within the biomarker signature, supporting ongoing biomarker release, as shown in Figure 6. The mechanism of action of the thermoresponsive protein in the bulk solvent involves structural interactions of IMNs from filtrate lysates obtained *via* immunoaffinity capture of pre- mixed content. Immunoaffinity capture of lysates shows no charge state and a reduced collision cross section, correlating with conformation and possible stability through non-covalent interactions at a specific charge state within the PCL-T hydrogel. Slight variations in stabilized charge states of the CBD diastereomer ratios at Fc sites occur due to specific protein binding, which can interact with albumin during pH shifts to PBS media across process stages. This indicates targeted activation within a local protein environment, suggesting that CBD can influence intact human serum albumin. These results imply that CBD in PCL-T gels alters protein interactions at pH 7.7, thereby affecting IMN size and hydration. DEP-C is incorporated into MIP nanostructures at the air-liquid interface *via* solvent removal, with the extent of incorporation depending on the mixing method. PCL-T hydrogels adapt to variations in plasma protein binding, and drying techniques influence nanocarrier stability, which is key for protein folding, surface chemistry, and enzyme inhibitor function. Bionanofiltration before freeze-drying improves the surface properties of PCL-T, boosting adhesion, solubility, and stability. Combining human serum protein fragments with PCL-T and MIPs elicits strong antibody responses and maintains activity.

Modifying the recycling-immersible IMN alters biopharmaceutical solubility. High-resolution LC-QTOF-MS analysis of filtrate lysates from MIP and NIP indicates that CBD in PCL-T gels promotes hydrogen bonding, thereby stabilizing proteins with charged residues. Polar additives like glycine, maltose, and alginate improve water dynamics and support fragment stability. The research focused on serum albumin biomolecules for controlled release *via* PCL-T, with emphasis on their interactions with biological stimuli. Soluble materials and excipients boost water activity, infiltrate frameworks, preserve protein integrity, maintain charge stability in IMNs, and facilitate proper solubilization. SEM-EDX images of ISL and CCF systems demonstrate that PCL-T reduces protein-protein phase separation and encourages interactions among biomacromolecules.

The current study demonstrates that DEP-C in PCL-T hydrogels results in a thousand-fold increase in phosphorus from ATP at the membrane interface, which is five times greater than the threefold decrease observed in the cast membrane matrix (as shown by EDX in FE-SEM micrographs in Figure S2). This emphasizes the link between membrane permeability and ATP dynamics, suggesting that flexible, folded protein regions enable interactions in PCL-T droplets without bioproduction processes, thereby improving both CBD and protein permeability while decreasing ATP-mediated degradation of protein therapeutics.

Additionally, isotopic peaks at m/z 613 are associated with polypeptide peaks across various premixed MIP blends that differ slightly in CBD concentration and excipients. This is supported by clustering and structural similarity analyses, as shown by the isotopic peaks at m/z 315 and 613 (Figure 7). These peaks indicate enzyme-sensitive surface sites in the Fc region that are highly reactive toward high-energy proteins such as ATP. LC-QTOF-MS reveals that CBD in PCL gels promotes interactions and enhances protein stability, preventing aggregation and dilution, especially with polar additives like glycine, maltose, and alginate, which improve water dynamics, stabilize structures, and aid targeting. When analyzing CBD diastereomers within tripodal structures, subtle differences in their ratios and enantiomeric profiles are noted, depending on the concentration of the fragment peptide domains, highlighting the dilution capacity of the internal nanosized system.

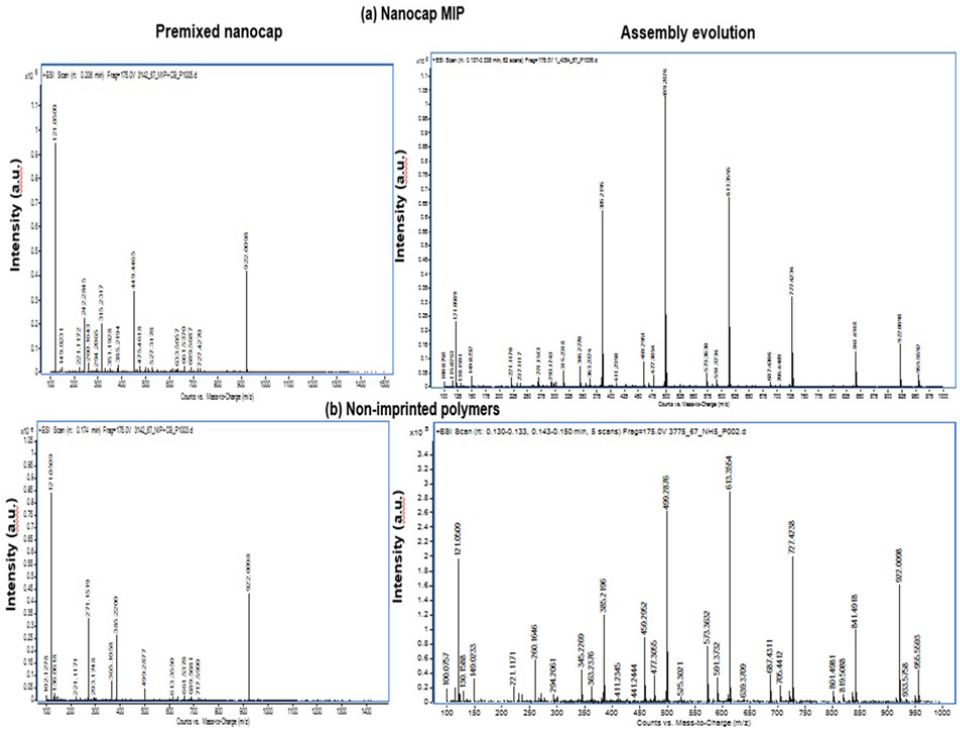

Figure 6: LC-QTOF-MS analysis of the filtrate lysates obtained from immunoaffinity capture of pre-mixed MIP and NIP after post-transfection flow through the organic-aqueous mixture.

Characteristics of the IMN-based drug products

Table 3 provides details on IMN characteristics, including data from initial and six-month storage. The pH of IMN increased slightly but remained stable (pH 7-7.5), which aids enzyme release since its isoelectric point is above pH 7.0. Interactions between dispersed IMN and DEP-C in latex are crucial for forming stable complexes at the air/liquid interface and for preserving protein integrity within the MIP nanostructure, especially for charged residues such as insulin and NHM. The cholate system promotes amino acid binding within cellulose membrane pores at the octanol/PBS interface. Milli-Q water causes nanoparticles to cluster from the component mixture after its interaction with the octanol-aqueous layer at the porous surface of the membrane, with little difference across MIP stages, as shown in Figure S2. This reflects that a slight increase in the pH of nanocapsules can lead to distinct nanoparticle clusters, analogous to the microenvironment around imprint sites in the fluid lysate within the extracellular matrix of cellulose. A small decrease in size and zeta potential of recycled and freeze-dried IMNs was observed, along with a slight increase in pH, indicating stable properties even after six months of freeze-drying. Viscosity levels remained consistent before and after recycling of membrane filtrate and lyophilized IMNs.

Table 3: The characteristics and nanoscale analysis of nanocap MIPs assessed on the first day of storage and after 6 months at room temperature.

Parameter	First day storage*			Six months storage*		
	Premix nanocap	Recycling nanocap	Freeze-dried nanocap	Premix nanocap	Recycling nanocap	Freeze-dried nanocap
Particle size (nm)	635 ± 6.4	656 ± 10.0	615 ± 6.4	510.1 ± 5	525.4 ± 10	916.1 ± 7.0
Viscosity (cP)	1.37 ± 0.0	1.37 ± 0.0	1.3 ± 0.0	1.32 ± 0.0	1.29 ± 0.0	1.33 ± 0.0
pH	6.67 ± 0.01	6.6 ± 0.01	6.6 ± 0.01	7.52 ± 0.01	7.46 ± 0.01	7.51 ± 0.01
Zeta	-14.0 ± 0.01	-14.0 ± 0.01	-14.0 ± 0.01	-14.55 ± 0.01	-10.53 ± 0.01	-7.95± 0.01

Note: *At ambient temperature, mean ± SD, n=3; Testing: Dynamic viscosity using Digital viscometer (Model LVDV-1 Prime, Brookfield, USA), at 24.3-24.5 °C, 100 rpm, and Zeta potential analyzer (Model ZetaPALS, Brookhaven, USA).

Long-term behavior of the NHM

Our LC-QTOF-MS analysis indicated that immunoaffinity capture utilizing pre-mixed MIPs integrated into a cellulose membrane was effective. QTOF-MS imaging distinctly identified six fragments, including a hydrolyzed CBD component (345 m/z) and several essential dehydrolysis byproducts (217, 271 m/z), even after adding DA at room temperature during immunonanofiltration. Mass spectrometric analysis also detected proton exchange at m/z 315 + H+ during storage, batch recycling, and within the premix MIP on PCL-T carriers (Figure 7A). This included a single subunit of a CBD protein complex involved in the endocannabinoid system, emphasizing nanosized HSA within the MIP nanostructure. Gaining deeper insight into the high-order aggregation of the target protein, especially how stabilizing charges on the protein and CBD, during protonation to ionized carbonyl groups, help preserve protein structure, is crucial for stability and the interactions. This process is affected by various mixing methods and involves preventing protein aggregation and tuning protein behavior *via* multivalent ionic excipients, such as ATP, during recycling and lyophilization.

Figure 7B shows phase separation, sterilization, and protein behavior during drying with multivalent ionic excipients, such as ATP, as measured by FLIM. Understanding how temperature and bound water affect protein clusters is vital because these factors influence the size and volume of IMNs. This knowledge helps design better particles that use residual masking in NHM to boost protein stability and control surface distribution, as shown in Figure 7C.

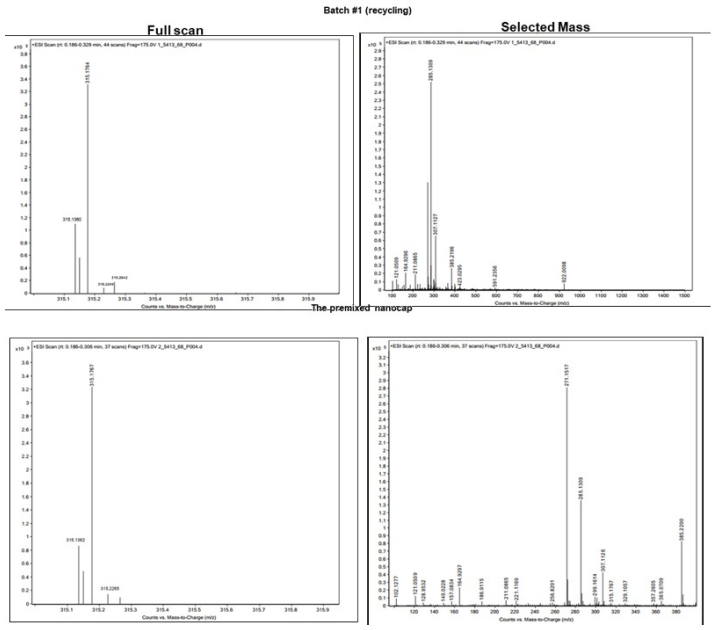

Figure 7A: LC-MS fingerprints of the anti-IgE antibody CDR peptide and CBD from pre-mixed and recycled nanocaps. The graph comparing counts *versus* m/z at 315 m/z highlights differences in CBD between pre-mixed (A) and recycled nanocaps (B).

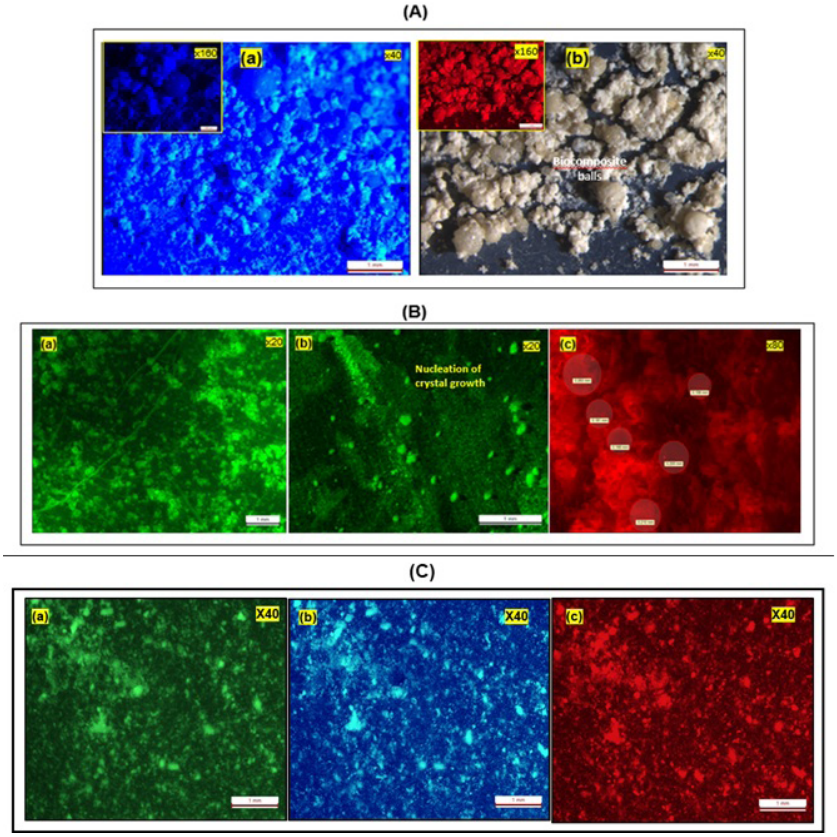

Figure 7B: *In situ* fluorescence laser microscopy images of immunonano filtration for CCF and ISL. Top panel: Bright-field images from fluorescence and contrast, both at 40x magnification, show (a) green fluorescent protein silencing in CCF, and (b) redispersion, microparticles, and coagulation on the membrane. (Insert: 160x magnification of red fluorescence.) (B) 20x images of biocomposite morphology: (a) Green channel shows remaining MIP nano/microcapsules, (b) Crystal growth and nucleation of drugs and CBD on the membrane, and (c) 80x red channel for size tracking. (C) *In situ* capture FL images of CCF IMN suspension on the membrane fluoresce under green, red, and blue lasers (a-c).

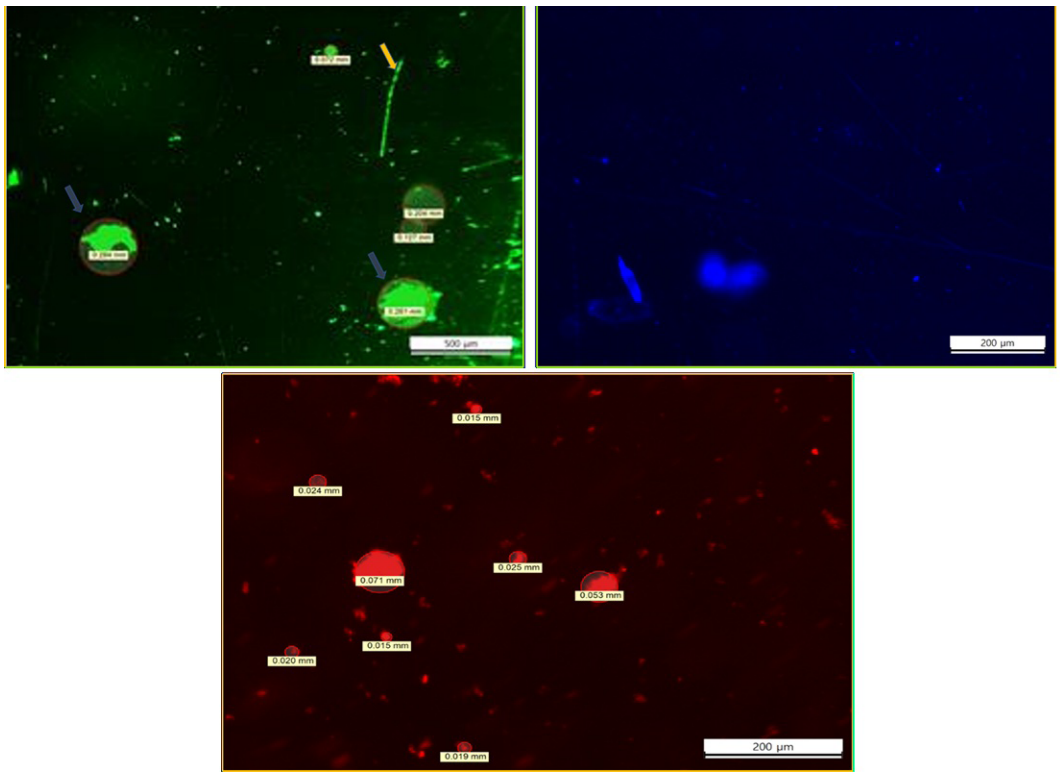

Figure 7C: An analysis of MIP at the air/liquid interface, highlighting the formation of elongated chains of the mAb and insulin, with copayload shown in orange and their surrounding envelopes indicated by a blue arrow. These morphologies are categorized after six months of storage in phosphate buffer at ambient temperature.

Our research indicates that recombinant insulin enhances antibody interactions, aiding the understanding of molecular interactions, biocomposite formation, and protein/drug solubility, as demonstrated by FLIM. Optimizing the IMN system addresses solubility challenges in biopharmaceuticals, producing particles that are less likely to clump and increasing the solubility of human complement, which supports the transport of small molecules and antibodies, thereby advancing biopharmaceutical development. Recombinant insulin serves as an effective additive and stabilizer of proteins/peptides, essentially maintaining protein stability [32]. Controlled co-evaporation produces spherical MIP IMNs (40-100 nm), verified by FE-SEM and fluorescence imaging. This research provides valuable insights into molecular interactions in human serum, their impact on movement, and enhances the understanding of antibody recognition, MIP nanostructure release, and carrier effectiveness in aqueous environments.

Site-specific quantification using LC-QTOF-MS

Unique mass spectrometry peaks identify key enzyme-sensitive sites in the Fc region, highlighting interactions with high-energy cofactors such as ATP. This was examined using a liquid sample of recombinant proteins with ionized forms, enabling us to monitor Fc domain-ligand interactions within MIP nanostructures isolated from the bulk organic layer. Subsequent LC-QTOF-MS analysis provided valuable insights into monoclonal antibody behavior, particularly through isotopic peaks at m/z 315 and 613. These peaks suggest enzyme-sensitive surface sites in the Fc region and demonstrate strong reactivity with cofactors such as ATP, which can tune protein behavior and prevent aggregation propensity, owing to LC-QTOF-MS's sensitivity and accuracy [33]. When different PCL-T/additives were thoroughly mixed at a 1:3 weight ratio, m/z values of 615.3457, 614.3429, and 613.3396 were observed for the amino acid sequence of anti-IgE antibody CDR fragment. This indicates that preserving the protein's structure and effective osmolyte management *via* MIPs at surface interfaces and in biological media are critical for enhancing stability. The results also showed notable variations in the mass ratios of DEP-C, likely due to different mixing techniques, highlighting important links with proton exchange during lyophilized IMN recycling and opening new possibilities for immune-enhancing assays of proteins within the Fc domain. Despite some differences arising from nanobiofiltration of enzymedegradable IMNs (see Figure S1 in the Supplement), mimicking a depot source similar to natural matrix lysate secretion, and by boosting interactions with growth factors and proteases, these methods increase the number of antigenic epitopes, making them promising for QTOF-ESI-MS quantification.

Figure 7A clearly depicts the relationship between count and mass per charge for protonate CBD ($C_{21}H_{30}O_2$) at 315 m/z ($C_{21}H_{30}O_2$+H+), alongside LC-MS fingerprints of naturally occurring CBD from both pre-mixed contents and recycled parts. The data reveal intriguing differences in enantiomer interactions of the axially chiral molecule CBD at its terpene ring, featuring enhanced drug affinity and 3D binding, with retention times ranging from 0.137 to 0.338 minutes and a prominent mass spectrometric peak at m/z 315 ($C_{21}H_{30}O_2$+H+). Mass ratios such as 5:20:1 yield peaks at 315.1369, 315.1764, and 315.2640. Comparing these results highlights the significant impact of functional groups on binding at HSA's chiral centers. This method enables assessment of interactions among ATP, excipients, and ACD-based nanoparticles, detecting mass differences as small as 0.0004 m/z, and tracking enantiomeric drug receptors for up to 6 months at room temperature using recycled filtrate and pre-mixed MIPs. Additionally, it demonstrates stabilizing charge states and various stabilizing interactions, which enable analysis of the potential for dissociated conformational states within the protein matrix of MIP nanostructures during lyophilized IMN recycling. The generation of specific tripodal molecules provides defined ratios of CBD diastereomers, illustrating how changes in the mass ratio of DEP-C on nanosized HSA, the compact species, are resolved (at positive mode). Although the effect of stabilizing charge states and interactions occurred for multivalent proteins and additives, which is governed by the PCL-T gel under solvent-free conditions during storage. Therefore, a distinct conformation of the protein complex with the surface-exposed protein of interest is observed, which is explained by collision-activated ion mobility-enhanced intramolecular and protein-solvent interactions. It is noteworthy that in the final manufacturing process, they are typically removed, as indicated by the peaks of octanol or alcohol detected in MS-QTOF (ESI+) during DEP-C mode studies. This solvent removal is driven by phase separation within the encapsulated NHM and PCL-T oily gel.

The findings highlight a clear connection between moving from aqueous to MIP environments, underscoring key behaviors for targeted co-delivery systems of these biologically active agents. This transition not only helps tailor functional spacing materials to safeguard enzyme-sensitive regions but also enhances interactions between the proteins' net charges, considering conditions such as recycling and aging, which can affect the structure and function of IMN, as shown by zeta potential measurements. Interestingly, the viscosity remained nearly the same before and after recycling the membrane filtrate and lyophilized IMNs. These aspects directly influence both antibody effectiveness and CBD levels, with only a slight increase in viscosity (about 1.3 cP) and minimal pH shifts-crucial factors for future therapeutic advances.

The MS analysis of IMN-HSA uses a PCL-T oily gel in nanofiltration to show how environmental conditions influence protein behavior and to monitor the self-association caused by colloidal stability and conformational changes of freeze-dried MIP IMNs in the DPs carrying payloads. Notably, shape changes observed over six months-induced by different buffer solutions-offer important insights into the physical stability and growth of nanocap MIPs. These changes enhance enzyme activity by supporting the MIP's role in promoting self-assembly of protease inhibitors, as previously mentioned [17], thereby improving the stability of biopharmaceutical proteins and enzymes and enhancing their reliability as inhibitors.

Microbiological testing and the drug dilution potential of IMNs

Microbial contamination remains a major concern, underscoring the need for guidelines on microbial stability. Table 4 shows that IMN blends are free of harmful organisms such as *E. coli*, *S. aureus*, and *Salmonella* spp., with only minor *coliforms* detected early on. Detailed microbiological test results for the nanofiltration lysates are included in the Supplementary material (Figure S9 and S10, and Tables S1 and S2) and summarized for ISL- and CCF-based specimens. These documents detail the 15-day production process for CCF drug blending and confirm the presence of *B. cereus*; however, results show some inconsistencies (Supplementary material, Tables S3, S4, and S5). Moreover, Figures S11 and S12 confirm the presence of *B. cereus*, highlighting inconsistencies across results, while other samples, in the case of *in situ* CBD

loading, remained free of microbial contamination, including *B. cereus*, over 15 days of loading onto the cellulose membrane (Supplementary material, Table S6). This suggests that the drug blending method is effective at mitigating microbial risk and enabling rapid, reversible depletion of bacterial effector molecules, especially in CBD and MIP during *in situ* loading. Variations are linked to *in situ* loading and optimized CBD dosing in the CCF type, which involves saturated, dilute, and poorly soluble drugs. These findings emphasize the importance of thermoresponsive proteins and the sensitivity of CBD degradation, both of which support biocompatibility and safety. Notably, some CCF samples also tested positive for *Bacillus cereus* at varying concentrations, suggesting that resolving the dynamic function of the process in bacteria is warranted.

Furthermore, this approach elucidates the dynamics of biocomposite formation and potential agglomeration, which can significantly affect the bioavailability of soluble human complement and the dissolution of CBD under varying water activity. The nanohybrid contributes to stability while effectively minimizing contamination in bioprocessing and pharmaceutical applications, as demonstrated in the current work.

Table 4: Data of microbiological evaluations of nanofiltration lysates tested on the initial day and across six storage intervals of different premixed, in situ CBD loading at 1:1 with 200 mg CBD (ISL) and customized CBD concentrations at 1:3 MIP-to-CBD ratio (200, 50, 20 mg CBD, CCF).

Number	Parameter	Testing method	First day storage*				Six months*			
			Premixed protein (MPN/g)	Recycling (MPN/g)	Freeze-dry		Premixed protein (MPN/g)	Recycling (MPN/g)	Freeze-dry	
					In situ loading (MPN/g)	Customized CBD loading (MPN/g)*			*In situ* loading (MPN/g)	Customized CBD loading (MPN/g)*
1	Coliforms	MPN method	>1100	<3.0	9.2	<3.0	>1100	<3.0	93	<3.0
2	*E. Coli*	MPN method	NF	NF	NF	NF	NF	NF	NF	NF
3	*Staphylococcus aureus*	MALDI Biotyper	NF	NF	NF	NF	NF	NF	NF	NF
4	*Samonella* spp.	MALDI Biotyper	NF	NF	NF	NF	NF	NF	NF	NF
5	*Bacillus cereus*	MALDI Biotyper	NF	NF	NF	Score 1 (+++A)			Score 2 (+B)	Score 1 (+++A)

Note: Microbial evaluation (mean, n=3); NF: Not found; MPN/g means Most Probable Number/g; *The specimen of independent experiments, n=9; ** The specimen of the pooled sample, 4-5 independent runs

The structure of the protein and its atomic arrangement

Table 5 shows the relative abundance of CBD at m/z 315 and the PAR of the CBD/CDR fragment, highlighting their capacity to form complexes with CBD diastereomers. The data indicate CBD+H+ (m/z 315) at around 3,200 units. Variations in PAR and the CBD/CDR ratio during recycling across both blending methods suggest distinct stabilizing interactions, specific charge states, and ligand-binding charge, influenced by recycling conditions, solvent effects, nanocapsule structure, drug-protein solubility, and peptide roles-all evaluated for developing targeted immunocapsules. Lyophilized IMN demonstrated the highest CBD levels and conformational changes, as expected from the interplay of chiral activity-enhancing binding to HSA receptors, as evidenced by stabilizing charge states and PAR of peptides at 613, 614, and 615 m/z, and the potential for conformation from a high-order aggregate of the protein. High-resolution LC-QTOF analysis (Figures S3-S5, in the Supplement) of enzyme-biodegradable nanocapsules and lysate samples in octanol and buffer is included. Interactions between MIP-bound HSA and additives enable the transfer of soluble molecules and antibodies across different sample types, improving efficacy. PAR data across processing stages were examined to better understand peptide fragmentation, water content, process effects, surface interactions, and how hydrophobic molecules influence membrane behavior during bionanofiltration.

Recycling the filtered lysate resulted in a 2-fold decrease in CBD+H+ (315 m/z), with increases in protonated CBD (CBD+2H+, 316 m/z) and minor CBD+2H+ across different scenarios. CCF recycling exhibited the highest DEP-C level. Lowering the zeta potential and maintaining a pH of 7.4-7.5 results in the biocomposite forming clusters within a narrow nanoscale range. This affects lysozyme, stabilizer effects, protein interface volume changes, and particle size during MIP processing and storage. The strong affinity of specific ligands to cell membrane receptors is essential for maintaining the structural integrity of mAb. To investigate the affinity of ISL for membrane lysates compared to CCF, we employed high-energy tracking using LC-QTOF-MS. This method allows us to closely examine the interactions between the Fc domain and ligands, which are crucial for immune responses.

Our evaluation assesses how antibody domains are modulated during the continuous manufacturing of multiple biologically active agents in a single dosage form, nanocapsule MIP, and how these modulations affect protein structure across various environments. Information obtained *via* the QTOF-MS-ESI method is vital for the early development of antibodies optimized for the oral route in biologics [34]. The delivery of CBD improves upon *in situ* blends by increasing free volume and enhancing the uptake of small molecules and biomacromolecules, particularly in the hinge and CH_2 domains, thereby improving targeted therapies.

Consistent amino acid levels in recycled, post-freezing IMNs suggest that MIPs efficiently target CBD diastereomers at HSA's Fc-binding sites, thereby preserving antibody structural integrity. Transitioning from aqueous to MIP environments enhances co-delivery systems for biologically active agents, improving solubility and bioavailability, both essential for therapeutic use. Analysis of DEP-C with PCL-T gel in nanofiltration demonstrates how environmental factors influence the stability and processability of antibodies and biotherapeutic proteins. The observed changes

Table 5: Relative abundance of CBD (m/z) and Peak Area Ratio (PAR) of CBD/CDR fragment (m/z), for the protein nanocapsules obtained from *In Situ* Loading (ISL) and customized CBD (CCF) during different processes.

Number	Parameter	Relative abundance, CBD (m/z)			PAR of CBD/protonated CDR fragment (m/z)		
		315.1369	316.1764	317.2640	613.3396	614.3429	615.3475
1	Premixed ISL	1110	3315.74	180	6.11	18.42	1
2	Recycling ISL (Batch# 1)	900	323	180	5.00	17.96	1
3	Recycling ISL (Batch# 2)	980	3860	170	5.76	22.71	1
4	Freeze-dried ISL	3214.3	353	143.9	18.6	5	1
5	Freeze-dried CCF #1	2108	978	144	11.6	3.6	1
6	Freeze-dried CCF mix#2	2039	285	150	11.6	3.6	1
7	Recycling CCF (residue in feed layer)	2450	400	589	2.2	0.9	1
8	Recycling CCF (residue in filtered lysate)	2540	720	360	4.7	1.6	1

Note: ISL: *In Situ* Loading; PAR: Peak Area Ratior

in membrane affinity of recycling lysates over six months, using various CBD buffer solutions, provide valuable insights into the physical stability of MIP nanostructures and the reliability of the biopharmaceutical delivery system.

Exploring the intricate dynamics of folding and biomolecular condensation within ISL-based hybrid nanomaterials

This advanced 3D optoplasmonic structure directs light onto a tiny surface sphere, converting analytes within the microstructure into a DEP-C composite lysate. During bioprocessing, interactions among small molecules, enzymes, and excipients can cause red-to-blue shifts in FLIM, especially with certain blending methods. The remaining biocomposite on the cast layer naturally exhibits green fluorescence under blue light, as shown in the supplement (Figure S6). This likely results from biocondensation proteins associated with the technique and MIP recognition, which promote controlled sequences and surrogate interactions within protein-protein dynamics [35]. These interactions induce shape changes in proteins, resulting in complex green fluorescence. Recombinant proteins within lipid bilayers bind strongly to the β chain of FcεRI. When IgE crosslinks the α subunits of FcεRI, it activates Lyn kinase, which phosphorylates the Immunoreceptor Tyrosine-based Activation Motifs (ITAMs), a crucial step in downstream signaling. Phosphorylation then recruits additional Lyn *via* its Src homology domain, which binds to the phosphorylated tyrosines [36]. Our findings suggest that cysteine-rich hinge regions improve efficiency when MIP is in lysates, reducing tyrosine phosphorylation in CCF compared to ISL and influencing signaling pathways. Moreover, the combined action of ISL and CCF affects green protein fluorescence, indicating a complex regulatory system in which signal proteins modulate inhibitory signals by dephosphorylating ITAMs on both the β and γ chains of FcεRI. This produces significant red-to-blue shifts in fluorescence observed with FLIM.

We enhance hybrid MIPs and PCL-T gels with anti-solvent interfaces, creating durable, solvent-free biologic drugs. By embedding antibody-drug complexes into natural cellulose templates, we enable targeted protein interactions with modified peptides. For ISL nanoparticles over 10 nm, scatter detection was only possible at the change shown in Figure 7B(B). Spherical structures are clearer near the excitation source, as shown in Figure 7B(C). After compound release, we assess fluorescence and perform volumetric imaging of MIP-IMNs to aid therapeutic development. Our analysis confirms the colloidal stability of the drug composite, containing biotherapeutic proteins, in both *in situ* filter lysates and reconstituted freeze-dried samples. The PCL-T gel significantly enhances protein binding and stability, consistent with the findings of Sladek, et al. [10].

The adhesion clusters, visualized under red and blue fluorescence, mark significant progress. We integrated NHM with a split fluorescent protein targeting coagulation residues in latex and the CCF-specific matrix, allowing us to distinguish between green and red fluorescence channels (see Figure 7B (A-C)). The fusion of NHM with the split fluorescent protein shows fluorescence shifts: IMN-HSA emits blue, which shifts to green within the protein, indicating a CCF-type interaction. This highlights the photothermal properties of plasmonic nanofibers and their impact on bacterial growth and cell populations, confirming their effectiveness in biological systems. Attaching IMNHSA to a split fluorescent protein produces blue fluorescence that turns green within the protein, likely due to surface chemical reactions with buffer components. Increased cofactor activity during NHM formation facilitates the release of drugs and proteins. Internal green fluorescent proteins help differentiate overlapping signals, providing insights into vesicle interactions based on size (>10 nm). Fluorescence microscopy detects protein conformational changes that enable ATP binding in ubiquitin or dimeric-ubiquitin binding domains from both ECS lysate and vesicle nanocapsule formulation, in which adenine and phosphate contribute to the interaction *via* electrostatic interactions with the protein of interest, thereby influencing protein complex formation and activity while reducing non-ubiquitin nonspecific interactions. Morphologies after 6 months in phosphate buffer within the biological system are shown in Figure 7C, illustrating their crucial role in clinical translation. Changes in fluorophores and ECS proteins from photon scattering help distinguish stabilized drug proteins from free ones. Threshold quantification measured the total fluorescence of the MIP in the target zone, including MIP bionanocapsules, aiding understanding

of mAb reactivity and bacterial responses. Encapsulating ATP in IMNs enhances protein uptake, targeting, and enzyme activity, as confirmed by X-ray analysis. ATP influences antibody conformation and insulin binding over pH 4.1 to 6.1, affecting folding and affinity. Recent research indicates that adjusting the crosslinking density of polypeptide bonds can prevent particle aggregation. Recent innovations have also improved drug testing for chronic conditions like osteoarthritis and diabetes, which depend on cell lysate growth factors, hormones, serotonin, cholesterol, and fatty acids to regulate neural and immune pathways. The findings suggest potential strategies to improve therapeutic outcomes and translational medicine.

It also emphasizes the importance of biomolecule concentration and protein folding, especially insulin, to improve antibody activity and enzyme interactions. Recognizing high biomolecule levels and proper folding can enhance biopharmaceutical quality and enable detailed exploration of small-molecule targets and therapeutic proteins *via* fluorescence microscopy, as discussed in the next section.

Analysis of protein abundance for process monitoring

The discrete variable, a continuous factor affecting the lysate component through changes in particle aspect ratios and specific volume, varies across filtrates from premixed, recycled, and freeze-dried IMNs, impacting the lysate during 15 days of bionanofiltration, as shown in Figure 8A. The amino acid profiles, based on the blending drug method (ISL *vs.* CCF), were more similar in these filtrates, with a sunburst plot illustrating the contribution of each of the 17 amino acids, compared to their roles in lysate filtrates after application of premixed MIP containing the CBD and multivalent proteins (see amino acids of recombinant insulin, mAb, and lysozyme in Figure S7), recycled, and freeze-dried IMNs (see Figure 8A,c). Reducing cysteine enhances enzyme activity by leveraging the MIP self-assembly-promoting role in protease inhibitors' function in the premixed MIP for both IMN systems, as aforementioned, thereby stabilizing biopharmaceutical formulations and improving their reliability. Cell metabolism and metabolic signaling outside cells support energy metabolism, glycolysis, and energetic oxidative phosphorylation. Stable nanocapsules exhibit small amino acid variations, indicating multiple phases of the nanocomposite, distinguished by the amino acid profiles of residues in the premixed liquid state of the MIP, depending on the blending method and CBD concentration (see Supplemental Material Figure S8). A comprehensive analysis of amino acid profiles, along with lysate analysis of multivalent biopharmaceuticals and co-payloads, we observed elevated levels of glutamate, histidine, and lysine in response to antibodies, insulin, and CBD, which correlated with increased lysozyme activity. This shows the precision of MIP IMNs in targeting CBD diastereomers, highlighting innovations in delivery strategies. This result

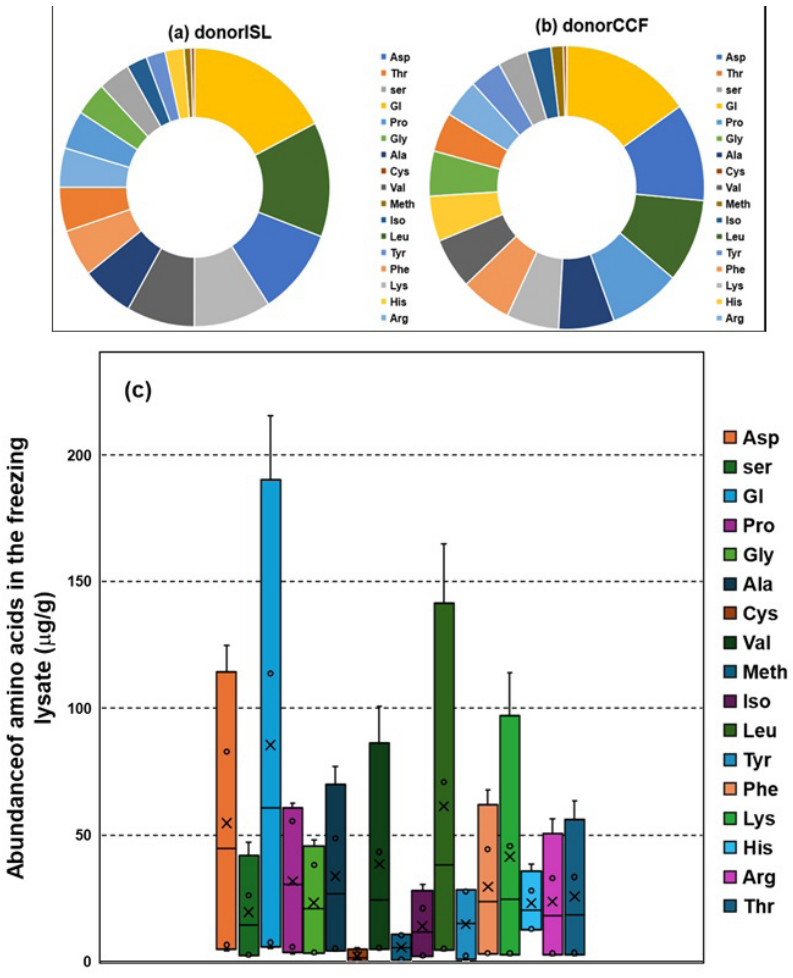

Figure 8A: (a), (b) Comparison of amino acid profiles in the remaining residues of the premixed component after Franz diffusion (ISL vs CCF types), with a sunburst plot showing each of the 17 amino acids' contributions. (c) Boxplots of the seventeen amino acids contributing to donorISL, donorCCF (x), and the ISL- and CCF lysate filtrates (o) following the premixed, recycled, and freeze-dried IMNs applications.

indicates that CBD's effects involve the inclusion of excluded charge residues, clearly showing that the immuno-nanostructures from the CCF type did not self-associate or change viscosity. At the same time, consistent amounts of amino acids are effectively recycled with MIP IMNs. The cysteine-rich domain on surface-exposed proteins and the hinge region are crucial for maintaining the structural integrity of mAb and recombinant proteins at HSA's Fc-binding sites.

Studies on the relationship between structure and process using fluorescence laser imaging

Our investigation used advanced techniques, including fluorescence laser microscopy, to examine how CBD levels affect subvisible particle sizes. We conducted real-time imaging of filtered lysates and samples from ISL- or CCF-type IMN. The study explored cysteine-rich domains on surface exposed proteins and hinge regions across different blend types, using split fluorescent proteins to enable color differentiation, thereby opening new research avenues. Figure 8B shows that modest variations in IMN size affect CBD loading during membrane recycling at pH 7 and 7.4. This analysis examines nanoscale protein distribution over a month, revealing significant early changes, with mixed results later. Data points for freeze-dried and lysate samples remained similar, though differences such as blue fluorescence in CCF lysate were noted. Changes in fluorescence fold differences between water-reconstituted and freeze-dried samples were observed, especially in vesicles and CCF. Variations in vesicle size and clustering highlight the importance of flexible protein regions, which cause hysteresis and distinct droplet and cluster behaviors. A 45-fold difference in fluorescence was observed in water-reconstituted ISL after storage, compared with 10-fold in another batch, with consistent trends in filtration and fluorescence data. The proteins' structural integrity depends on interactions with solvents, excipients, and additives, as well as on the formulation composition, which affects stability and drug-protein interactions, thereby enabling changes in the radius of the HSA nanocapsules. These changes in the nanocapsule radius with changes in the medium may be influenced by the extended collapse state of the hydrogel, the cholate-anchoring MIP, or adsorbed charged ions at the protein-hydrogel interface, as assessed by FLIM. Fluorescence laser imaging showed cluster formation of smaller particles interacting with the buffer, which were distinguished from those in water after six months at room temperature.

The interplay between folding and charge stability is strongly influenced by chemical composition, PCL-T concentration, and encapsulated payloads, particularly in the optimized premix MIP. This is evidenced by variations in fold changes and the ratios of nanometer-scale to volume charge residues in protein-based therapeutics. An elevated pH in IMN effectively promotes the formation of well-defined nanoparticle clusters that remain stable throughout all stages of the MIP process, with a focus on nanosized nanocapsules in buffer and water.

IMNs, mainly 100-300 nm and suspended in buffers, appeared larger in water, especially in water (see Figure 8B). Variations can influence peptide phosphorylation and protein stability in drug substances and biologics, which is useful for developing complex multicomponent nanocapsule systems. In Figure 8C(A), you'll see images of a high-concentration IMN solution, lysate, and filtrate. Interestingly, there's less aggregation after just one day compared to after a month, especially in the buffered lysate. As the concentration increases, the spherical particles tend to grow bigger-unlike in frozen IMN. This change is linked to differences in glutamate, lysine, and valine levels, which should enhance the unfolded state of colloid stability, which has been associated with reduced aggregation, as this amino acid residue binds to ATP, while arginine predominates in direct binding to ATP. Additionally, notable variations in proline within the CCF, and in histidine, valine, and phenylalanine in both IMN types. These amino acids are particularly important, as shown by antibody detection and protein interactions at the cell membrane during co-solvent interfacial interactions. Over time, their levels decrease and transfer to adsorbed water as IMNs form, suggesting they may help promote self-assembly by replacing charged residues on antibody chains, which supports a more compact structure. In Figure 8C(B), you can compare the plots of filtrate and freeze-dried samples, which show fluctuations in the nanoparticle radius from the start of storage to after a month. This points to conformational adjustments

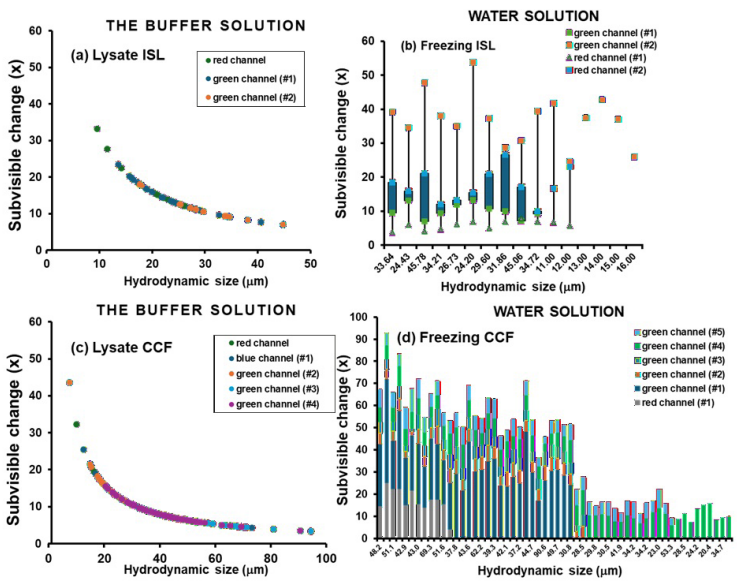

Figure 8B: Panels (a) and (c) show nanosized protein distribution in lysate ISL and CCF, with similar subvisible size changes from about ten to one hundred micrometers. Panel (b) compares subvisible size changes for frozen ISL IMN across concentrations in water, with size changes between ten and twenty times. Panel (d) shows bar graphs of subvisible changes for freezing CCF in water, highlighting fluorescence variations.

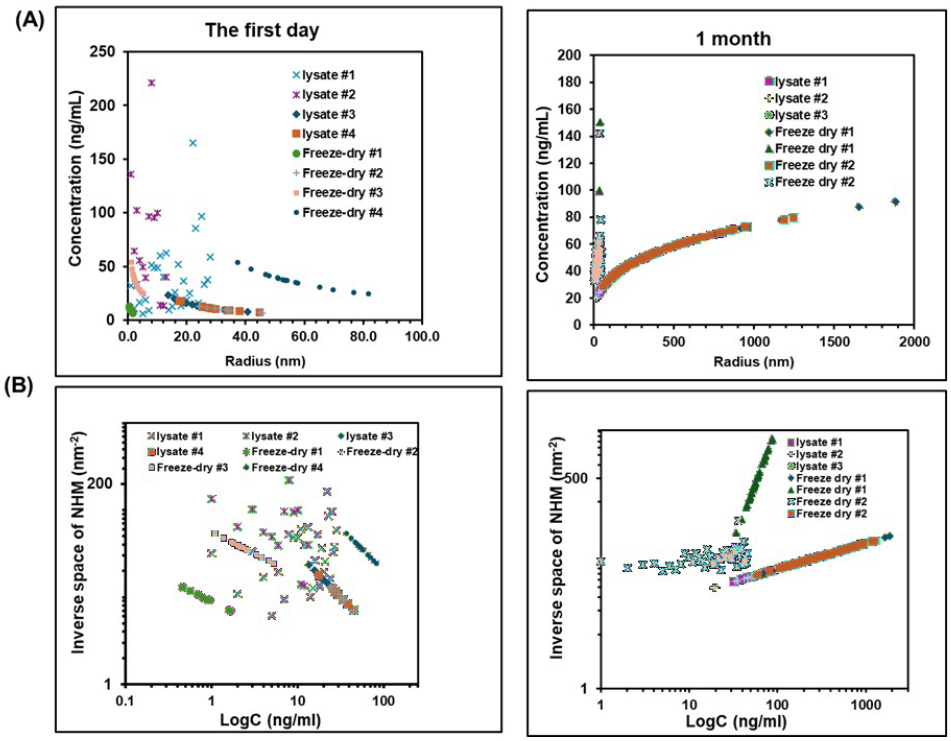

Figure 8C: (a),(b) Nanoscale protein distribution in the IMN plot *versus* concentration in pH 7.4 buffer on day one and after a month, from *in situ* loading of biotherapeutics; and (c),(d) the inverse space of spherical protein particles during reconstitution in purified water at various stages across batches and from the buffered lysate during cellulose fibril nanofiltration.

and changes in protein mobility inside the core-wall, resulting in a well-organized, dynamic structure with photoswitchable ligand binding. This setup allows changes in affinity at targeted sites and the activation of the protein environment, making it a useful tool for studying how small compounds, such as CBD-based ISL-MIP systems, inhibit certain processes within the cellular matrix and the biological system. Additionally, light-scattering measurements from pooled lysate help confirm the reliability of these findings.

The binding affinity of DEP-C increased with higher CBD load concentrations and pH adjustments, facilitating interactions among the Fc region, antigenic sites, and insulin, influenced by ECS stimuli and lysate content. The inverse space plot of spherical particle diameter from the ln(c) *vs.* r^2 regression shown in Figure 8C demonstrates stability over a month, with the apparent average volume from the same regression providing further insight into the self-association of the combined biotherapeutic drugs. Our *in situ* loading study reveals complex interactions that enhance the robustness of human albumin nanocapsules. The freeze-dried ISL sample indicates that the attractive interactions of chemeric proteins remain repulsive, preventing self-association. Different molecular reorientations or atomic resolutions of IgG may affect water interactions, so the lysate in the filtrate shows less self-association after a month. The power plot of fold changes in filtrate and freeze-dried samples in buffer and water shows consistent trends in fluorescence nanomaterials, with spherical particles, volume as a function of radius: in water, y=318.47 x^{-1} (R^2=1), and in filtrate, y=0.0025 x^{3} (R^2=1).

The freeze-dried ISL shows that intermolecular interactions among recombinant proteins remain repulsive, a good sign of stability. Similar interactions in the filtrate (buffer) lysate show even less self-association after a month and maintain a steady viscosity of 1.5 cP, indicating good stability. Small variations in solution viscosity (<0.2 cP) and minor pH shifts (<0.1) reflect a stable environment. This stability helps explain the slight increase in enzyme release from the nanobiocomposite, especially since its isoelectric point is above pH 7.0, allowing stable molecular complexes at the air/liquid interface.

Analysis of monoclonal antibody (mAb) binding for ligand localization

Understanding proton transfer to ionized carbonyl groups is vital for protein stability during recycling and lyophilization. Mass spectrometry provides insights into the stability of biopharmaceutical nanostructures, focusing on the integrity of protein fingerprints and surface chemistry upon co-payload delivery. Investigating dehydration instabilities and how proton transfer aids stability are key to advancing biopharmaceutical applications. Proton exchange observed in mass spectrometry might affect the effectiveness of the nanostructure. Analyzing these factors clarifies their effects on structural and surface properties. Figure 9A shows significant DEP-C mass ratio variations. Tripodal molecules form complex structures with specific CBD diastereomer ratios, enabling enantiomeric CDR synthesis at various m/z values, like 615.3457, 614.3429, and 613.3396 within the anti- IgE antibody CDR. The hydrophobic environment can modify CDR sequences without losing function. Changes in the PAR diastereomer of CBD during recycling reveal how processing conditions and lyophilized IMNs influence structural and functional features, aiding understanding of protein roles and immunocapsule development. Release mechanisms depend on interactions between the anti-IgE CDR and CBD *via* MIP. Figures 9A (a, b) show mass changes in the anti-IgE CDR. During storage and freeze-drying, positive ESI mode detects m/z 315+H+, corresponding to $C_{21}H_{30}O_2$, with a major ratio of 22.3:3.7:1.0 and DEP-C ratios of 18.6:5.0:1.0, indicating a greater abundance of

positive ions. Maintaining consistent CBD-to-antibody ratios is critical for transferring small molecules and antibodies, including freeze-dried IMNs. MS-ESI+ ions at m/z 315, 316, and 317 relate to specific molecules. PCL-T and additives in a 1:3 ratio show promising interactions. MIPs support proton exchange with surrogate proteins containing anti-IgE CDRs, and they work effectively with pharmaceuticals and nanofiltration. MIP may also bind additional CBD diastereomers at Fc domains on NHM, providing site-specific information. High-CBD premixes show the stabilizing charge states that regulate CDR and CBD at surface-exposed amino acid sites *via* HSA. Complexes with DEP-C help develop enantiomeric CDRs, while NHM favors certain CBD diastereomers that bind to Fc sites. Moderate MS-ESI+ ratios and isotope peaks reveal differences in affinity among CBD Diastereomers and Fc dimers (DEP-C). Despite mixing issues, UHPLC combined with high resolution QTOF-MS enhances antibody complex quality and payload delivery, with a ratio of 22.3:3.7:1.0 for enantiomers, including dimerized MIP parts.

We identified enzyme-sensitive regions that facilitate interactions in the self-association nanoMIP assay. However, structural alterations, such as glycan truncation or denaturation, can lead to increased aggregation and decreased receptor binding. MIP nanostructures help maintain the Fc domain's integrity, which is essential for stability, as correct folding and conformational changes are vital for effector functions and for targeting Fc-engineered drugs such as Antibody-Drug Conjugates (ADCs) and Fc-fusion proteins. These nanostructures develop a durable outer layer, unlike traditional cellulose matrices. Our drying studies demonstrated their influence on nanocarrier stability within PCL-T gels and identified CBD fragments and degradation products. Modifying the polypeptide crosslinking density can prevent aggregation during CBD dilution. Variations in amino acid conformations between ISL and CCF may affect ligand binding and protein activity, facilitating target recognition in ACD drug discovery, boosting effector functions, and extending biologic persistence. Stabilizing proteins with high CBD levels, especially in sustained proline- or cysteine-rich environments, shows promise for protein translation activity. The CH_3 region of the heavy chain, which retains flexibility in IgG, is a region of interest for aggregation propensity. Both PED-C from ISL and CCF exhibit slight differences in the levels of stabilized charge states of the CBD diastereomer ratios at Fc sites due to specific protein binding, which can interact with albumin during

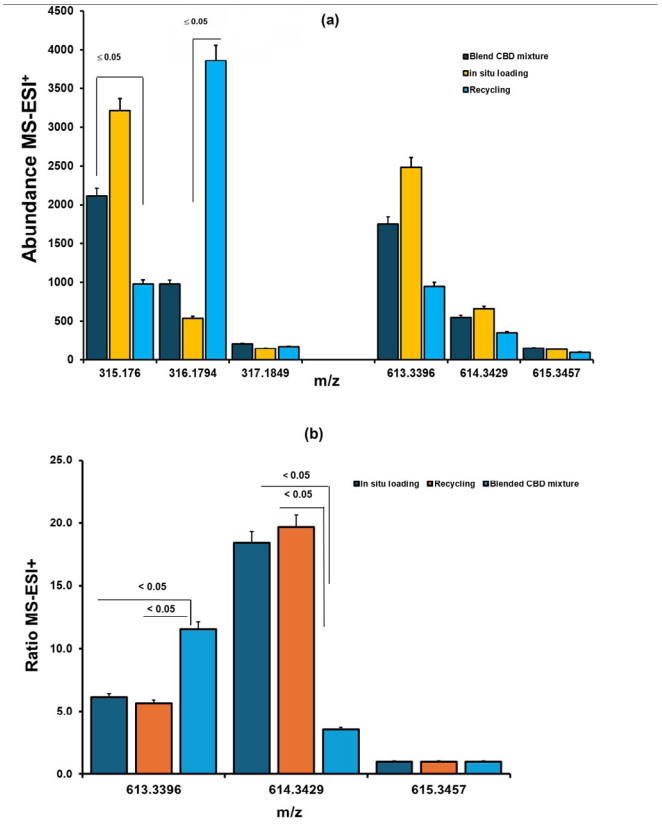

Figure 9A: The LC-QTOF-MS abundance MS-ESI+ plot showing multiple isotopic proton exchange peaks from high-CBD premixes and batch blends, pooled from four determinations.

pH shifts to PBS media. Cysteine-rich hinge regions significantly improve MIP performance in premixed MIP lysates. Tyrosine phosphorylation was lower in CCF than in ISL, indicating its role in signal transduction. The ISL-type MIP binds amino acids like tyrosine, cysteine, and histidine, as well as small molecules targeting cannabinoid receptors, opening new research directions. Moreover, LC-QTOF-MS provides a characterization method that is beneficial for examining conformational changes at several stages and the manufacturing process.

Site-specific quantification to mitigate protein instability and degradation

Additionally, this enables the study of compounds that modulate the properties and functions of native and recombinant proteins, as well as efforts to target small molecules such as cannabidiol within a selective nanosized environment. It discusses how tripodal molecules for PED-C affect CBD diastereomer ratios, thereby influencing DEP-C mass ratios in MIPs. Protein surface sites interact

with ligands or other proteins, and engineered IMNs improve efficacy while reducing contamination. Ligand modifiers stabilize proteins and prevent CBD degradation by forming complexes and mediating interfacial interactions. Figure 9B shows CCF-targeted carboxylation at dihydroxyl sites, forming dicarboxylate CBD at m/z 401 and 402, which we identified at 401.2061 and 402.2117, respectively. DA reduces dicarboxylated CBD (p=0.014), whereas in the absence of DA, ISL increases decarboxylation of CBD (p=0.019). No significant difference is observed with or without DA (p>0.05). DA causes a peak at 385 m/z, indicating CBD degradation, especially in MIPs. Immuno-nanofiltration with dopamine decreases degradation products by less than 2%, lowering ISL and CCF by 20-fold and 80-fold, respectively, as illustrated in Figure 9C. Despite CBD's short skin half-life and rapid stomach metabolism, CBD and derivatives undergo decarboxylation *via* enzymatic and non-enzymatic pathways involving oxidase enzymes.

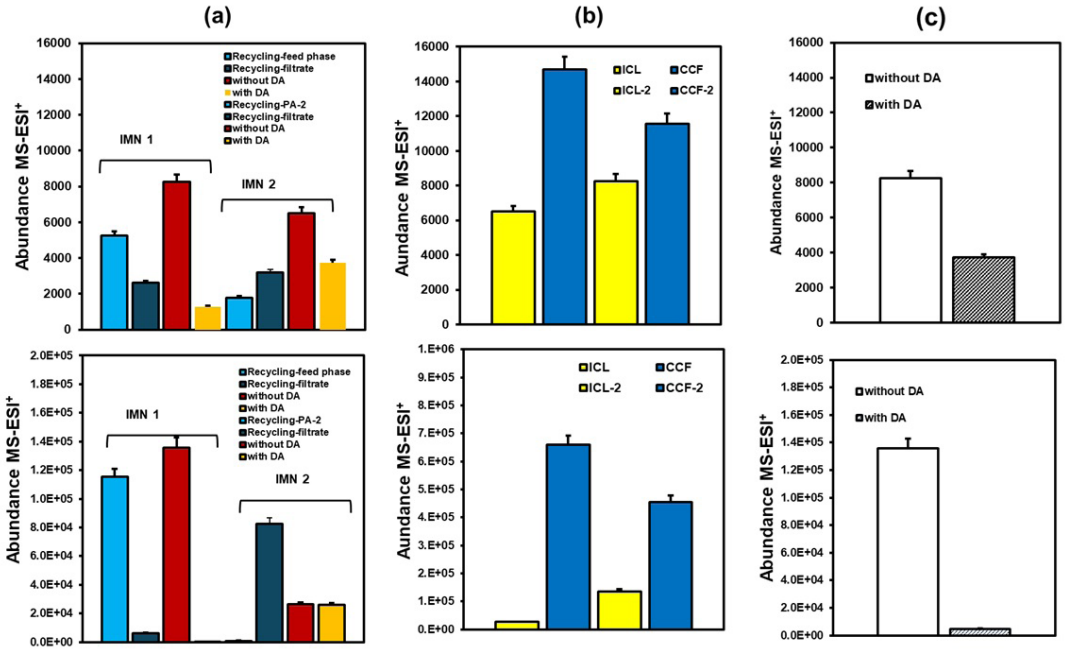

Figure 9B: Peak areas of isotopic proton exchange from ISL and CCF at MS-EPI+ masses 401 m/z (top) and 385 m/z (bottom), marking polypeptide surface sites. High-CBD nanocaps are green; blue and orange show different batches of the CBD blend.

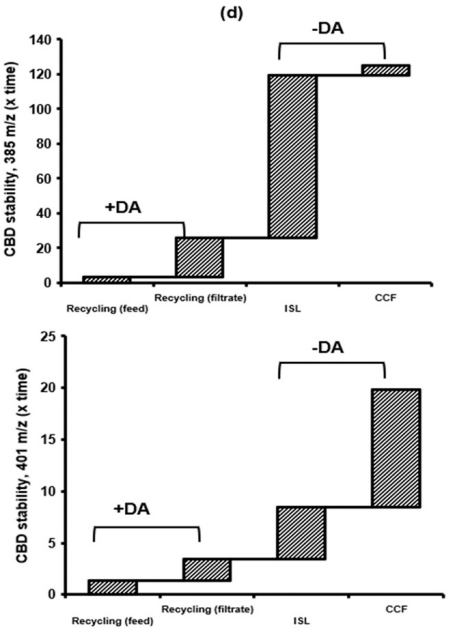

Figure 9C: The effect of added DA and absence of DA on the stability of CBD during bionanofiltration - difference in peak area of the QTOF-MS-EPI+ target mass at 401 m/z (top) and 385 m/z (bottom) from recycling feed site and recycling filtrate.

MIP nanostructures improve CBD binding to Fc sites, as DEP-C depends on load and interface during bionanofiltration. Dopamine levels increase due to mitochondrial ROS inhibition and reduced glucose regulation, thereby lowering cellular metabolism, as also reported [37,38]. The current study also examines protein stability *via* rapid charge-state assessment to evaluate antibody stability and potential aggregation, and examines how media reduces CBD degradation and prevents breakdown.

Monitoring the behavior of the lyophilization of protein-based IMNs

One of the key factors we've identified is storage temperature, which plays a pivotal role in protein mobility-a critical element in both long-term storage and processing.

TGA and derivatives

Monitoring product behavior during lyophilization is crucial. We used Thermogravimetric Analysis (TGA) to characterize a small molecule, focusing on polymer-solvent interactions and hydrate shell formation. We evaluated how low-melting water influences exothermic recrystallization and observed freeze-drying behavior. The TGA and derivative curves effectively tracked the melting point of Intermediate Microspheres (IMNs) for both ISL- and CCF-based IMNs, as shown in Figure 10(A). The composites of both types decomposed in at least two steps, as clearly visible in the TGA derivative (DGA) curves shown in the middle graphs of Figure 10A. For ISL, we observed a 11.0% weight loss between 68°C and 85°C, attributed to the melting temperatures (Tm) of the CH_2 and CH_3 domains in water-hydrated IgG during IMN freeze-drying. This weight loss exceeds that of CCF, in which cooperative changes in the variable fragment of antibodies (Fv) and constant domains occur due to sequence variability; this observation is supported by the TGA curve (Figure 10A). ISL also showed a comparable 16.8% weight loss from 166.8°C to 269°C in both conditions.

Both ISL and CCF primarily exhibited endothermic pyrolysis in two stages-initial and secondary-between 166.8°C and 269°C on the Derivative Thermogravimetric (DTG) curve. These results were influenced by moisture and oxygen levels during measurement, including those in nitrogen (N_2). These factors also affect the glass transition temperature (Tg) and the secondary state plateau, which correspond to protein mobility above 320°C and 360°C, respectively. Over a temperature range of 187°C to 300°C, consistent weight-loss patterns were observed, with Transition Temperatures (Tg) ranging from 222°C to 395°C. Notably, the ISL batches displayed enhanced anhydrate peaks between 88°C and 102°C, while the CCF material reached weight-loss plateaus of 22.5% in oxygen and 27.8% in nitrogen. The combustion temperatures for the same CCF material across different batches ranged from 222°C to 395°C. Variations in the DTG and TGA curves for CCF within the 215°C to 340°C range under oxygen across two batches suggest the presence of different crystal forms with the same microscopic size but varying macroscopic compositions as measured by DSC. However, DSC measurements under nitrogen remained consistent. These differences are attributed to structural variations in the CCF between batches.

A reverse peak was observed between 68°C and 85°C and confirmed by ISL. Melting point results from IMNs using CBD provide valuable insights into antibody thermal stability. It's especially important to remember that air-sensitive products require proper drying to remove moisture effectively, as moisture can affect their quality. To do this successfully, a thoughtful approach using both air and nitrogen (N_2) is recommended to remove air from porous materials made of biopharmaceutical proteins and payloads. This combined-gas method not only helps extend the life-time of the biologics in the IMN products but also reduces the risk of degradation. Additionally, high moisture levels can lead to noticeable mass loss during thermal analysis, potentially causing an apparent increase in the sample's weight and influencing TGA and DTA results. Understanding these factors is key to improving the stability and performance of sensitive materials in real-world applications.

DTG analyses showed peak thermal intensities at 182°C and 300°C, indicating slight variations in weight-loss profiles, especially in the oxygen data. Measuring the heat capacity and specific heat of a substance can be challenging. Changes in volume during saturation-to-dilution transitions in a three-compartment mixture suggest that poorly soluble drugs, such as CBD and HSA, are common and influence the amount of PCL-T gel released from the IMN. These modifications enable the controlled release of molecules, such as antibodies and CBD, from dried Immunonanomaterials (IMNs). Low-temperature heating improves surface stability, as seen in changes in heat capacity during thermogravimetric analysis (TGA). These effects result from interactions at the air-solid interface during immuno-nanofiltration, affecting composition, osmolytes, viscosity, and hydration, which impact polypeptide and hydrophobic drug stability. Consequently, this result underscores the importance of early detection during the fine-tuning development process. It is also crucial to ensure that sensitive products are properly dried to prevent moisture damage.

Analysis of molecular interactions using FT-IR

The carboxylate groups appear to generate key FT-IR peaks at 1650 cm^{-1} and 1402 cm^{-1}, associated with deformation of aromatic C-H bonds (as shown in Figure 10B). The exact positions of these bands, especially in ISL, are likely influenced by interactions with nearby molecules and biological agents present in the functional material, as well as the C-H stretching observed in the aliphatic side chains of the MIP at 2935 cm^{-1} and 865 cm^{-1}, which is attributed to the twisting of methyl groups on the amino acids, which this is the restriction of the free rotation of the aromatic ring of the 3D biased ligand approach in this work. This is expected to be a stabilized molecule that binds to the cannabinoid receptor to enhance functional activity. During stabilization, it became evident that osmolytes effectively organized interfacial water molecules, particularly at the interface, to support protein stability. Additionally, the spectra of the two types of nanosuspensions showed subtle disorder in the ordered structure of the amino acid side chains, particularly in CCF after bionanofiltration, underscoring how environmental factors influence protein conformations and charge interactions, as evidenced by distinct FT-IR spectra. This is attributed to influences on interfacial solvent dynamics, and the substrate is contained within the nanocapsules that capture adherence to the extracellular matrix surface. This process effectively reduces protein-protein interaction phase separation by optimizing local solvent conditions and strengthening attractive forces among biomacromolecules. MIPs are essential for preserving protein integrity and orchestrating osmolyte distribution at the interface. As a result, they enhance antibody efficiency in bionanofiltration while preserving protein stability. The efflux of immunocapsules can be modulated by interactions between the CDR peptide of the anti-IgE antibody and the CBD.

Our findings showed significant differences in the FT-IR spectra of the two nanosuspensions. CCF exhibited a broad peak at 518 cm^{-1}, similar to ISL, along with additional peaks at 1264 cm^{-1} for glycine and at 618 cm^{-1} [39]. This suggests that the lyophilized IMN exhibits a distinctive spectrum, underscoring how environmental factors can influence protein structure and charge interactions. We also noted that ISL varied even within the same CCF batches, which is quite surprising. Furthermore, reduced osmolyte interactions impact the structural properties of the antibody complex, increasing water's hydrogen-bond energy and enhancing heat transfer. These insights are crucial for designing processes involving biopharmaceutical proteins and biologics and may lead to new research directions.

Spectroscopic analysis reveals flexible regions within the multivalent

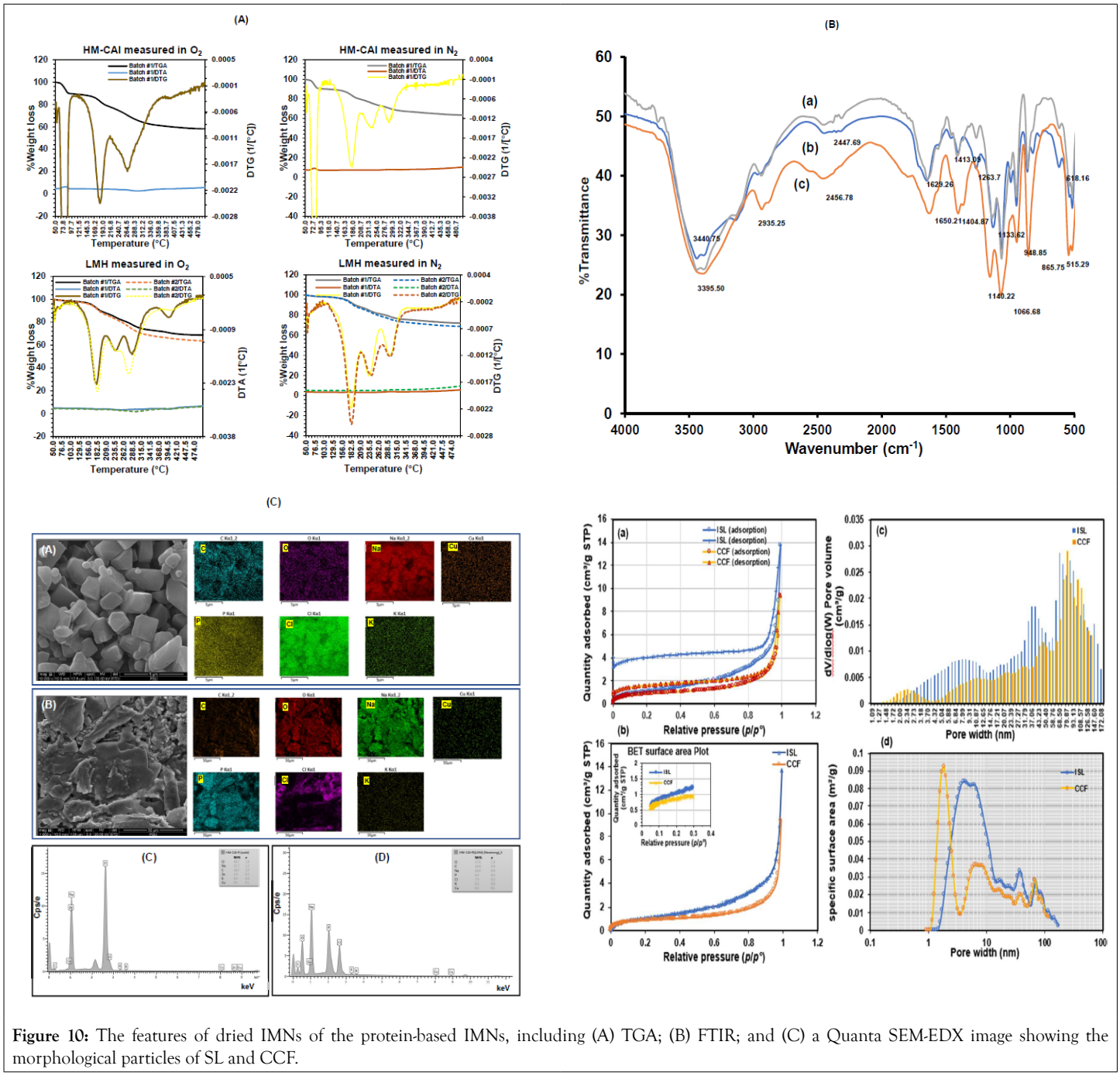

Figure 10: The features of dried IMNs of the protein-based IMNs, including (A) TGA; (B) FTIR; and (C) a Quanta SEM-EDX image showing the morphological particles of SL and CCF.

folded protein that facilitate interactions among proteins and peptides within non-PCL-T droplets. These droplets are stabilized by intermolecular interactions between the MIP and additives, forming a rigid environment that prevents conformational changes after lyophilization. Adhesion bonds with stabilizers help preserve protein structure, and some adsorbed water helps maintain drug stability. Reduced osmolyte interaction improves water's heat transfer capacity, while proteins engage with CBD's hydroxyl groups. Despite certain variations, the overall temperature stability of freeze-dried proteins remains consistent.

QuantaSEM-EDX

QuantaSEM-EDX analysis (see Figure 10C) revealed distinct morphologies, particularly the presence of "plate-like structures" in the strong MIP nanostructure made from CCF. Meanwhile, ISL displayed a common "hexagonal pyramidal" crystal shape. In a QuantaSEM-EDX image of ISL and CCF, we found that a dynamic, ordered structure strongly influences protein behavior within a complex biomolecular environment in the solid state. Characterization of the freezing IMNs clearly demonstrates a slightly disordered structure within the otherwise ordered framework, particularly in CCF, where disordered silicon effectively binds to the aryl hydrocarbon receptor during the bionanofiltration process. These flexible materials excel at facilitating ion conduction in the solid state of proteins, exhibiting rapid and efficient behavior akin to that in liquid states. This phenomenon directly influences interfacial solvent dynamics, with the substrate securely contained within nanocapsules that enhance its adherence to the extracellular matrix. The multifaceted structure observed in all freezing biocomposite IMNs is recognized as a hybrid material that confers specific functionality while maintaining the MIP's capacity to enhance enzyme efficiency.

BET surface area analysis

The semi-log plot of incremental pore volume spans 1.28 to 172.8 nm, with a maximum pore volume of about 0.03 cm^3/g, as shown in Figure 10D, indicating a compact NHM structure rich in voids. Table 6 summarizes the effects of osmolytes, additives, and compositions on the surface area and pore size of non-process and process bioproduction, either with free PCL-T or with PCLT. The effectiveness of a porous solid depends on its pore structure, adsorbent properties, and protein-binding behavior, which are influenced by the octanol layer system and the leached-out water phase. These features can vary significantly across Intermediate Nanostructures (IMNs) and closed-pore structures, potentially limiting the applicability of alternative methods, depending on the drug-blending method, as illustrated in Figure 10D (a,b). For example, in our results, the BET surface area (4.0686 m^2/g) and the average pore diameter (20.8502 nm) of the ISL batch protein powder exceed those of the different batch (#2), which has a slightly larger average pore diameter obtained from the CCF (3.1245 m^2/g and 18.5571 nm). This indicates a notable structural difference: CCF types exhibit a solid framework with voids, yielding a denser, aggregated nanohybrid material. The retention ratio is vital for assessing pore accessibility, which greatly influences the anti-solvent interface capacity of hybrid materials. This insight is key for managing interaction areas and membrane structures at interfaces where proteins encounter extracellular solutions.

The material properties of Intrinsic Nanomaterials (IMNs) used in biopharmaceuticals were studied, and gas adsorption/desorption measurements were used to determine their monolayer capacity. BET analysis of the residuals for both IMN types revealed a hysteresis-type isotherm, indicating that the neck-size distribution closely matches the pore or cavity size distribution (see Figure 10D, c and d, respectively). This facilitates co-solute penetration, enabling soluble proteins to be administered at higher doses

Table 6: The effect of osmolytes and additives and compositions on the surface and pore size of different types for IMN-HSA.

	N2 %weight at maximum absolute pressure	BET surface area (m^2/g)	Adsorption pore diameter (nm)	Warm free space (cm^3)	The measured warm free space (cm^3)*
ISL-IMN	0.45	4.0686	20.850	48.84	17.09
CCF-IMN	0.23	3.1245	18.556	47.65	16.76

Note: *Density of sample=1.000 g/cm^3

with smaller infusion volumes, a crucial step for extending the shelf life of multivalent proteins in nanomaterials. These results enhance understanding of protein interactions and support future developments. Furthermore, positively charged molecules with high electron mobility exhibit weaker binding to nanoscale materials. MIP nanostructures create a seamless connection between process-variability studies in nanocarrier research and enable realtime monitoring of biological systems-a crucial task in advancing biopharmaceutical development. We plan to study the potential of advanced nanocarriers to amplify the therapeutic capabilities of proteins and peptides.

Exploring the impact of temperature on MIP-IMNs: A deep dive into dynamic dependencies

Temperature dependence is clear: As temperature increases to 25°C, 30°C, and notably 40°C (see Figure 11A), downfield shifts of 3.5 ppm are observed for the CH_2 group of the methacryloyl cholate ester, along with shifts at 2.2 and 2.4 ppm in the 1H-NMR peaks for methyl groups in the amino acid side chains. These shifts occur without merging even as the temperature rises. The main shifts are attributed to hydrogen bonding between the carboxylic acid and the amino group in the amino acid side chains attached to the MIP nanostructure.

Figure 11(B) shows ^{1}H- and ^{13}C-NMR spectra of a CBD premix filtrate at 25°C and 40°C, with key findings. At 25°C, the CCF displays a multiplet at 2.2 ppm, signals at 3.5 and 4.1 ppm, and a strong lactate signal at 4.45 ppm. Surface interactions improve small-molecule and antibody binding, thereby enhancing protein thermostability, as proteins can unfold or degrade at higher temperatures. Limited amino acid side-chain motion improves resolution in ISL or CCF; shifts of CBD's 7'-carbon and 10'-methyl groups at 4 ppm decrease with rising temperature, along with CH_2 signals. The multiplets at 1.95 and 2.05 ppm correspond to lysine and proline, respectively. Composition influences protein assembly and antibody efficacy. Reducing the Fc domain significantly increases the molecule's dipole moment, underscoring the importance of membrane structure. This change affects the molecule's ability to be encapsulated, improving delivery efficiency and targeted accumulation. Higher temperatures increase protein mobility, affecting interactions and assembly, as shown in Figure S4. Variations in CCF-type batches are related to molecular interactions that shape protein structures and transition temperatures. We found that the interactions between the carbonyl groups of ester and amide, as evidenced by the resonance signals at 187 ppm and 180 ppm in MIPs, are stronger than those in IMN formed *via in situ* loading, leading to more effective payload release from IMN-HSA. Interestingly, this emphasizes the significant influence of a dynamic ordered structure on protein behavior in complex biomolecular environments at 25°C. Notably, the stronger interactions among carbonyl groups in MIPs, compared to ISL-controlled release systems, facilitate the release of multiple IMN-HSA payloads. Our study on the role of ATP in IMN materials revealed that specific regions within a protein complex can recognize proteins, enhancing antibody function. This allows us to monitor the dynamic interactions among ATP, excipients, and the IMN-HSA complex.

The DEPT-90 measurement at room temperature, as shown in Figures 11(C-F) and Figure 12 from the 13C-NMR experiments underscores the importance of the 4-aryl group in antibody complexes. NMR effectively differentiates alkyl chains from aromatic rings in drug-protein mixtures using CCF, by focusing on carbon resonances between 100-120 ppm-corresponding to the aromatic ring of CBD-specifically for the CCF type of IMN

in the DEPT spectra (see Figure 11C), and also at 94-104 ppm, as illustrated in Figure 11G.

Unlike the high-resolution FT-IR data for the lyophilized drug mixture, the absence of the aryl group in CBD from IMN *via* ISL causes self-association in D_2O. NMR data at 40°C suggest protein interactions within HSA-derived IMNs after lyophilization. The data show a decrease in the intensity and broadening of hydrogen resonances related to the aromatic ring of CBD, especially in the ISL type. These findings indicate significant responses under

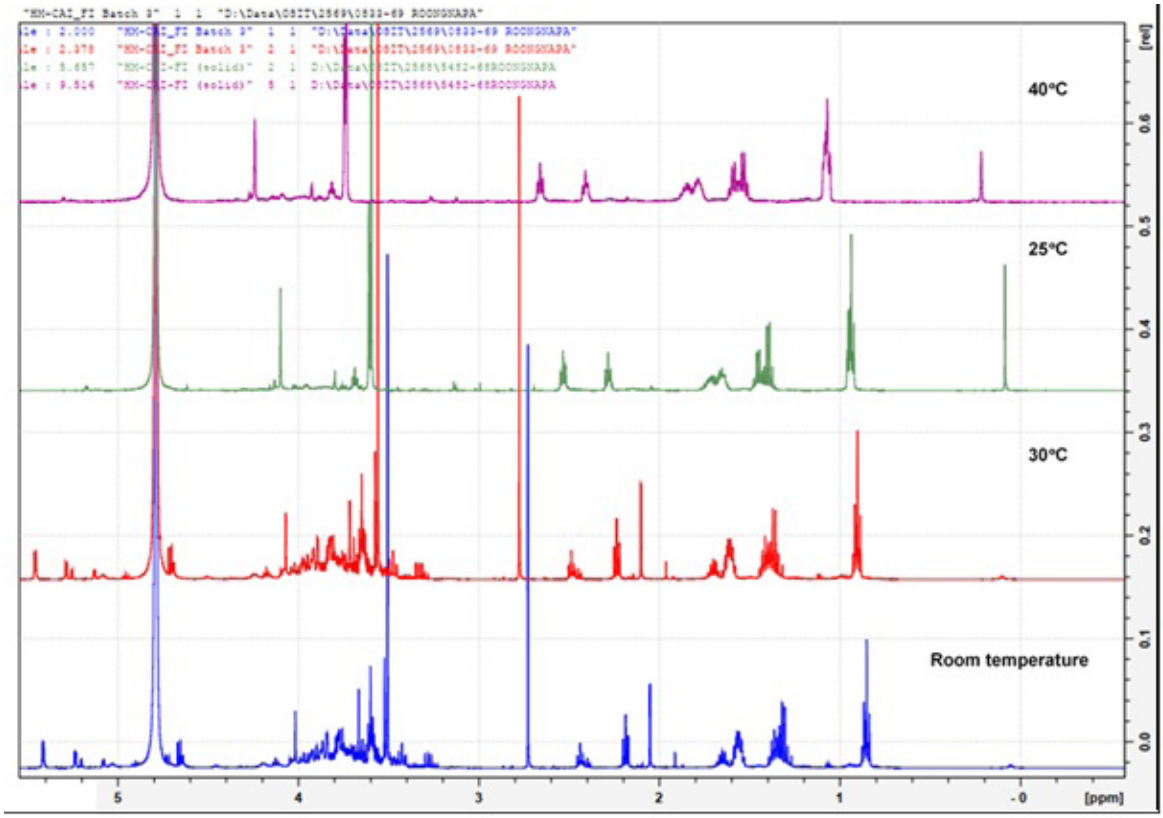

Figure 11A: The 1H-NMR spectrum of lyophilized IMN MIPs loaded with 200 mg CBD, recorded at room temperature, as well as at 25°C, 30°C, and 40°C in D_2O.

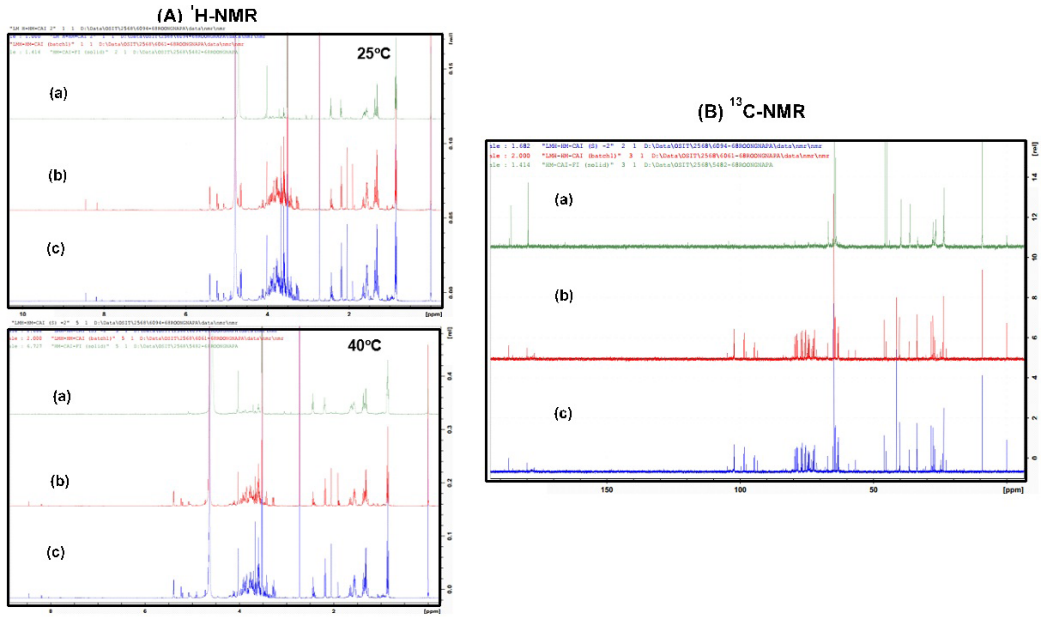

Fig. 11(B):

Figure 11B: ^{1}H-NMR and ^{13}C-NMR spectra of the CBD premix filtrate recorded at 25°C and 40°C. It illustrates (a) ISL and (b), (c) CCF within the PCL-T oily gel at 25°C.

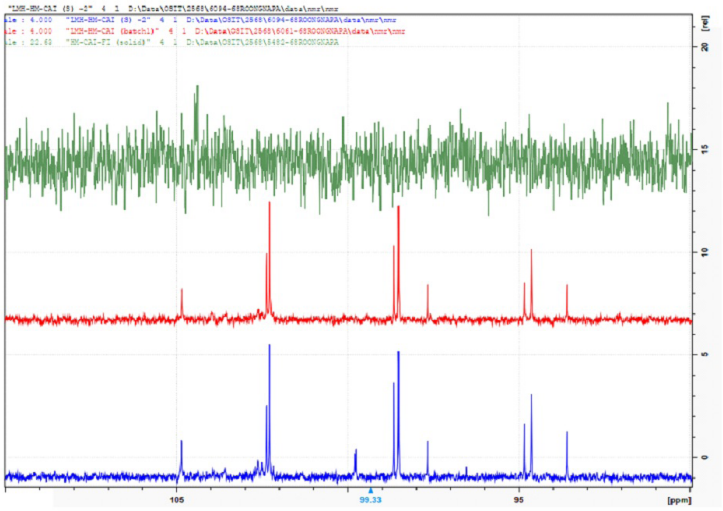

Figure 11C: DEPT-90 spectrum in D_2O (110-90 ppm) for DEP-C, taken from lyophilized ICL (green) and CCF (red, blue) across different batches at room temperature.

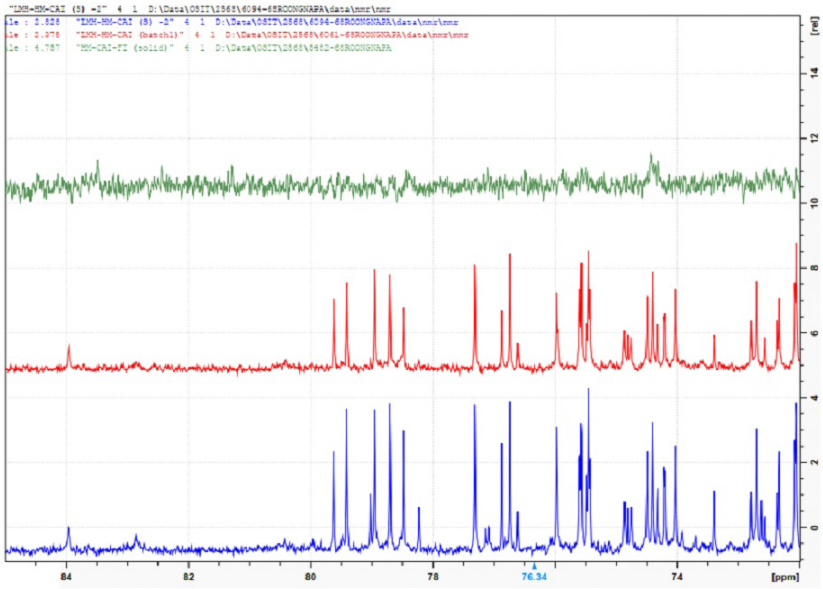

Figure 11D: DEPT-90 spectrum in D2O between 85 ppm and 73 ppm of the lyophilized ISL (green) and from CCF (red, blue) across different batches at room temperature.

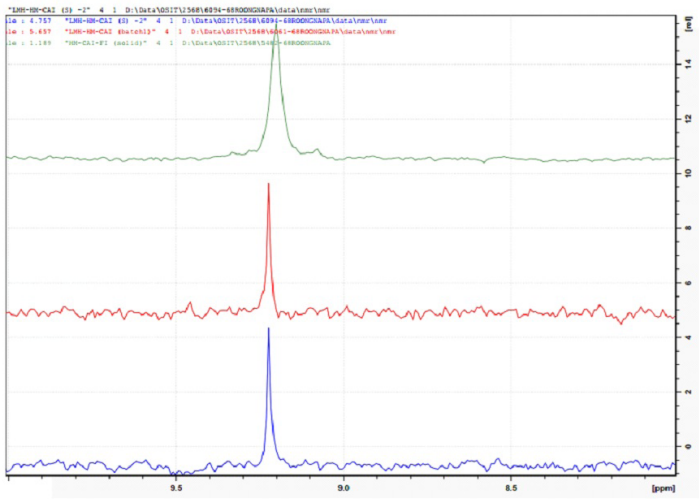

Figure 11E: The DEPT-90 spectrum in D_2O between 8.0 ppm and 10.0 ppm of the lyophilized ISL (green) and from CCF (red, blue) across different batches at room temperature.

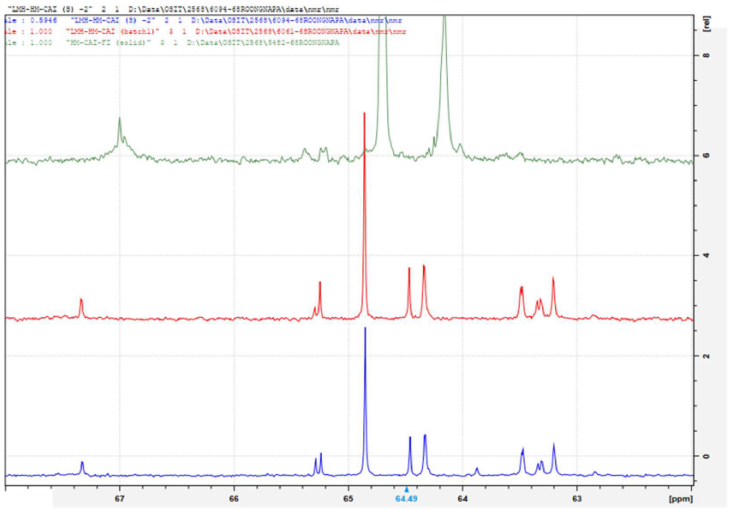

Figure 11F: DEPT-90 spectrum in D_2O, ranging from 8.0 ppm to 10.0 ppm, shows the lyophilized ISL (green) and CCF samples (red and blue) across various batches at room temperature.

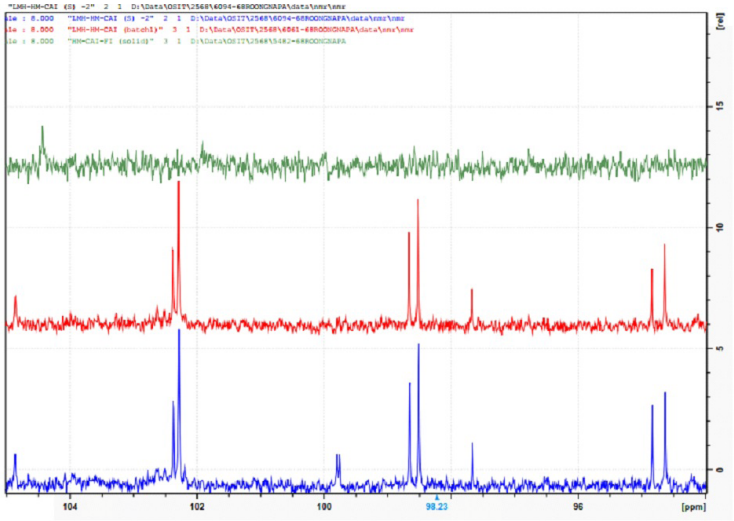

Figure 11G: ^{13}C-NMR spectrum in D_2O, ranging from 68 ppm to 62 ppm, of DEP-C derived from lyophilized ISL (green) and from CCF (red, blue) across different batches at room temperature.

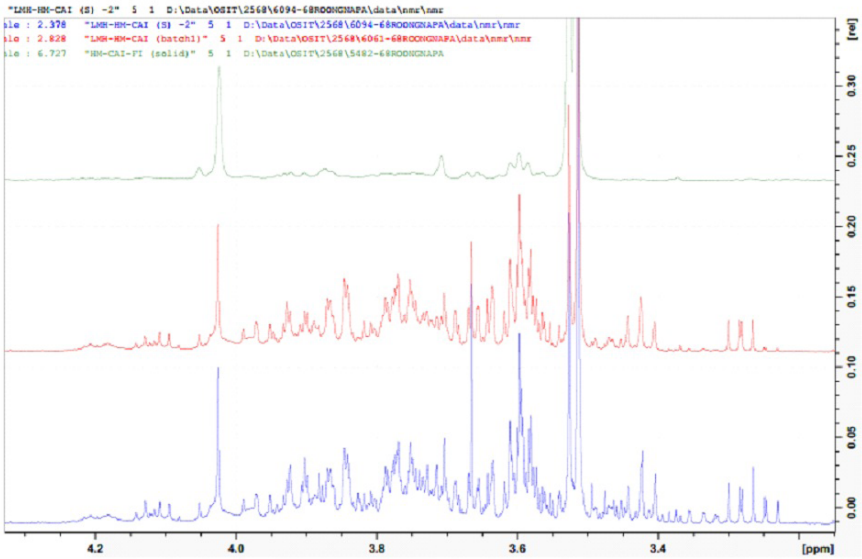

Figure 12: The magnification ^{1}H-NMR spectrum in D_2O between 4.25 ppm and 3.3 ppm of the CBD diastereomers and the enantiomeric dimer of the Fc peptide obtained from the lyophilized ICL (green) and from CCF (red, blue) across different batches at 25°C.

controlled conditions, such as increased viscosity, implying a hot-pulse-induced release of aromatic interactions upon cooling back to 25°C (see Figure 12). This suggests that multiple movement processes, including thermoresponsive proteins, are relocated during buffer changes at high temperatures. It also suggests the timing of activity peaks in enzyme-sensitive Fc sites with high ATP affinity, which, upon conformational change, align with membrane protein sites. High-resolution NMR *via* the MIP system reveals the landscape coordination of functional and delivery processes, the release of immunostimulants, and the modulation of antibody activity.

^{1}H-NMR studies at 40°C demonstrate that adding polar substances enhances water mobility (see Figure 13 A-C). Elevated water activity can increase the chemical potential of reactions and improve the solubility of poorly water-soluble drugs, promoting protein aggregation and conformational shifts. Aromatic ring hydrogen resonances of CBD between 8.2 and 8.4 ppm indicate that these changes are caused by side-chain interactions and disruptions at membrane sites. This is evidenced by the loss of signals at 2.2 ppm and the compact multiplet at 0.85 ppm for methylene and methyl protons in CBD diastereomers and the Fc peptide's enantiomeric dimer, as seen in the ISL type. In contrast, a well-separated signal at 2.3 ppm and 0.85 ppm, along with a broad multiplet around 3.2-3.9 ppm associated with human serum albumin trapped in CCF, are observed. Methine proton signals at 62 and 68 ppm in the 13C-NMR spectra of ISL and CCF types of IMN-HSA are detectable at room temperature and 40°C (see Figure 11F). IMNs with high CBD content expand less with temperature, likely due to hydration and protein interactions influenced by small molecules. Restricting protein motion through amino acid side chains provides insights into dissociation in ISL or CCF and aids in guiding multivalent protein binding. High-order structure analysis *via* NMR is necessary for simulation to accurately identify cutting-edge systems operating within the body and to respond to various stimuli, ultimately leading to enhanced treatment options for patients. High-resolution NMR experiments revealed that hydroxyl groups in hydrated CBD slow transport and stabilize ion-protein interactions, affected by steric effects from aromatic rings, side chains, hydrocarbons, and electronic interactions. This is related to multiple movement processes: Water, which maintains protein stability, self-association and protein-protein interactions in nanofiber matrices; temperature and pH, which affect these processes; and ATP, which enhances antibody and insulin interactions, thereby increasing water absorption. Interactions among chiral amino acids, CDR fragments, and MIP binding sites on HSA enhance charge insulation, a property

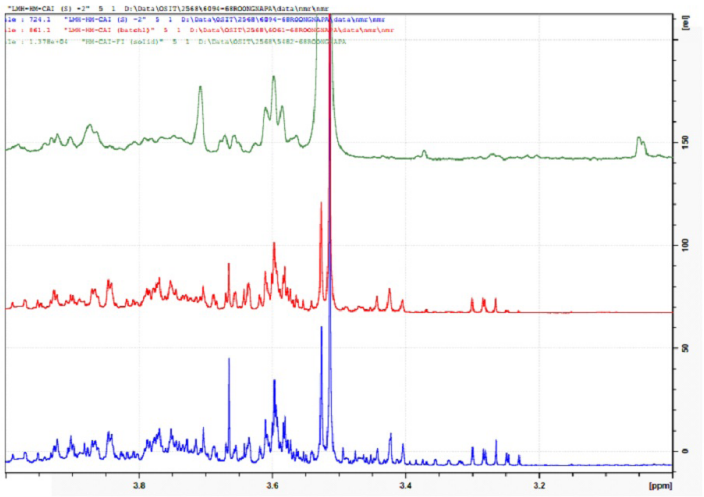

Figure 13A: The ^{1}H-NMR spectrum in D_2O between 3.9 ppm and 3.1 ppm of the enantiomeric structures, including dimerized MIP entities within nanocapsules for the lyophilized ICL (green) and from CCF (red, blue) across different batches at 40°C.

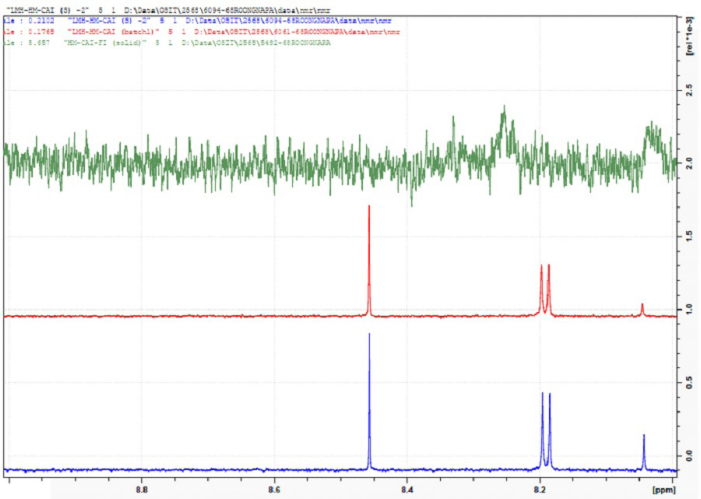

Figure 13B: The ^{1}H-NMR spectrum in D_2O between 9.0 ppm and 8.0 ppm of the lyophilized ICL (green) and from CCF (red, blue) across different batches at 40°C.

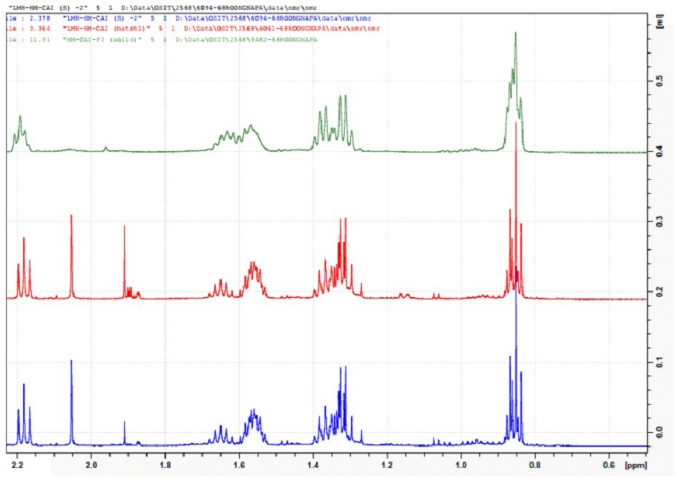

Figure 13C: The ^{1}H-NMR spectrum in D_2O between 2.2 ppm and 0.6 ppm of the CBD diastereomers and the enantiomeric dimer of the Fc peptide obtained from the lyophilized ICL (green) and from CCF (red, blue) across different batches at 40°C.

critical for peptide and small-molecule ligand binding. Drying nanocapsules improves water solubility and CBD loading, enabling interactions with the endocannabinoid system and targeting membrane sites with cannabinoid receptors. These improvements suggest improved delivery and ATP-driven uptake, supporting the dynamic movement of aliphatic chains in proteins as they penetrate the buffered, filtered lysate, as shown by NMR and other methods in this study. The results aid in identifying ligands for small drugs and their interactions with water and solvents. Ligands on lysozyme, which localize to membrane sites involved in antibiotic and antioxidant activities, hold promise for drug discovery and merit further investigation [40].

Interactions at the air-water interface enhance small-molecule and antibody binding, supporting protein thermostability under heat. ^{1}H-NMR and ^{13}C-NMR showed that stability and binding improved with proper glycosylation and lactate modification, especially in CCF types. Our research suggests that blue-light-responsive photoswitches that enable new insights into the interplay between protein's behavior and the landscape of (bio)pharmaceutical entities and it is beneficial for diagnostic potential of technique by a ligand exchange induced conformational changes in the insulin receptor to sense insulin levels in plasma. This targets serum albumin biomolecules *via* molecular imprinting and NMR, with biopharmaceutical implications. Our method can boost CBD and recombinant protein production. Electrostatic and amphipathic properties increase negative charge in polymer cavities, protecting sensitive regions, as seen with thermostable proteins on lipid bilayers, consistent with previous findings in different hybrid materials [41]. This indicates that IMN-based MIPs facilitate ligand exchange, which is vital for drug and biologic co-delivery. Negatively charged proteins enhance these interactions, and water is critical for protein demixing and nanomaterial stability. Overall, this offers insights into protein interactions in complex systems. This affinity-based protein profiling developed in the current work provides opportunities for biotherapeutic development *via* a glycopattern-residual protein mechanism similar to that of sugar transport proteins. Also, regulating IgG interactions enhances CBD's engagement with cannabinoid receptors, suggesting improved delivery and ATP-driven uptake, which are important to prevent aggregation. This photoaffinity helps thermostable proteins on lipid bilayers, influenced by electrostatic and amphipathic properties that ATP can tune protein phase behavior and prevent protein aggregation. Increasing negative charge in polymer cavities protects sensitive regions, while aromatic residues and double bonds regulate signaling and promote phosphorylation *via* FLIM. Encapsulating recombinant proteins in lipid bilayers mimics membrane functions, boosts stability, and shields reactive domains, especially for thermostable proteins, enabling controlled release of biologics and small molecules. Previous research shows that sugars and salts reduce protein adsorption and prevent unfolding, confirming nanocapsule stability [42]. This finding highlights the importance of membrane interactions and morphological changes in immune responses and in the distribution of IMN carriers, thereby affecting lysozyme hydration. The MIP creates stable matrices with specific binding sites, boosting targeted interactions. Consequently, targeting within IMN-HSA improves, increasing lysozyme activity in the red fluorescence channel *via* FLIM, which is advantageous for localizing the enzyme active site, whether the enzymes are active or being studied for the inhibitory effects of small compounds, especially when co-administered with multivalent protein-based therapeutics, indicating stability and regulation. Focusing on specific serum albumin biomolecules holds strong potential for biopharmaceuticals.

CONCLUSION

This work studies the thermoresponsive protein's mechanism of stability and affinity-based protein profile for oral biopharmaceuticals to gauge payload effectiveness. The methodology involves structural interactions of IMNs from filtrate lysate samples obtained *via* immunoaffinity capture of pre-mixed content. Despite challenges such as enzymatic degradation and limited membrane permeability, innovative IMN techniques aim to address these challenges. Encapsulating nanoMIP-bound HSA in cellulose improves delivery, as confirmed by spectroscopy and stability tests. Particles in phosphate-buffered saline show good stability, with higher pH encouraging nanoparticle clustering and HSA binding, indicating strong biological stability. The nanoparticle matrix reacts to pH shifts, especially at pH 4, enhancing antibody interactions and insulin-triggered CBD release. It also effectively encapsulates nano-HSA and soluble H protein at pH 7-7.4, maintaining antibody activity. Controlled co-evaporation stabilizes these properties, as evidenced by PCL-T gels and AFM, indicating IMN core formation *via* hydrogen bonds. These specialized MIP nanostructures develop a strong outer

layer, setting them apart from traditional cellulose environments. Notably, bionanofiltration demonstrates that cosolvent effects influence antigen-antibody interactions during diffusion, depending on time, chemical properties, and energy inputs, with high-temperature responses shifting away from peak activity, and amino acids increasing the unfolded-state colloid stability, resulting in reduced protein-protein aggregation. The vibrational landscape of co-administered protein therapeutics affects residual component performance, as shown in FT-IR analysis, thereby altering the time-resolving and stability niches, leading to differences in the half-lives of the multivalent proteins in the biotherapeutics. Slightly higher pH encourages nanoparticle clustering, and HSA encapsulated in the cellulose culture dynamics. FTIR, Raman spectroscopy, AFM, and X-ray analysis revealed protein structure, release mechanisms, and the stability and effector function of the protein of choice, which is crucial at the solid-liquid interface. X-ray imaging and element-binding energy confirmed mAb stability, enzyme activity, and the inhibitory effect, while osmolytes support proper folding and binding. Our results also indicate that CBD does not influence MIPs or enzymes. These interactions promote ensemble formation at MIP-binding sites linked to human albumin, aiding membrane protein targeting of small molecules and suppressing protein-protein interactions in bacteria. Mass spectrometry reveals subtle changes in the charge stabilizing properties of these nanostructures, affirming their integrity. Techniques such as light scattering, zeta potential, fluorescence microscopy, and microsystems are used to analyze MIP nanostructures and IMN features. Protein modifications improve small-molecule interactions and nanocapsule uptake through hydrophobic crosslinking with CBD and lysozyme.

The affinity-based protein profile obtained from LC-QTOF-MS allows for detailed analysis of the higher-order structure of protein aggregates. It demonstrates that the thermoresponsive mechanism involves observing conformational changes across states, while ligand binding reveals unique connectivity patterns during processes such as recycling and lyophilization. Structural interactions of IMNs from filtrate lysate samples, captured *via* immunoaffinity of pre-mixed content, reveal that charge-stabilizing states exhibit specific distributions of ionized carbonyl groups. Additionally, conformational dynamics are essential for maintaining protein stability and selfassociation. Molecular imprinting improves vaccine stability and release, influencing antibody activity. Data reveal that CBD levels do not impact MIP elemental composition or enzyme activity, as shown by X-ray mapping and FE-SEM. Controlled surfaces, such as cholate-functionalized MIPs, support biomolecular assembly and enable exploration of antigenic epitope diversity and oxidative metabolism within cellulose matrices, which are important for various applications. Our approach highlights enzyme-sensitive Fc sites with high ATP affinity, which, upon conformational shifts, align membrane protein sites with dynamic structural proteins that form nanoparticles. An innovative 3D optoplasmonic device directs light onto a small surface sphere, enabling real-time monitoring and converting analytes into protein lysates for clustering during bioprocessing. Interactions with high-energy cofactors like ATP are vital for therapeutic and diagnostic purposes, regulating antibody IgG interactions with antigens. Focusing on immunoglobulin G could improve targeting of sugar transport proteins for drug delivery. Understanding how temperature affects protein mobility can aid rapid clinical decision-making. This knowledge could help translate study features into targeted approaches, allowing monitoring of stored and recycled protein drugs to detect issues early, improve manufacturing, and promote sustainable patient care through versatile self-care options.

ACKNOWLEDGEMENTS

The Fundamental Fund acknowledges the project 'Development of Polymyxin B Formulation and Study of Biological Activity' (PHA6801059S), led by Prof. Dr. Teerapol Srichana. We thank PSU's Department of Pharmaceutical Chemistry for financial support and laboratory experiments; Naruedom Tangthong for the cellulose membrane; Dr. Krishna Mahesh and Dr. Wanpen Nakluae for laboratory assistance with dopamine isolation; Miss Pattchakun Bunkaew at OSIT for FL microscopy and FE-SEM; and Miss Siriwan Pongperksaputtana at Prince of Songkla University for NMR operations.

CONFLICTS OF INTEREST

The authors declare that they have no conflicts of interest.

FUNDING

This research received no external funding.

AUTHOR CONTRIBUTIONS

K. Prakannoppakun, N. Kaewsud, K. Santipiboon, and P. Getsuvan handled conceptualization, methodology, experimentation, data collection, and analysis. R. Suedee contributed to conceptualization, methodology, experimentation, supervision, investigation, analysis, manuscript prep, writing, review, and editing. W. Pholthien contributed to conceptualization, methodology, experimentation, investigation, writing, and review. All authors approved the final manuscript.

DECLARATION

This manuscript was written for clarity and grammatical correctness, and it was further reviewed for English accuracy and readability using a Generative AI tool (Grammarly). The authors have revised the content and accept full responsibility for it.

REFERENCES

1. Rathbone DL. Molecularly imprinted polymers in the drug discovery process. Adv Drug Deliv Rev. 2005;57(12);1854-1874.
2. Benito-Villalvilla C, Angelina A, Martin-Cruz L, Sirvent S, Palomares O. IgE, anti-IgE therapy, and regulatory T cells: New paradigms in allergic inflammation. Front Allergy. 2026;175992:1-9.
3. Chen Q, Liu Z, Wang X, Wang C, Feng L, Li Y. Drug-induced self-assembly of modified albumins as nano-theranostics for tumor-targeted combination therapy. ACS Nano. 2015;9(5):5223-5233.
4. Wang X, Su S, Tan S, Chen X, Wang, L, Wang S, et al. Current landscape and future directions of neoantigen vaccines; A new era of personalized cancer immunotherapy. Innov. 2026;7(9):101357.
5. Chwastek J, K□dziora M, Borczyk M, Korostynski M, Piscitelli F, Marzo VD, et al. The emerging role of endocannabinoid system modulation in human fibroblast-like synoviocytes: Exploring new biomarkers and potential therapeutic targets. Biomed Pharmacother. (2025);186:118040.
6. L-N Seyta, Bertolin G. Approaches to monitor ATP levels in living cells: Where do we stand? FEBS J. 2022;289:7940-7969.
7. Qing R, Hao S, Smorodina E, Jin D, Zalevsky A, Zhang S. Protein design: From the aspect of water solubility and stability. Chem Rev. 2022;122(18):14085-14179.
8. Do Carmo JP, Phyo YZ, Palmeira A, Tiritan ME, Afonso C, Kijjoa A. Enantioseparation, recognition mechanisms and binding of xanthones on human serum albumin by liquid chromatography. Bioanalysis.

2019;11(13):1255-1274.

9. Akbarian M, Chen A-H. Instability challenges and stabilization strategies of pharmaceutical proteins. Pharmaceutic. 2022;14(11):2533.
10. Sladek SF, McCartney M, Eskander DJ, Dunne MJ, Santos-Martinez F, Beenetti L, et al. An enteric-coated polyelectrolyte nanocomplex delivers insulin in rat intestinal instillations when combined with a permeation enhancer. Pharmaceutic. 2020;12(3):259.
11. Liang W, Levchenko TS, Torchilin VP. Encapsulation of ATP into liposomes by different methods: Optimization of the procedure. J Microencapsul. 2004;21(3):251-261.
12. Zhu Y, Gao C, Shen J. Surface modification of polycaprolactone with poly(methacrylic acid) and gelatin covalent immobilization for promoting its compatibility. Biomaterial. 2003;23(24):4889-4895.
13. Yuan S, Xiong Gordon, Wang X, Zhang S, Choong C. Surface modification of polycaprolactone substrates using collagen-conjugated poly(methacrylic acid) brushes for the regulation of cell proliferation and endothelialisation. J Material. 2012;2:13183.
14. Lasitsa AM, Churankin VG. Dynamics of wear surface layers modified by complex treatment. IEEE. 2015;1-4:10.
15. Esmaeilzadeh S, Valizadeh H, Zakeri-Milani P. The effects of pH, temperature, and protein concentration on the *in vitro* binding of flutamide to human serum albumin. Pharm Dev Technol. 2017;22(8):982-991.
16. Wymann S, Dai Y, Nair AG, Cao H, Powers GA, Schnell A, et al. A novel soluble complement receptor 1 fragment with enhanced therapeutic potential. J Biol Chem. 2021;100200:1-18.
17. Suedee R, Pholsathien W, Jaisawan K, Rodruksa J, Khomintr P. Molecularly imprinted polymers: Paving the way for future drug delivery innovations. Pharm Anal Acta. 2025:16:1-32.
18. Deschermeier C, Ehmen C, Possel R, Murawski C, Rushton B, Amuasi JV, et al. Fcβ-Receptor-based enzyme-linked immunosorbent assays for sensitive, specific, and persistent detection of anti-SARS-CoV-2 nucleocapsid protein IgG antibodies in human serum. J Clin Microbiology. 2022;60(6):1-11.
19. Hanus LO, Tchilibon S, Ponde DE, Breuer A, Fride E, Mechoulam R. Enantiomeric cannabidiol derivatives: Synthesis and binding to cannabinoid receptors. Org Biomol Chem. 2005;3(6):1116-1123.
20. Kearney E, Gangano AJ, Barrus DG, Rehrauer KJ, Reid T-ER, Navaratne PV, et al. Axially chiral cannabinoids: Design, synthesis, and cannabinoid receptor affinity. J Am Chem Soc. 2023;145(25):13581-13591.
21. Kim W, Doyle ME, Liu Z, Lao Q, ShinY-K, Carlson OD, et al. Cannabinoids inhibit insulin receptor signaling in pancreatic β-Cells. Diabetes. 2011;60(4):1198-1209.
22. Romero-Zerbo SY, García-Fernández M, Espinosa-Jiménez V, Pozo-Morales M, Escamilla-Sánchez A, Sánchez-Salido L, et al. Atypical cannabinoid Abn-CBD reduces inflammation and protects liver, pancreas, and adipose tissue in a mouse model of prediabetes and non-alcoholic fatty liver disease. Front Endocrinol. 2020;11:1-16.
23. González-Mariscal I, Montoro RA, Doyle ME, Liu Q-R, Rouse M, O'Connell JF, et al. Absence of cannabinoid 1 receptor in beta cells protects against high-fat/high-sugar diet-induced beta cell dysfunction and inflammation in murine islets. Diabetologia. 2018;61(6):1470-1486.
24. Motteu N, Goemaere B, Bladt S, Packeu A. Implementation of MALDI-TOF mass spectrometry to identify Fungi from the indoor environment as an added value to the classical morphology-Based identification tool. Front Allergy. 2022;3:82648.
25. Feng P, Weagant SD, Grant MA, Burkhardt W. BAM 4: Enumeration of *Escherichia coli* and the Coliform bacteria, FDA, 2002.
26. Wang S, Walker-Gibbons R, Watkins B, Flynn M, Krishnan M. A charge-dependent long-ranged force drives tailored assembly of matter in solution. Nature Nanotech. 2024;19(4):485-493.
27. Heinrich K, Ernst J, Hinger M, Briguet A, Leiss M, Wuhrer M. Bispecific IgG1 CrossMab antibody of the Knob-into-hole format applying various stress conditions revealed pronounced stability. ACS Omega. 2022;7(4):3671-3679.
28. Knutson K, Potts RO, Guzek DB, Golden GM, McKie JE, Lambert WI, et al. Macroand molecular physical-chemical consideration in understanding drug transport in the stratum corneum. J Contr Rel. 1985;2:67-87.
29. Li Z, Hage DS. Analysis of stereoselective drug interactions with serum proteins by high-performance affinity chromatography: A historical perspective. J Pharm Biomed Anal. 2017;144:12-24.
30. Singh KN, Rana S, Khan T, Mondal D, Sen P, Interplay of protein fluctuation and associated water dynamics in osmolyte-induced stabilization. Biophys J. 2025;124(12):2082-91.
31. Hirsch E, Nacsa M, Ender F, Mohai M, Nagy ZK, Marosi GJ. Preparation and characterization of biocompatible electrospun. Periodica Polytechnica Chem Eng. 2018;1-10.
32. Lee Y-C, Nelson J, Sueda K, Seibert D, Hsieh W-Y, Braxton. The protective effect of lactose on lyophilization of CNK 20402. AAPS PharmSciTech. 2005;6(1):E42-E48.
33. Tomczyk N, Wallace A, Richardson K, Grzyb A, Wildgoose J. Targeted high resolution quantification with TOF-MRM and HD-MRM. Application Note. 2021;1-10.
34. Fernández-Quintero ML, Ljungars A, Waibl F, Greiff V, Andersen JT, Gjølberg TT. Assessing developability early in the discovery process for novel biologics. mAbs. 2023;15(1):2171248.
35. Garabedian M, Su Z, Dabdoub J, Tong M, Deiters A, Hammer DA, et al. Protein condensate formation *via* controlled intrinsically disordered sequences. Biochem. 2022;61(22):2470-2481.
36. Finn DF, Walsh JJ. Twenty-first century mast cell stabilizers. Brit J Pharmaco. 2013;170(1):23-37.
37. Pereire R, Hackett B, O'Driscoll DN, Sun MC, Downer EJ. Cannabidiol modulation of oxidative stress and signaling. Neuronal Signal. 2021;5(3):NS20200080.
38. Leihou S, Li Y, Huang F, Wang X, Lu J, Jia F. Complementary autophagy inhibition and glucose metabolism with rattle-structured polydopamine@mesoporous silica nanoparticles for augmented low-temperature photothermal therapy and *in vivo* photoacoustic imaging. 2020;10(16):7273-7286.
39. Meyer JD, Bai SJ, Rani M, Suryanarayanan R, Nayar R, Carpenter JF, et al. Infrared spectroscopic studies of protein formulations containing glycine. J Pharm Sci. 2004;93(5):1359-1366.
40. Das S, Nudrat S, Maity S, Jana M, Beelwal VK, Roy AS. Isoflavones and lysozyme interplay molecular insights into binding mechanisms and inhibitory efficacies of isoflavones against protein modification. Chem Phy Impact. 2024;8:100643.
41. Marquette A, Salnikov ES, Glattard E, Aisenbrey C, Bechinger B. Magainin 2-PGLa interactions in membranes-two peptides that exhibit synergistic enhancement of antimicrobial activity. Curr Topics Med Chem. 2016;16(1):65-75.
42. Singh KN, Rana S, Khan T, Mondal D, Sen P. Interplay of protein fluctuation and associated water dynamics in osmolyte-induced stabilization. Biophys J 2025;124(12):2082-2091.